

**UNIVERSITY OF GENOVA**

**POLYTECHNIC SCHOOL**

**DIME**

**Department of Mechanical, Energy, Management  
and Transportation Engineering**



**MASTER OF SCIENCE THESIS  
IN  
MECHANICAL ENGINEERING**

**Characterization of Secondary Air System circuits in a  
Gas Turbine engine**

**Supervisor:**

Chiar.<sup>mo</sup> Prof. Ing. Alessandro Bottaro

**Co Supervisor:**

Dott. Alessio D'Alessandro

**Candidate:**

Valerio Lanata

March 2019

# **Caratterizzazione dei circuiti di Aria Secondaria di una turbina a gas**

## **Sommario**

All'interno del sempre più competitivo mercato degli impianti per l'energia, la necessità di un sistema integrato per la predizione delle performance di un impianto in condizioni nominali e di forte off-design è sempre maggiore. L'elaborato seguente si concentra sulla caratterizzazione dei circuiti d'aria secondaria di una turbina a gas in suddette condizioni di off-design. Per poter simulare il comportamento dei circuiti di Aria Secondaria una rete fluida 0D è stata implementata in una routine basata sull'analisi dimensionale e sul teorema  $\Pi$  di Riabouchinsky-Buckingham. Basandosi su queste basi teoriche, il sistema utilizza i dati derivanti da varie simulazioni della rete fluida per generare le curve caratteristiche dei circuiti. Queste curve sono state generate in modo da poter essere associate con le curve caratteristiche degli altri componenti del turbogas. Le curve sono state inoltre suddivise in due macro contributi (Cooling e Leakage) e successivamente classificate per ottenere un'elevata risoluzione spaziale dei flussi d'iniezione in turbina.

# **Characterization of Secondary Air System circuits in a Gas Turbine engine**

## **Abstract**

In a more and more competitive power market, the necessity of an integrated system for a plant's performance prediction, both in nominal and off-design conditions, is always greater. The following text is focused on the characterization of the Secondary air System circuits of a gas turbine engine, in the above mentioned off-design conditions. To simulate the behaviour of the Secondary Air circuits a 0D fluid network has been implemented in a routine based on the dimensional analysis and on the Riabouchinsky-Buckingham's  $\Pi$  theorem. Basing on these theoretical fundamentals, the system utilizes the data coming from many simulations of the 0D fluid network to generate the Secondary Air System circuits' characteristic curves. These characteristic curves have been defined in order to be interfaced with the other Gas Turbine components' curves. The characteristic curves have been split in 2 macro-contributes (Cooling and Leakage) and subsequently classified to obtain an elevated spatial resolution of the turbine injection flows.

## **Ringraziamenti**

Ringrazio innanzitutto il Prof. Ing. Alessandro Bottaro, insegnante appassionato ed ispiratore, che mi ha concesso l'opportunità di svolgere questa attività presso Ansaldo Energia.

Ringrazio il Dott. Alessio D'Alessandro per la disponibilità, la cura dei dettagli e la professionalità con cui ha seguito l'intera attività.

Ringrazio Andrea, Elena, Francesco, Marco, Roberto e Vera per avermi accolto nel loro gruppo, per aver corretto i miei errori e per avermi mostrato la passione che mettono nel loro lavoro.

Ringrazio infine mia madre che dal primo giorno mi ha spronato a seguire i miei sogni, sempre pronta ad aiutarmi in qualsiasi modo.

# Contents

<b>Sommario</b> .....	I
<b>Abstract</b> .....	II
<b>Ringraziamenti</b> .....	III
<b>1. Introduction</b> .....	1
1.1 Gas Turbine introduction.....	3
1.2 Basic Gas Turbine thermodynamics .....	3
1.3 Blade cooling .....	8
1.4 Energy market.....	10
<b>2. Gas Turbine Secondary Air System</b> .....	13
2.1 Secondary air system main objectives .....	14
2.1.1 Turbine Blade Cooling .....	14
2.1.2 Turbine Vane Cooling .....	14
2.1.3 Turbine sealing system .....	15
2.1.4 Rotor Axial Thrust Balance .....	21
2.1.5 Passive clearance control .....	22
2.1.6 Leakages .....	23
2.1.7 Optimal and robust SAS design.....	24
<b>3. Secondary Air System Numerical Integration</b> .....	26
3.1 Secondary Air System network solver .....	26
3.2 CalculiX.....	26
3.2.1 Newton-Raphson scheme .....	27
3.2.2 Drawbacks of the Newton-Raphson Method.....	29
3.2.3 Implementation .....	32
3.2.4 Convergence criteria.....	36
3.2.5 User interface.....	37
<b>4. Dimensional analysis on Secondary Air System</b> .....	38
4.1 Dimensional analysis for Gas Turbines .....	38

4.2 Dimensional analysis .....	38
4.2.1 $\Pi$ Theorem .....	41
4.3 $\Pi$ theorem applications .....	42
4.4 $\Pi$ theorem application to Secondary Air System .....	43
4.5 Application of Blade and Vane Characteristic Curves .....	45
4.6 Characteristic curves matching.....	47
4.7 Secondary Air System characteristic curves production .....	48
4.7.1 Internal lines .....	50
4.7.2 External lines .....	55
4.7.3 Pumping work.....	56
4.7.4 Design of Experiments .....	56
4.7.5 Characteristic Curves Post Processing.....	57
<b>5. Fluid Network Assembly .....</b>	<b>58</b>
5.1 Internal line assembling.....	58
5.2 External line assembling.....	66
<b>6. Characteristic Curves Production .....</b>	<b>76</b>
<b>7. Conclusions .....</b>	<b>86</b>
<b>References.....</b>	<b>87</b>
<b>Nomenclature .....</b>	<b>89</b>

# 1. Introduction

This master thesis application has been carried on in collaboration with Ansaldo Energia: Ansaldo Energia is a leading international player in the power generation industry, to which it brings an integrated model embracing turnkey power plants construction, power equipment (gas & steam turbines, generators and microturbines), manufacturing and services and nuclear activities. Ansaldo Energia manufactures a complete range of heavy duty gas turbines for power generation applications, from E to H class technology, ranging from 80MW to 538 MW (ISO Power) in single unit configuration, allowing customers to operate their combined-cycle and open-cycle power plants with state of the art gas turbines in terms of all market drivers: efficiency, power output, reliability, operational and fuel flexibility, emission levels and cost-effectiveness. In order to meet all customer requirements Ansaldo Energia is active as full service provider with a broad portfolio on heavy duty gas turbines, offering complete maintenance solutions on power generation rotating equipment and plants, built both by itself or by other manufacturers. Ansaldo Energia boasts decades of experience in the production, design, development, sale and service of gas turbines and can count on a worldwide R&D organization that supports the continuous development and innovation of its gas turbines, designing manufacturing and testing products and solutions in line with market demand [1].



*Fig. 1.1 - Ansaldo Energia history*

Born formally in 1991 from Ansaldo Group, an established Italian engineering company based in Genoa, with interests in shipbuilding, aircraftbuilding, ironworking and weaponmaking, Ansaldo Energia already had experience in steam turbine power plant building and started its gas turbine development as manufacturer of engines from other original equipment manufacturer (OEM) under license contract: in 2005 Ansaldo Energia reached the total independence from licenses and began the development of its own 1st gas turbine engine. With the acquisition of Alstom's advanced heavy duty gas turbine business, Ansaldo Energia has complemented its R&D center with two additional key centers in Switzerland and Florida, further extending its skills and capabilities in this industry. It has also enlarged its gas turbine product portfolio and can rely on new facilities to test full scale prototypes, as well as on an additional combustor pressure test rig facility, which completes the range of laboratories available to the Group in the areas of combustion, fluid-dynamics with atmospheric wind tunnels, mechanical testing on materials, and metallographic and chemical analysis, which are fundamental to validate the design and innovation process.

## Standard Configurations

Gas Turbine	Gas Turbine Performance	Power Plant Configuration	Power Plant Performance
<b>GT36-S6</b> 	369 MW 42.3%	1+1	520 MW 62.3%
		2+1	1,046 MW 62.6%
<b>GT36-S5</b> 	538 MW 42.8%	1+1	760 MW 62.6%
		2+1	1,525 MW 62.8%
<b>GT26</b> 	370 MW 41.0%	1+1	540 MW 61%
		2+1	1,083 MW 61.2%
<b>AE94.3A</b> 	340 MW 40.3%	1+1	495 MW 60%
		2+1	992 MW 60.3%
<b>AE94.2</b> 	190 MW 36.3%	1+1	287 MW 55.8%
		2+1	578 MW 56.2%
<b>AE64.3A</b> 	80 MW 36.4%	1+1	120 MW 55.7%
		2+1	243 MW 56.4%

Fig. 1.2 - Ansaldo Energia GT engine fleet

This particular thesis application has been carried on in collaboration with the Ansaldo Energia R&D Gas Turbine Secondary Air System department: the main target of the thesis was the modelling of the Secondary air system circuits and their characterizations, in design and off-design working conditions. To achieve this target, with the constraints of an industrial time scheduling and an industrial required accuracy, a 0D tool for the fluid networks resolution has been implemented in a wider routine to predict the off-design conditions of the entire engine. The characterization of the gas turbine will occur as the integration of all the main components, in every working conditions: this thesis will show how the main components may be modelled and characterized in a stand-alone configuration and the how the result can be matched, with particular attention to the Secondary Air System.

## **1.1 Gas Turbine introduction**

The gas turbine engines are machines made for the energy production based on the Brayton cycle: gas turbines have recently been protagonist of an important revolution in the energetic technology. Mostly if combined with recovery steam cycles and using natural gas as primary fuel, they constitute, today, the an efficient, economic and environmental respectful solution for the electromechanical power generation. The relative simplicity of the machine and the incredibly wide power range that may be produced make the GT engine the 1<sup>st</sup> choice for the energy production, moreover the high power to weight ratio makes them particularly suitable for the aircraft propulsion application. From its conception in the late 1800 the gas turbine engine has undergone to many changes and improvements: to fulfil many different targets the basic engine has been subjected to a strong evolution and differentiation. Techniques, like the intercooling, the reheating or the post-combustion, have been adopted, to improve specific work or efficiency: the current gas turbine industry allows the final client to tune the gas turbine base model with additional features, leading to an extreme chance of customization, but also to a wide fleet of engine models. In the modern energy market the gas turbine engines are fundamental for the energy production system: from base to peak load, in cogeneration plants or in distributed generation, the GT engine may adapt to the situations with competitive levels.

## **1.2 Basic Gas Turbine thermodynamics**

The ideal Brayton cycle is composed by:

- 2 isobaric processes (combustion and atmospheric dispersion of the exhaust gases)
- 2 adiabatic isentropic processes (compression and turbine expansion)

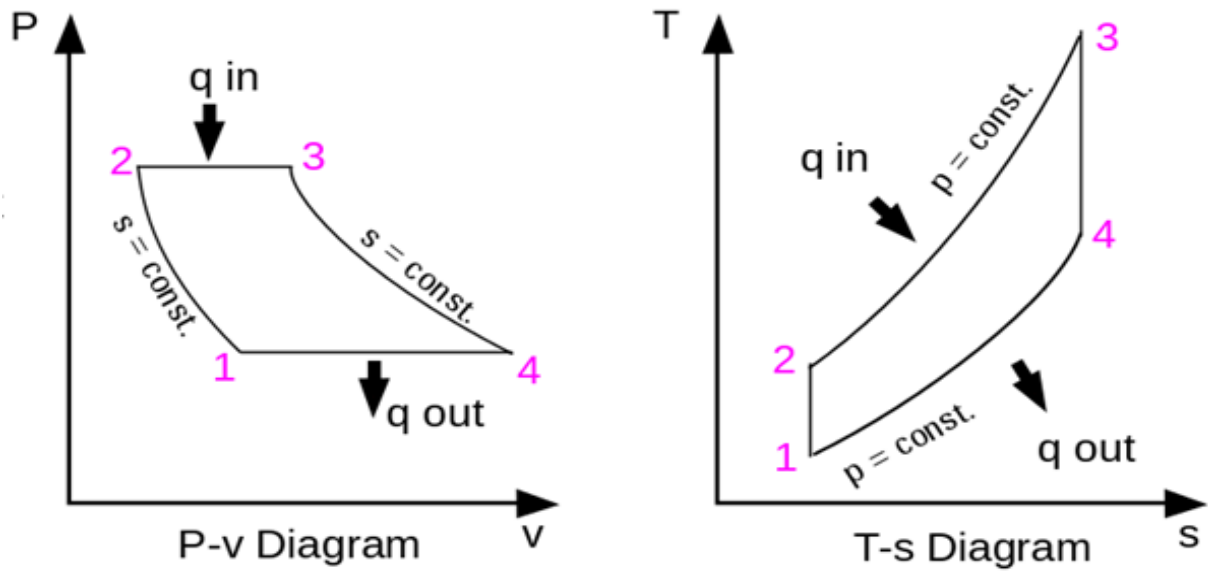


Fig. 1.3 - Brayton cycle

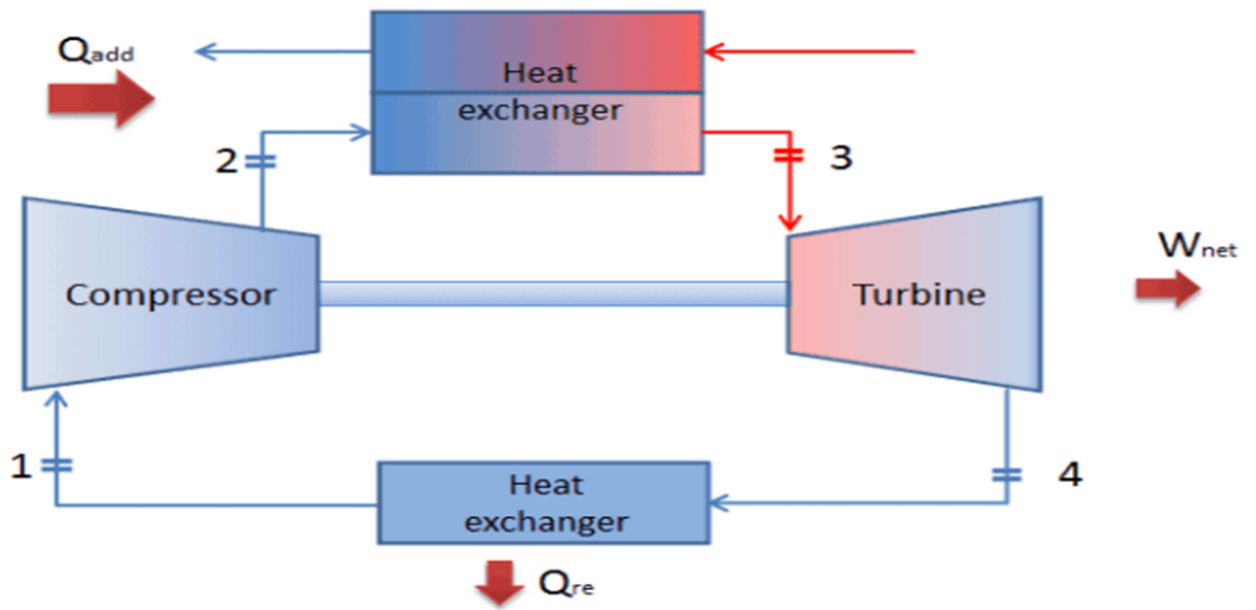


Fig. 1.4 - Closed Brayton cycle engine

From 1<sup>st</sup> principle analysis the cycle efficiency may be expressed as:

$$\eta = \frac{L_n}{Q_1} = \frac{L_E - L_C}{Q_1} = \frac{(h_3 - h_4) - (h_2 - h_1)}{h_3 - h_2} = \frac{c_p(T_3 - T_4) - c_p(T_2 - T_1)}{c_p(T_3 - T_2)} \quad (1.1)$$

$$= \frac{(T_3 - T_4) - (T_2 - T_1)}{T_3 - T_2}$$

Or

$$\eta = \frac{Q_1 - Q_2}{Q_1} = \frac{c_p(T_3 - T_2) - c_p(T_4 - T_1)}{c_p(T_3 - T_2)} = \frac{(T_3 - T_2) - (T_4 - T_1)}{T_3 - T_2} = \quad (1.2)$$

$$\eta = 1 - \frac{T_4 - T_1}{T_3 - T_2} = 1 - \frac{T_1 \left( \frac{T_4}{T_1} - 1 \right)}{T_2 \left( \frac{T_3}{T_2} - 1 \right)} \quad (1.2)$$

In the adiabatic transformations 1-2 and 3-4 the following relations rule:

$$\frac{T_4}{T_3} = \left( \frac{p_4}{p_3} \right)^{\frac{k-1}{k}} \quad (1.3)$$

$$\frac{T_1}{T_2} = \left( \frac{p_1}{p_2} \right)^{\frac{k-1}{k}} \quad (1.4)$$

If we pose:

$$\beta = \frac{p_2}{p_1} = \frac{p_3}{p_4} \quad (1.5)$$

$$\varphi = \frac{k-1}{k} \quad (1.6)$$

$$\beta^\varphi = \frac{T_2}{T_1} = \frac{T_3}{T_4} \quad (1.7)$$

$$T_2 T_4 = T_1 T_3 \quad (1.8)$$

$$\frac{T_4}{T_1} = \frac{T_3}{T_2} \quad (1.9)$$

So the efficiency

$$\eta = 1 - \frac{T_1}{T_2} = 1 - \beta^{-\varphi} \quad (1.10)$$

The ideal cycle efficiency depends only on the isentropic temperature rise given from the compressor: rising up the pressure ratio  $\beta$ , the global efficiency increases, striving to 1 for  $\beta \rightarrow \infty$

The net work is for definition given from the product of the heat given  $Q_1$  by the cycle efficiency  $\eta$ . Referring to a unitary weight fluid, we obtain:

$$\begin{aligned} L_N = \eta Q_1 &= (1 - \beta^{-\varphi}) c_p (T_3 - T_2) = (1 - \beta^{-\varphi}) c_p T_1 \left( \frac{T_3}{T_1} - \frac{T_2}{T_1} \right) \\ &= (1 - \beta^{-\varphi}) c_p T_1 \left( \frac{T_3}{T_1} - \beta^\varphi \right) \end{aligned} \quad (1.11)$$

For a fixed  $T_1$  (ambient temperature), we see that the net work is strongly influenced both from the maximum temperature  $T_3$ , both from the pressure ratio  $\beta$ . The work tends to 0 for  $\beta = 1$  (compression and expansion works null) and for  $\beta^\varphi = \frac{T_3}{T_1}$  or for  $T_2 = T_3$  (condition where the isentropic compression work is equal to the expansion one). Deriving the function  $L_N$  respect to  $\beta$ , we obtain a maximum for  $\beta^{-\varphi} = \sqrt{\frac{T_3}{T_1}}$ : the work is maximum for  $T_2 = T_4 = \sqrt{T_3 T_1}$ . It's possible to find an optimum pressure ratio  $\beta_{opt}$  that maximizes the net work: this value doesn't supply the best available efficiency for the ideal cycle.

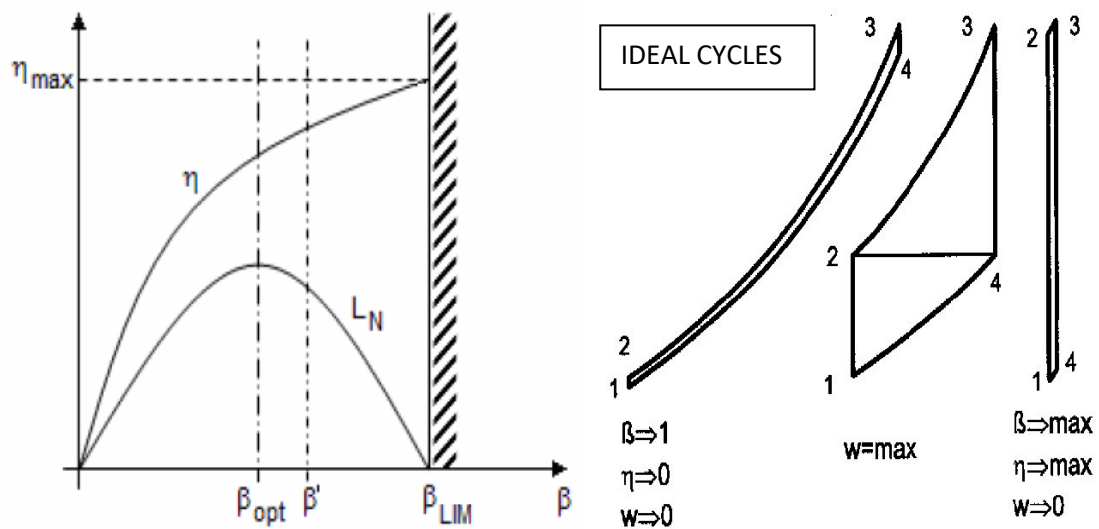


Fig. 1.5 - Efficiency and net work against the cycle pressure ratio (left) and Extreme Brayton cycles (right)

In the real open cycle the cycle is no more characterized by 2 isobaric and 2 isentropic processes, but admits real effects such as pressure and the heat exchange losses, mass losses (leakages), incomplete chemical reactions, mechanical losses. A Brayton type engine is made by 4 main components: compressor, combustion chamber, expander and a power conversion device such as a nozzle for aeronautic applications or an electrical generator for industrial applications; typically the compressor and the turbine are connected on a shaft to permit work exchange.

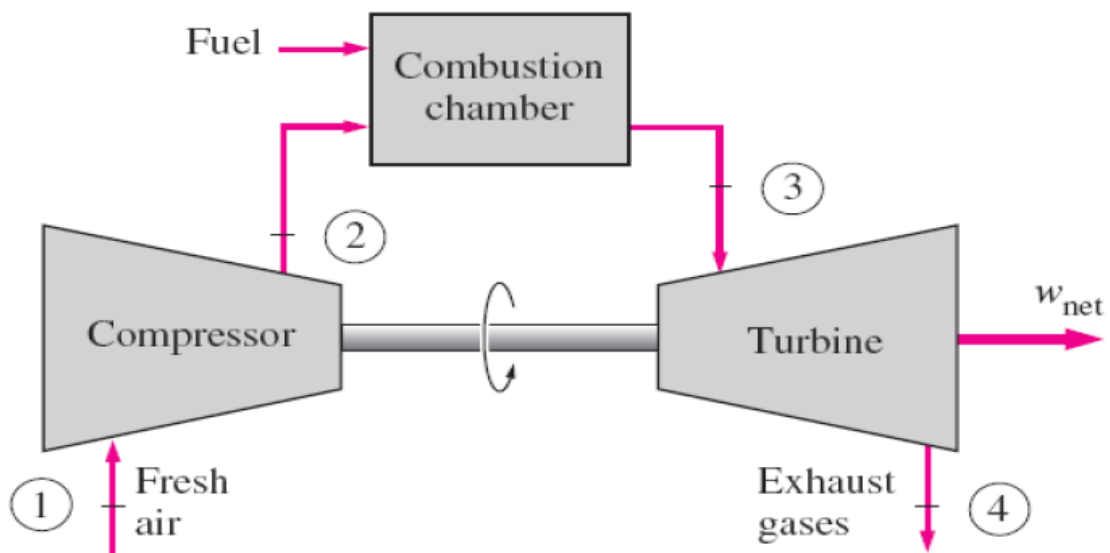


Fig. 1.6 - Brayton open cycle engine

The cycle can be summarized in:

- an adiabatic compression made by the compressor with the air at ambient temperature and pressure lower than the ambient (due to aspiration losses) (1-2')
- an heat exchange that happen thanks to the combustion of a fuel-air mixture, with combustion chamber pressure losses (2'-3')
- an adiabatic expansion made by the turbine that expands the compressed hot gases to a pressure higher than the ambient (due to discharge losses) (3'-4')
- an heat exchange that happens by dispersing the hot gases in the atmosphere

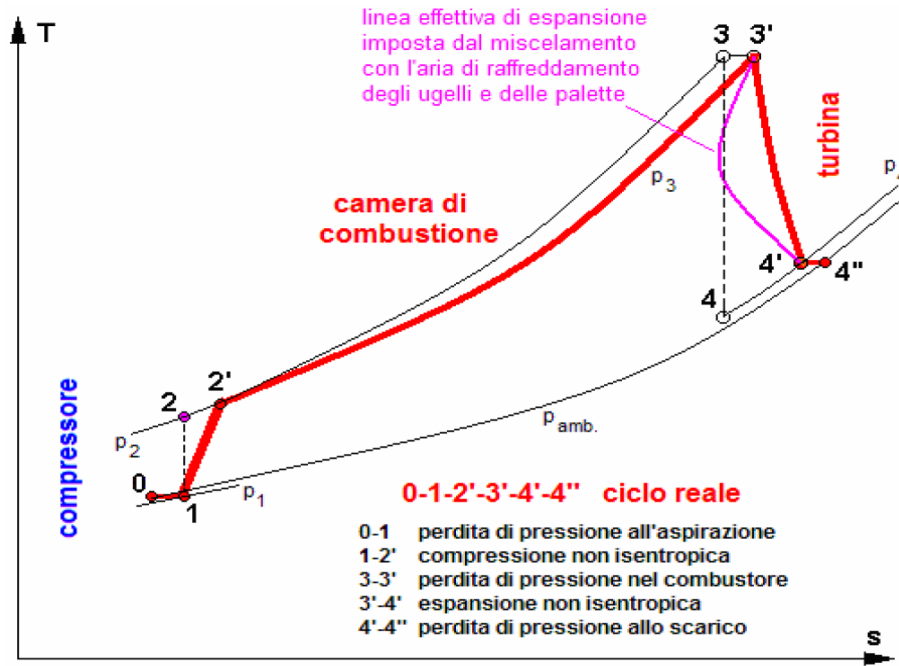


Fig.1.7 - Brayton real cycle

Considering the real machines:

$$L_{c,real} = h_2 - h_1 = \frac{h_{2is} - h_1}{\eta_{cis}} = c_p(T_2 - T_1) = \frac{c_p(T_{2is} - T_1)}{\eta_{cis}} = \frac{c_p T_1 (\beta^\varphi - 1)}{\eta_{cis}} \quad (1.12)$$

$$L_{t,real} = h_3 - h_4 = (h_3 - h_{4is})\eta_{tis} = c_p(T_3 - T_4) = c_p(T_3 - T_{4is})\eta_{tis} = c_p T_3 (1 - \beta^\varphi)\eta_{tis} \quad (1.13)$$

In Fig. 1.8 the efficiency is plotted against the specific work: every point has 3 parameters: the turbine inlet temperature  $T_3$ , the turbine and compressor polytropic efficiency  $\eta_p$ , and the pressure ratio  $\beta$ .

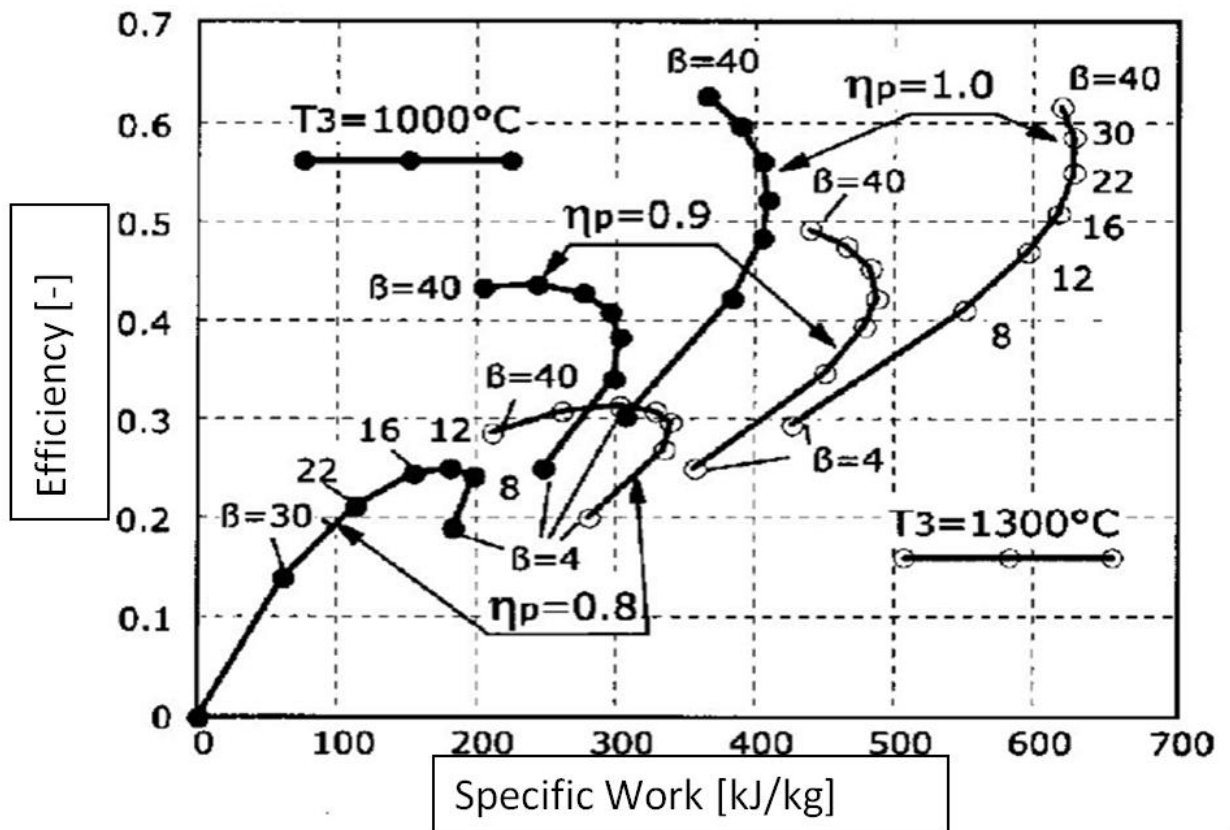


Fig. 1.8 - Efficiency and specific work in a real Brayton engine

The choice of the pressure ratio will have to be focused on the targets of the engine: an aircraft engine is designed to reach the maximum efficiency (medium-high pressure ratio) in a limited available size; while an heavy-duty gas turbine is more designed to pursue the maximum specific work allowable (middle range pressure ratio) and high mass flow rate, the latter proportional to the cross section of the first stage of the machine [2]. Other figures of merit are more and more important nowadays in a flexible energy market, such as a low Minimum Environmental Load (respecting the emission limits) and a fast start-up capability. Typically markets with high fuel availability and low cost of gas but poor electric network connections (Northern Africa, Middle East, Russia...) are more interested to the ability to fast recover an energy shortage in the network than to steady state performance. Moreover the growing up of renewable energy reserves more and more a network-supporting role to gas turbines: hence it also requires a GT fast reaction to variations of load demand (flexibility). This will have an impact on any part of the GT design including the secondary air as we will see. The non-ideal effects of the GT components and the wide variety of working conditions lead to the necessity of a component characterization that keeps in count these effects [3].

### 1.3 Blade cooling

The easiest manner to improve the value of the engine efficiency, as visible in Par. 1.1, is the increment of the maximum temperature of the cycle: the continuous research for higher Turbine Inlet Temperature (TIT) pushed the material technology to its own limits. Modern materials, implied in the most stressed rows of the turbine, fulfil both the resistance to high stresses and high temperatures even with the disadvantage of great costs. Research for higher cycle

efficiency has pushed the hot gases temperature beyond the maximum tolerable by the materials, decoupling the hot gas temperature from the material one through a cooling system: 3 main cooling methods have been implemented

- Internal forced convection (mechanism of heat transfer based on a fluid in motion, inside the blade itself, in which the fluid motion is generated by an external source)
- Film cooling (introduction of a cooling fluid along a surface exposed to a high temperature environment)
- Jet impingement (enhanced convection heat transfer due to an high velocity flow rate impinging on a solid surface)

All these methods imply the use of relatively fresh air to generate a fluid barrier between the hot gases and the blade's material: this air mass flow rate is typically bled from the compressor [4] [5].

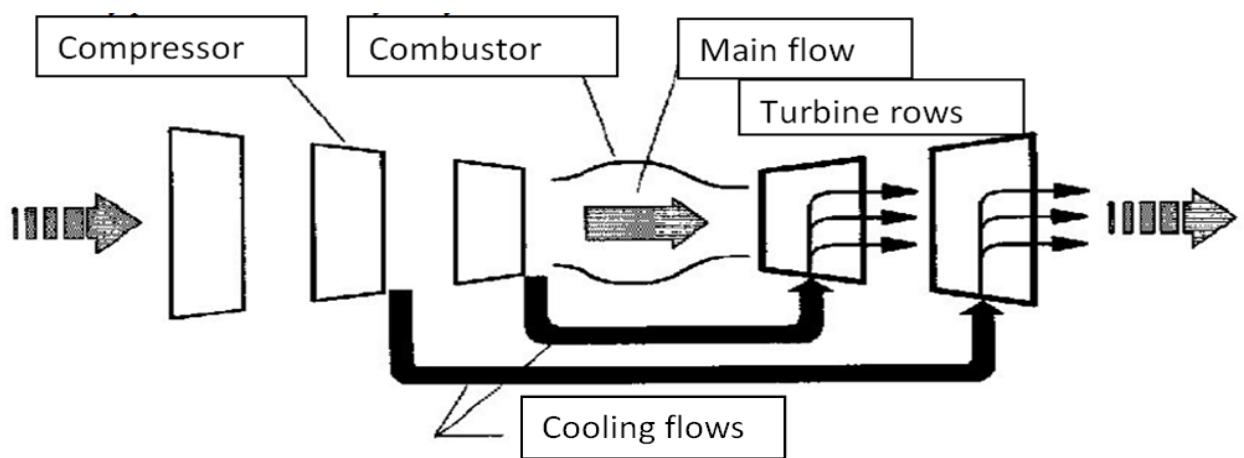


Fig. 1.9 - Modern GT engine scheme

Blades are designed to use one, or more, method of cooling: the choice of which method will be derived from various factors such as gas temperature, material stress limits, cost. For example the vanes, that are not submitted to centrifugal forces, have low constraints on the weight and wall thickness and may host a complex and bulky system like the jet impingement.

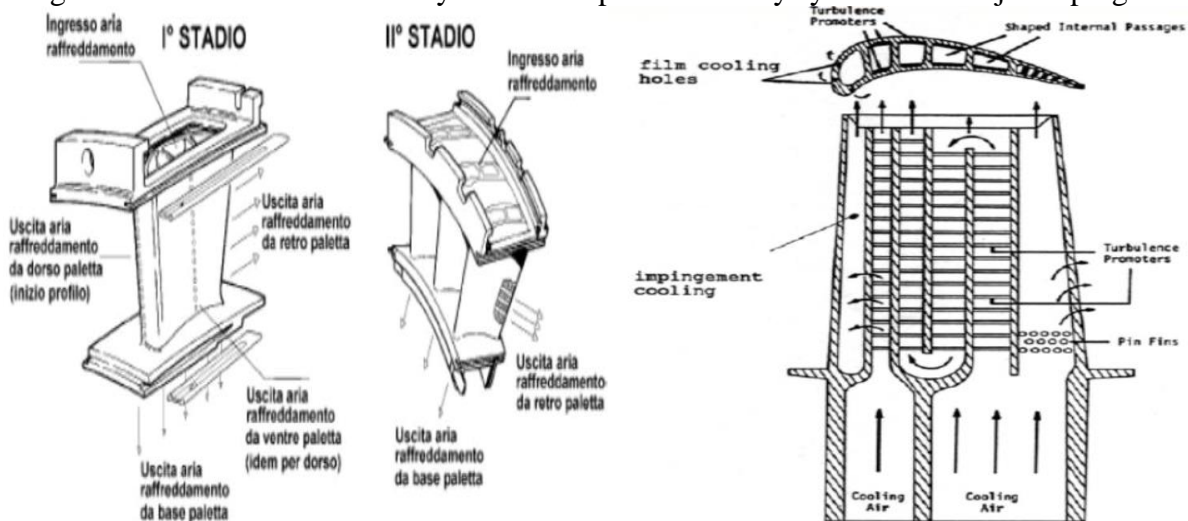


Fig. 1.10 - Examples of vane (left) and blade (right) cooling channels

The example in figure show the three main methods: the trailing edge part is cooled by internal convection, enhanced by turbulence promoters, the leading edge is instead cooled by a combination of film cooling and jet impingement. As visible in figure the internal path is very tricky, so the pressure losses are not negligible and the cooling air flows in a high pressure ambient: a relatively great pressure value must be necessarily guaranteed at the blade cooling channel inlet to ensure the driving pressure ratio necessary for the cooling flow rate.

The necessity of this coolant flow rate took to the birth of a 5<sup>th</sup> main component of a GT engine: the secondary air system. Different piping lines are used to supply the turbine blades with the coolant air in different locations: the extreme complexity of this pipe network integration, both mechanical and thermal, with the other components results a difficult task. The SAS system takes charge, not only of the distribution of the cooling flow rate along the turbine rows, but also of many different tasks that are summarized in paragraph 2.1.

#### **1.4 Energy market**

The structure of the electric energy generation portfolio in Italy has suffered deep changes in a very short temporal arc [6], accordingly to the ARERA [7] data, updated at the year 2017, collected below these changes regard essentially:

- The strong growth of renewable energies in the last 10 years, both in terms of installed power (45% in 2017 a front of 24% in 2004), both of production (35% circa in 2017, in front of 24% in 2004) and consequent reduction of the fossil sources incidence, mostly of the combustible oil, now almost unused (1% of the produced total in 2017). We also assist to an installed power decrease deriving from the disposal of the old thermoelectric plants, also the biggest ones, not fully compensated by the new installation of renewable energies fed plants (respect to 2015, reduction of 4.6 GW of traditional thermoelectric plants, in front of an increases of 1.7 GW from renewable sources)
- The correlated increase of the weight of random sources and in particular of solar and wind plants (respectively 25.1% of the installed power in 2017, in front of few more than 1% in 2014 and 14.5% circa of the produced in 2017 in front of few less than 1% in 2014)
- The weight increment of small size plants, prevalently connected to the distribution net. In 2015 the plants with a power inferior to 10MVA represented the 22.6% of the installed power: 18 percentage points circa more than in 2004. Their weight in terms of production is passed from 4.7% of 2004 to 17.8% of 2016, with a variation of 0.4TWh respect to 2015

In addition a reprise in the electric energy consumptions is happening: after having reached the minimum value (291 TWh) in 2014, also for the effect of the economic crisis, they recently have traced back to 302 TWh in 2017, remaining lower than the 2008 consumption of 319 TWh. Some thoughts about the renewable energy installation must be done:

- the renewable energy fed plants (particularly wind and photovoltaic solar) present variable costs null and high fixed costs
- the renewable energy fed plants are realized where the power source is available, not necessary where the electric energy is needed, and they produce when the source is available

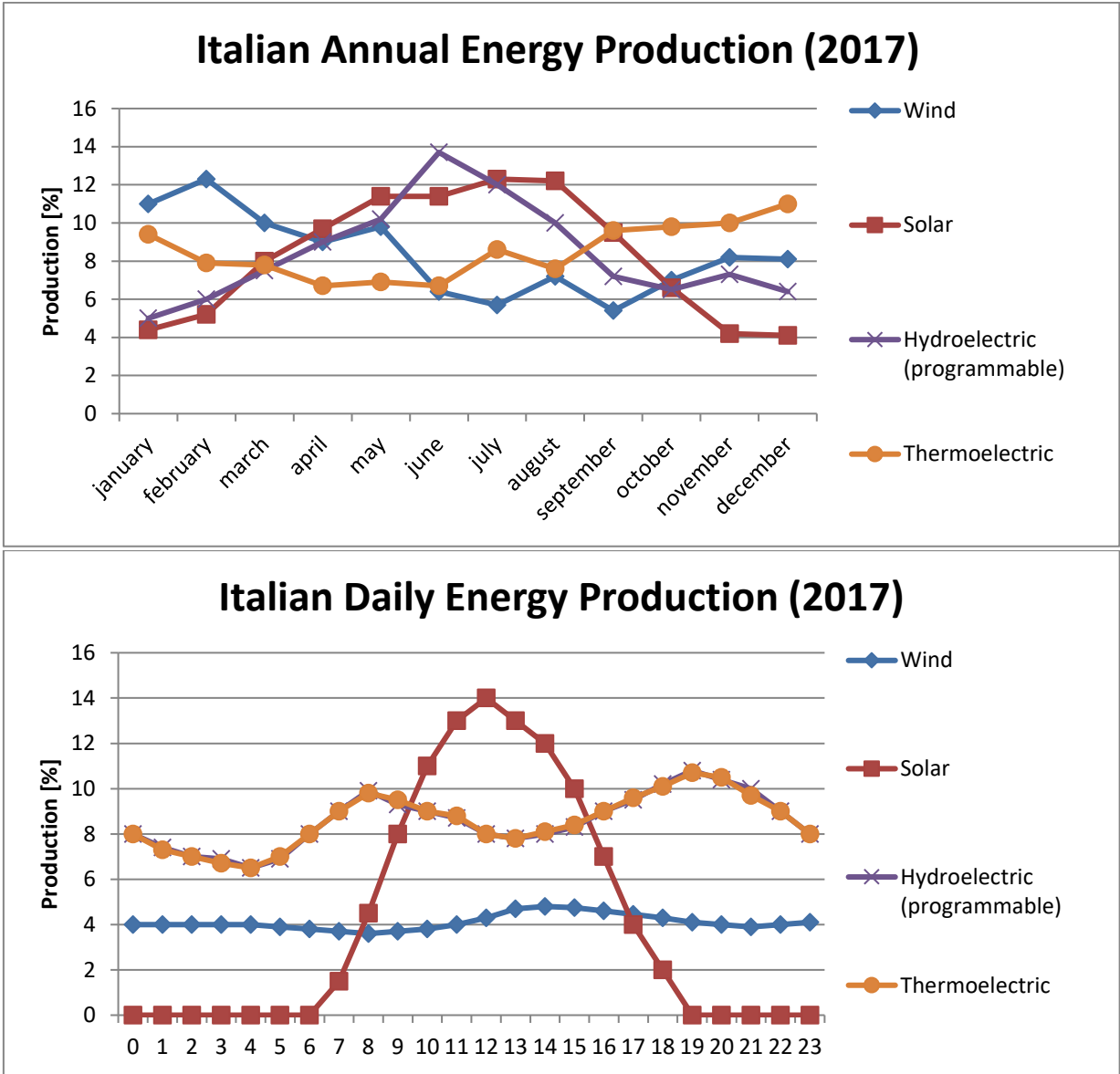


Fig. 1.11- Annual and daily Italian energy production

For example in the figures upon (Fig. 1.11) are reported the annual and daily production percentage of the total Italian energy production, divided per source and referred to the year 2017: it's clearly visible the seasonality and the great daily variation of energy production from the renewable sources such as the wind and the solar plants. Programmable energy plants such as the hydro basin and the thermoelectric are called to balance the net load request: because of this, the range of working conditions and the necessity of ramping capability requested to these plants has incredibly grown up.

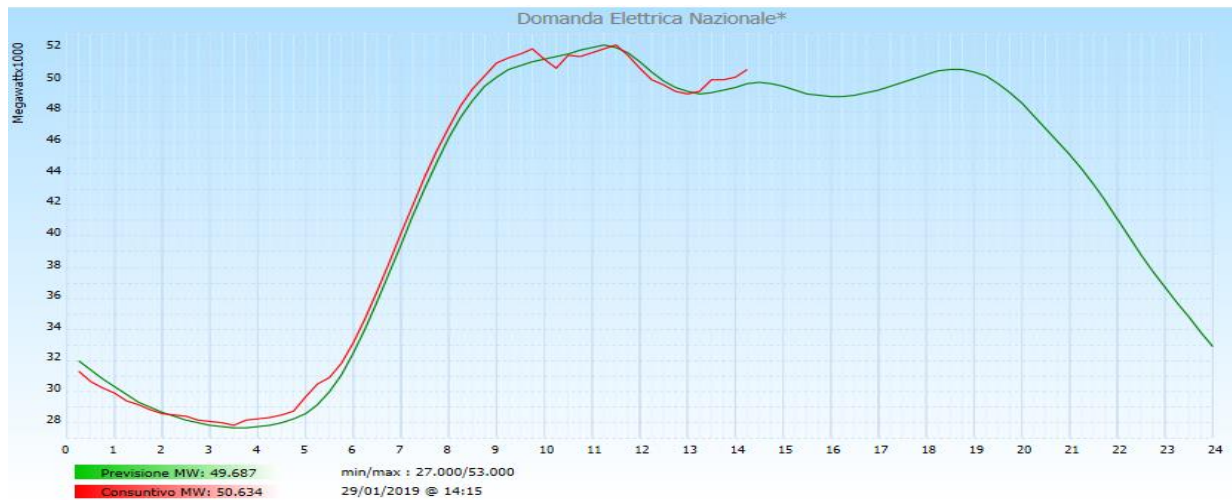
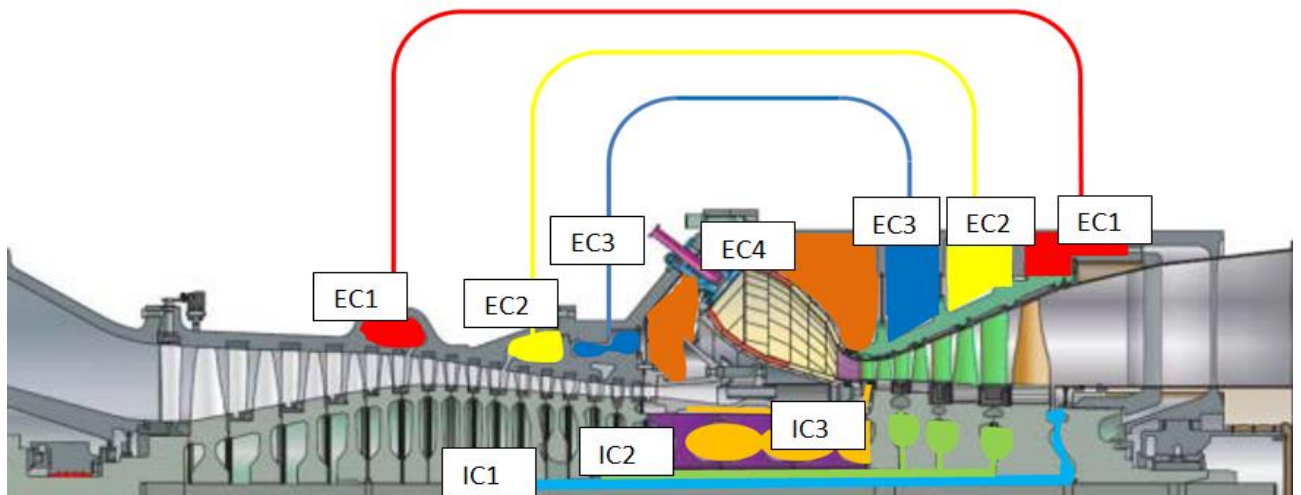


Fig 1.12 -Generic daily Italian energy request

In Fig. 1.12 the Italian electric request during a generic winter day is plotted[8], as visible, the request has a very inhomogeneous trend with valleys and peaks: because of the electric net nature, the main task of the regulatory body is to keep the power demand perfectly matched with the power produced, to avoid harmful fluctuations of the value of frequency and voltage of the electric net. To guarantee the power balance in every zone of the net and in every moment, the thermoelectric plants are called to vary their level of energy production: gas turbine powered plants do not cover anymore the base load but have to adapt their load to the net request. Power market evolution is heavily impacting thermal generation: the historical design guidelines have changed, chasing the market requests, giving precedence to values such as load factor reduction, number of start-up increase, with a direct effect on the profitability of these assets, often leading to hibernation or closure of these plants. These new design targets can lead to ancillary services revenues: ancillary services are all services which support elementary functions of electric power system such as the network frequency control or the reactive power and voltage control. The gas turbine engine behaviour knowledge in off-design conditions is nowadays a fundamental step to define the entire machine life cycle: from the product placement in the offer scenario, to the maintenance, to the performance optimization. The increase in flexibility is also reached broadening the permissible load range: criticalities in pollutant creation appear both at minimum load both at base load: when the engine operates close to its turndown load the compressor airflow is so high, compared to the fuel airflow, that the heat released by the flame cannot properly support the conversion of  $CO$  into  $CO_2$ . In such a condition, the power plant could not comply with the environmental legislation and must be operated at a higher load (minimum environmental load or MEL) or, worse, shut down. Another pollution problem comes from the  $NO_x$  production: the main  $NO_x$  production mechanism is the thermal one that happens in the zones with high fuel concentration and high temperatures, where the molecular nitrogen triple bond is broken and the high concentration of molecular oxygen enhance the  $NO_x$  combination. These conditions happen both at reduced loads, where the diffusive combustion mechanism is predominant respect to the premixed one, with the resulting generation of high temperature hotspots, both at base load, where the request of power is satisfied by the high fuel-air equivalence ratio in combustion chamber, with an increase in temperatures.

## 2. Gas Turbine Secondary Air System

The totality of the air flow of a gas turbine which does not take part in the useful work production is called Secondary Air System (SAS). This air is used to perform various tasks: cooling of the static and rotating components, sealing, clearance control and axial thrust control. All the components in the turbine and combustion chamber zones must be kept at a temperature below the material maximum allowable limit to prevent any damage of the machine and to avoid any hot gas ingestion. The air mass flow rate necessary to guarantee the SAS objectives is bled from the compressor flow path and is injected in the turbine flow path and in the CC shells: the air injected in the turbine flow path mixes with the hot gases so it's still possible to extract work from this flow rate in the turbine stages downstream the air injection and mixing location. The net work obtainable from this flow rate is quite low because the air extracted from the compressor is not subjected to the enthalpy increasing in CC and the compression work is not negligible: extracting the flow rate from the first stages of the operating machine is an effective way to reduce the negative impact on the global machine. The first engines that implemented the SAS network took all the air from the compressor's OGV exit, where air is at its maximum level of pressure and temperature: this air was used to supply both the high pressure components both the low pressure ones but this design took to heavy energy losses, mostly in turbulent energy dissipation, and to heavy leakage flow rates due to the great pressure ratio between the OGV and the last stages of the turbine. In the modern engines, different internal and external extraction lines for blades and vanes are located along the compressor flow path: this mass flow rate is at a level of temperature and pressure lower than the compressor discharge. In this configuration the negative compression power is lower and the coolant temperature is lower, enhancing the cooling effectiveness. The energy loss minimization is still subordinated to the necessity of the sealing and cooling requisites: the pressure ratio between the blade root and main channel must remain in a safety range, given from the blade internal flow characteristic, in every possible working condition. In addition, for the common used duct geometry, a great pressure ratio would also lead the flow to high Mach numbers, and to possible choking conditions: besides the problems that an high speed flow would generate (greater pressure drops, high turbulences, vibrations of the structural components), the control over the flow by the blade internal flow characteristic would not be effective, with problems in the engine off design.



*Fig. 2.1 - Example of a GT engine SAS lines*

## **2.1 Secondary air system main objectives**

An example of SAS lines design is pictured in Figure 11: it's common design to supply the blades and the vanes with different piping lines fitted both at the external of the turbine casing, both inside the turbine rotor, but the final design is a choice of the engine manufacturer. In this thesis application a simplified nomenclature has been used to refer to these lines: the main division is between the external circuits (ECX) and internal circuits (ICX), with the value X representing the order of the circuit seen from the compressor flow path, in the specific engine (Figure 2.1) there are 3 external lines and 2 internal lines in the compressor flow path and 1 external line coming from the compressor diffuser. From this simplified basic scheme, and consequently to the design philosophy chosen from the engine constructor, the external lines may be equipped with additional components such as regulating butterfly valves or cooling systems. Hereafter a short summary of the SAS main tasks are reported to permit a deeper comprehension of this thesis main job [9].

### **2.1.1 Turbine Blade Cooling**

Turbine blades are cooled by a combination of film and convection cooling. The first stage blades are cooled by a portion of air bled off from the main flow at the end of the compressor to guarantee the maximum possible pressure ratio to the blades. Furthermore, in modern gas turbines, one or many more additional flows may be fitted inside the rotor to supply the cooling air for other rotating stages. The cooling air for the turbine blades of stages 2, 3 and 4 in the example of Fig. 2.1, is extracted respectively from IC2 and IC3 and then led through two different passages in the central hollow shaft. In any case, the cooling air is driven, by centrifugal and pressure force, towards the cavities between the turbine rotor disks, to reach, through radial bores, the rotor cascades. Cooling air, which enters in the hot gas main stream, envelops the rotor hub in a film of air.

### **2.1.2 Turbine Vane Cooling**

Turbine vanes use both impingement, film and convection cooling. The cooling air for the first stage vanes and blades is directly extracted at the diffuser exit, where the pressure is at its maximum level. The outer extraction lines feed three different chambers contained between the rear outer casing and the turbine stationary vane carrier and then supplied at the vane roots.

Typically the external lines, for space requirements, are the only lines that can be equipped with the regulating butterfly lines that maintain a specific pressure ratio between turbine chamber pressure and compressor end pressure: this control allows the adjustment of the pressure ratio across the internal cooling circuits of vanes and then the consumption of cooling air, with good results in terms of regulations and flexibility.

### 2.1.3 Turbine sealing system

The term sealing includes whatever devices, mechanical or fluid dynamics, used to divide zones with different pressures, minimizing the mass leakages: due to cost reduction purposes the valuable materials are used only in specific components such as combustion chamber tiles or turbine blades. Parts, like the rotor disks, are made by cheaper materials that don't guarantee adequate performances in aggressive environments and, because of this, need to be protected from the hot gases interaction: to perform this task, part of the bled air is used to purge the hot gases away from these materials, separating the two zones through a fluid barrier (Fig. 2.2) [10].

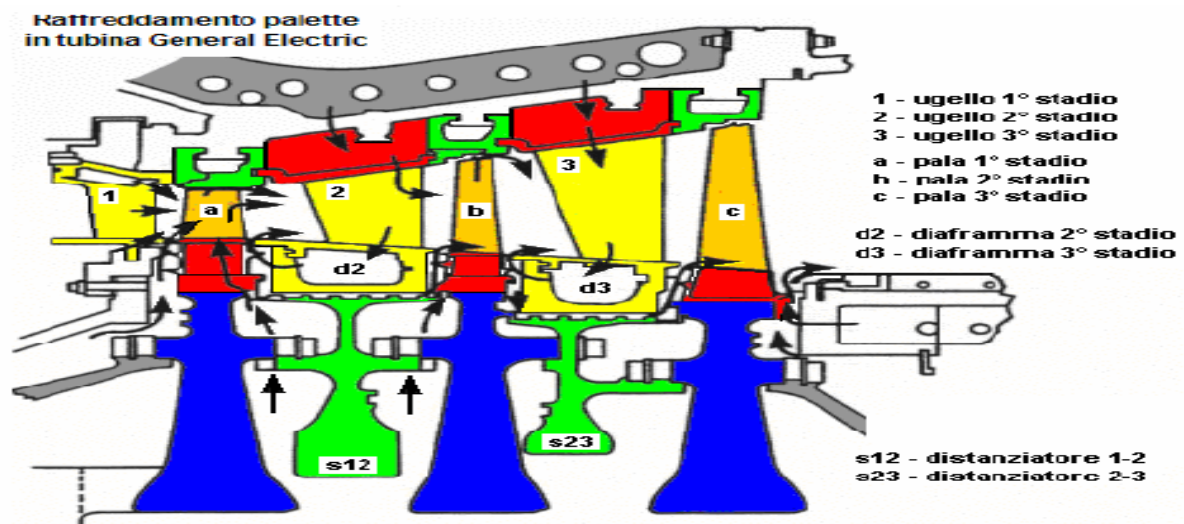


Fig.2.2 - Example of SAS turbine displacement

The efficiency of the turbine depends in part on the radial clearance or gap between the rotor disk assembly and a sealing structure of the adjacent stationary assembly. If the clearance is too large, excessive valuable cooling air will leak through the gap between the rotor shank and the inner shroud of the stationary blade, decreasing the turbine's efficiency. If the clearance is too small, the blade tip will strike the sealing structure of the adjacent stator portions during certain turbine operating conditions. In this regard, it is known that there are clearance changes during periods of acceleration or deceleration due to changing centrifugal forces on the buckets, due to turbine rotor vibration, and due to relative thermal growth between the rotating rotor and the stationary assembly. During periods of differential centrifugal force, rotor vibration, and thermal growth, the clearance changes can result in severe rubbing of, for example, the moving rotor tips against the stationary seal structures. Increasing the tip to seal clearance gap reduces the damage due to metal to metal rubbing, but the increase in clearance results in efficiency loss. Clearance control devices, such as abradable seals, have been proposed in the past to accommodate rotor-to-casing clearance change. This protection feature, applied to the rotating or stationary component tips, allows the designer to decrease the cold built clearances of the

turbine or engine, which decreases unwanted leakage, thus improving the performance and efficiency of the turbine or engine. The abradable seal or coating is typically applied to the stationary components, with a seal segments machined into and/or caulked into the rotor assembly. Labyrinth seals (Fig. 2.3) are mechanical seals that provide a tortuous path to prevent leakage. A labyrinth seal may be composed of many grooves that press tightly inside another axle, or inside a hole, so that the fluid has to pass through a long and difficult path to escape. These interlock, to produce the long characteristic path which slows leakage. For labyrinth seals on a rotating shaft, a very small clearance must exist between the tips of the labyrinth threads and the running surface. The pressure drop on every fin reduces the mass flow leakage. Brush seals are made of a fixed ring with thin metallic brushes that rub on a ceramic report that covers the shaft, and can be easily installed in combination together with a labyrinth seal (Fig. 2.3).

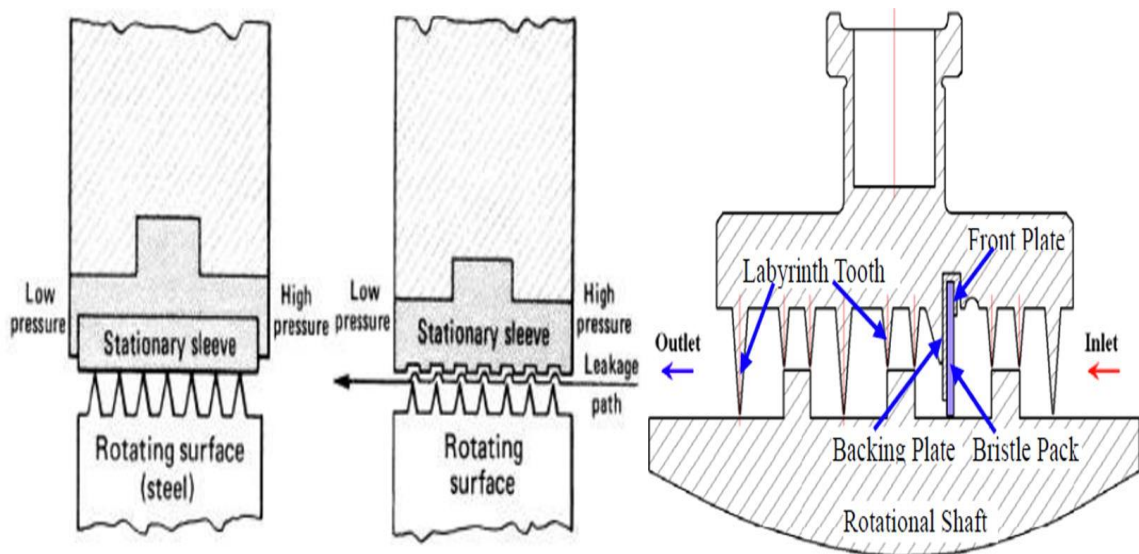
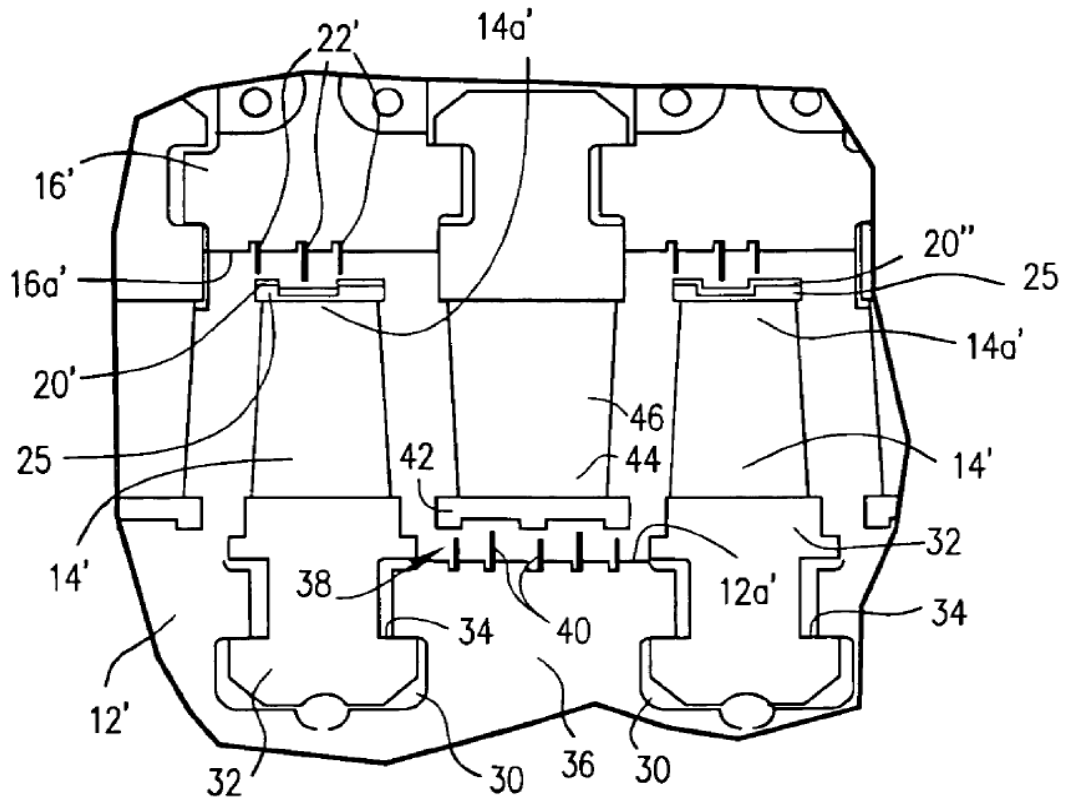
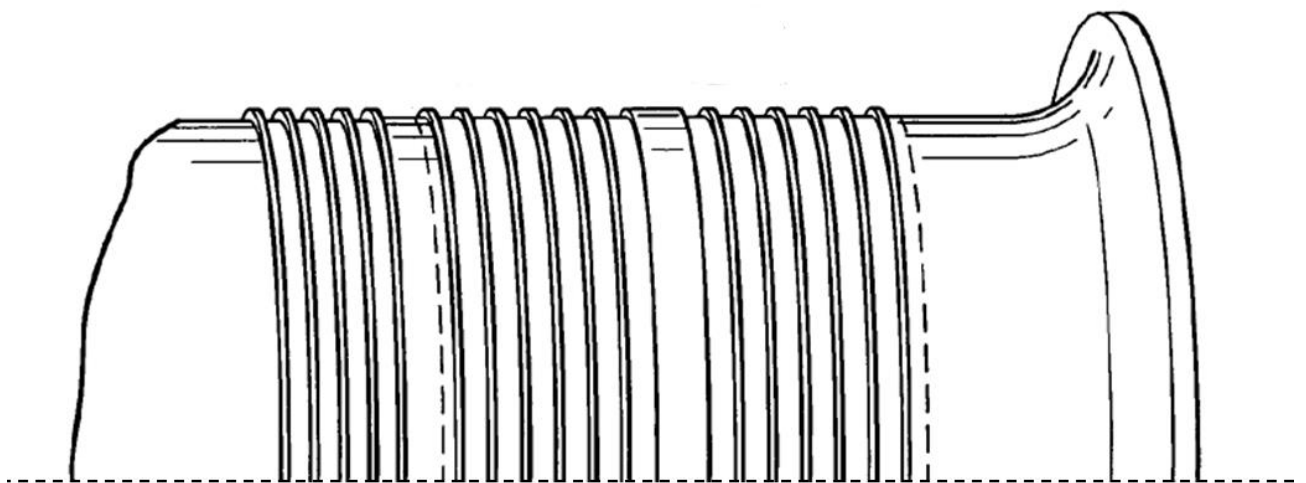


Fig. 2.3 - Example of labyrinth seal (left) and labyrinth seal with brush seal (right)



*Fig. 2.4 - Generic sealing displacement*



*Fig. 2.5 - General shaft sealing*

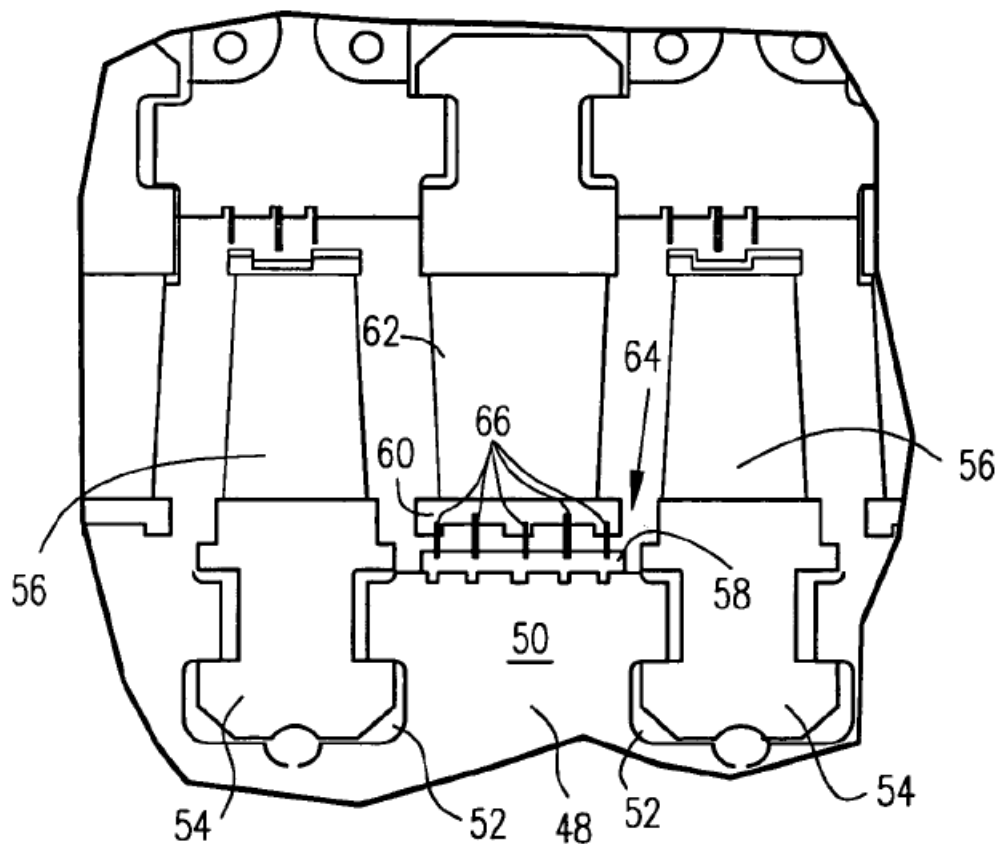


*Fig. 2.6 - Generic sealing displacement*

Figures 2.4, 2.5 and 2.6 show the application of both the strip seal and the abradable coating in 2 different configurations: in the 1<sup>st</sup> one (figures 2.4 and 2.5) the abradable coating is applied to the blade tips (20') and the knife edged strip are machined on the rotating shaft (40 and Figure 2.5); while the 2<sup>nd</sup> configurations (figure 2.6) shows the abradable sealing applied both on the blade tips and to the rotating shaft (58). Other leakage-reduction systems consist in extrusions, called seal plate fins of angel wings, applied on both the rotoric and statoric assemblies that extend axially in the stator-rotor cavity, overlapping and generating a shrinkage in the gap, with a consequent concentrated pressure drop, limiting the leakage flow rate.

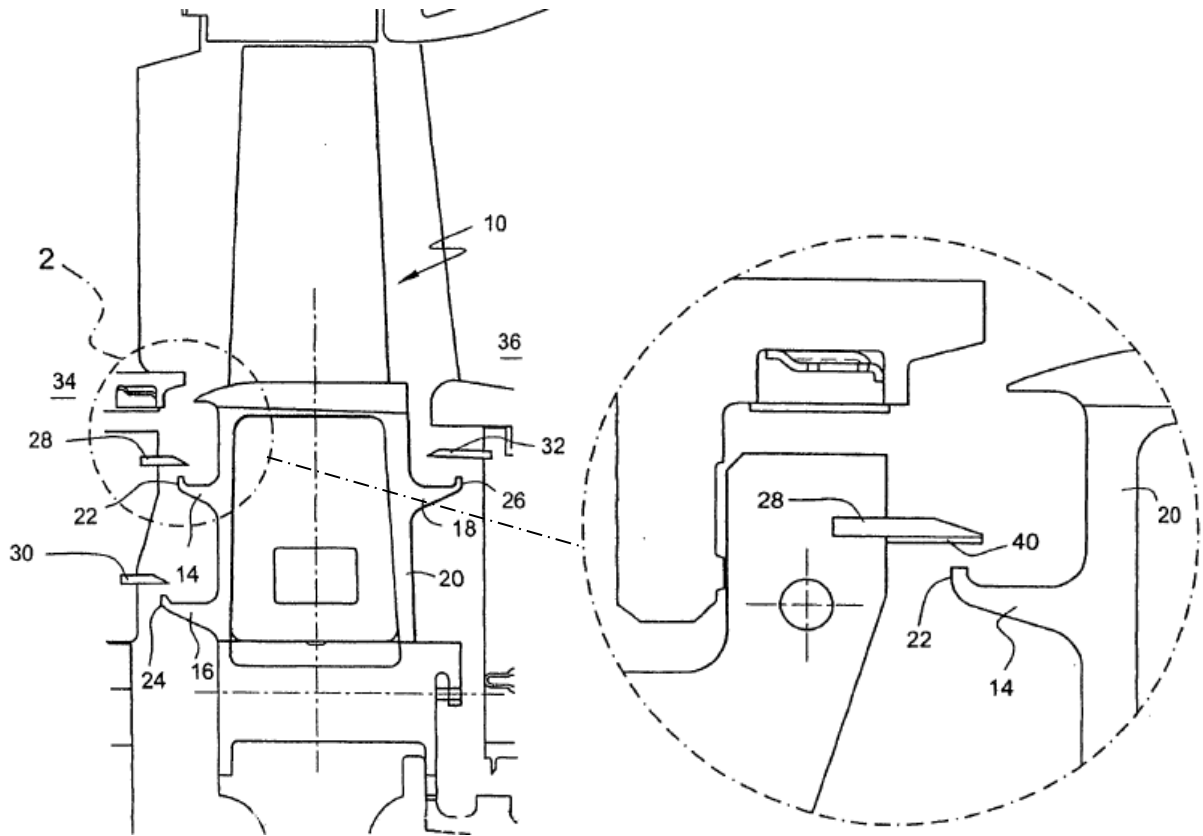


*Fig. 2.7 - Generic displacement of seal plates*

Ring seals are used in gas turbines to separate different extraction pockets in the turbine casing: they are made of a series of metallic rings placed in appropriate channels, housed in the casing. This configuration allows to obtain reduced clearances respect to the labyrinth seal because the rings can adapt to dilatations and deformations of the shaft moving themselves in the housings. Due to the great requested flexibility and ramping capability the clearances must be optimized also for the transients, with thermal dilatations different from the steady ones, avoiding labyrinth seals scrapings on the rotor, and guaranteeing sealing performances also if the teeth relative positions from opposite rows changes for the axial dilatations. Turbine wheel spaces are made of two stator-rotor cavities connected by a labyrinth seal against the seal-ring inner radius (Fig. 2.8). The pressure difference across labyrinth seals and the radial clearance define the amount of sealing air to the downstream cavity. Many GT engines use a relatively softer material fastened on the rotating components that are sacrificed, in case of creeping, to avoid consumption of the nobler material. Sealing air, coming from the same secondary air passages used for blade and vane cooling, flows through the vanes towards the seal-ring. Thus, the main portion of sealing air is led in the lower region of the cavity through cooling holes drilled in the vane shroud-ring. The other portion of air comes through the fir-tree of upstream rotating stage. Note that temperature of sealing air, after passing through the vane, is higher than temperature at the extraction point.

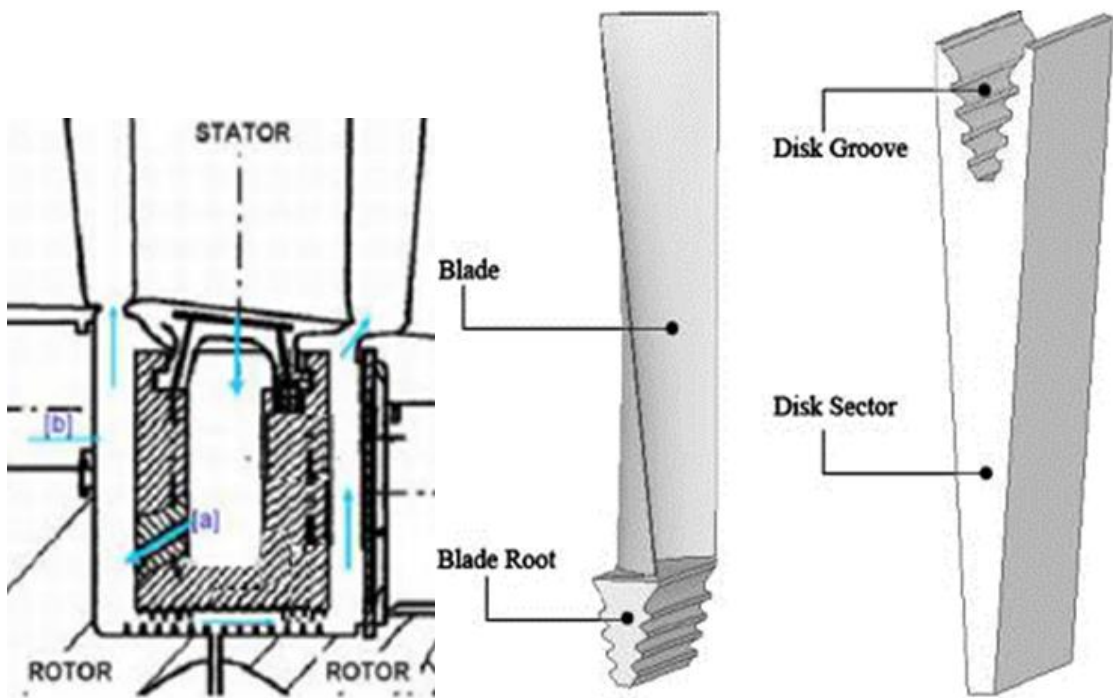


*Fig. 2.8 - Vane hub box with sealing hole (left) and blade mounting (right)*

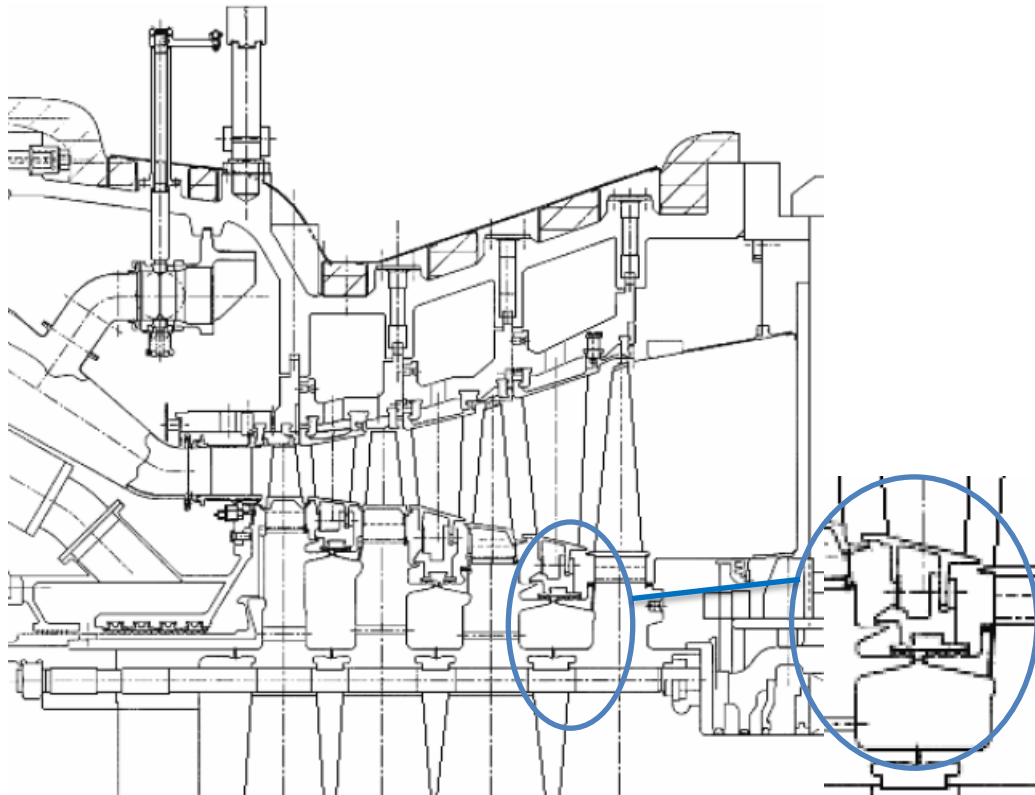


*Fig. 2.9 - Example of the hub vane sealing*

### 2.1.4 Rotor Axial Thrust Balance

The pressure gradient between the 2 sides of the compressor and turbine blades generate, beyond the tangential force used to extract power from the machine, an axial directed force that must be countered to keep the engine still in place. Due to the higher mechanical power associated to the turbine, relatively to the compressor, the axial forces result unbalanced generating a net axial force, called rotor axial thrust, that needs to be countered. Also the SAS system contributes to the overall axial thrust because the pressure difference applied to both side of a static-rotating cavity, that also possibly lead to secondary flows [11].

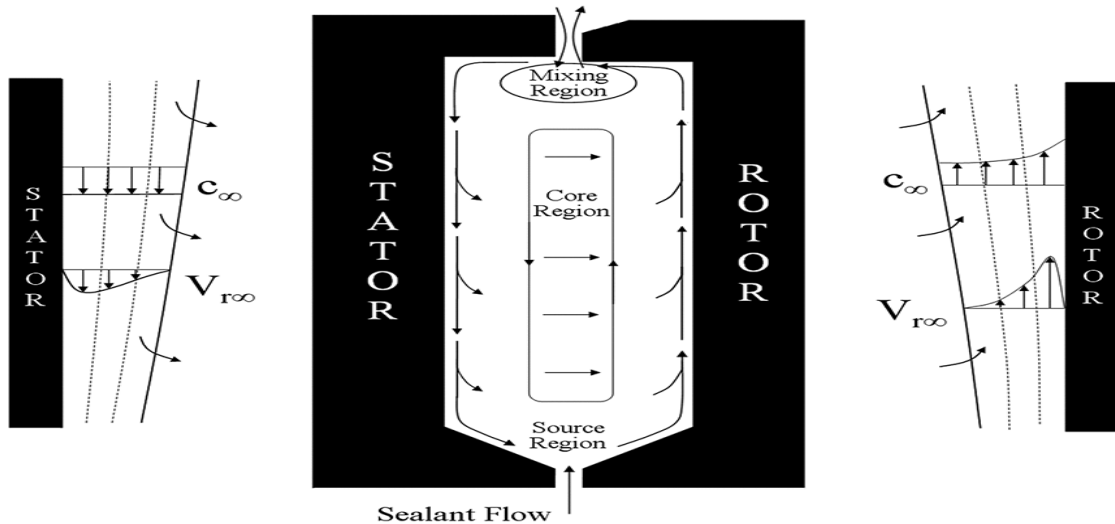


Fig. 2.10 - Fluid motion inside a stator-rotor cavity

Only a mechanical thrust bearing, designed to balance the entire engine thrust would be too big and expensive: in common design practice, to compensate the rotor axial thrust, part of the turbine is designed as a balancing piston. This balancing piston is essentially a surface subjected to a pressure gradient oriented against the rotor axial thrust (Fig. 2.11 and 2.12): the gradient of pressure applied to the surface generates a resulting force useful to counter the axial thrust, relieving the axial bearing of part of the load given by rotor thrust. The balancing piston may be modelled as a rotating surface contained in a static casing: the pressure gradient and the clearance present in the stator-rotor coupling inevitably lead to the necessity of an adequate sealing to ensure the proper pressure level of the thrust piston. Figure 19a shows an aircraft engine schematization, while Fig. 2.12 shows a centrifugal compressor application.

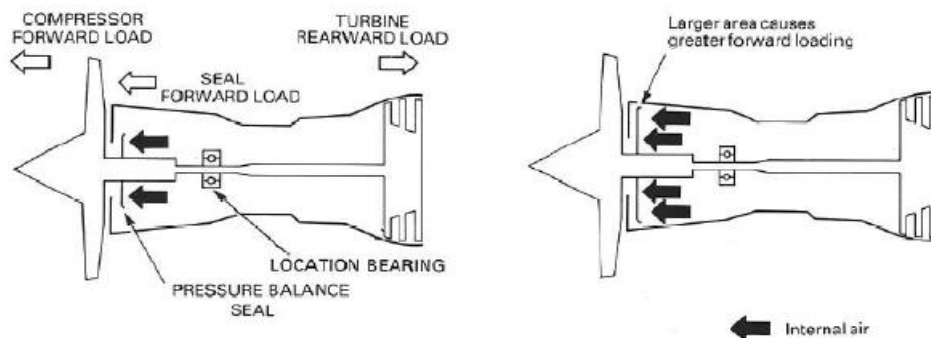
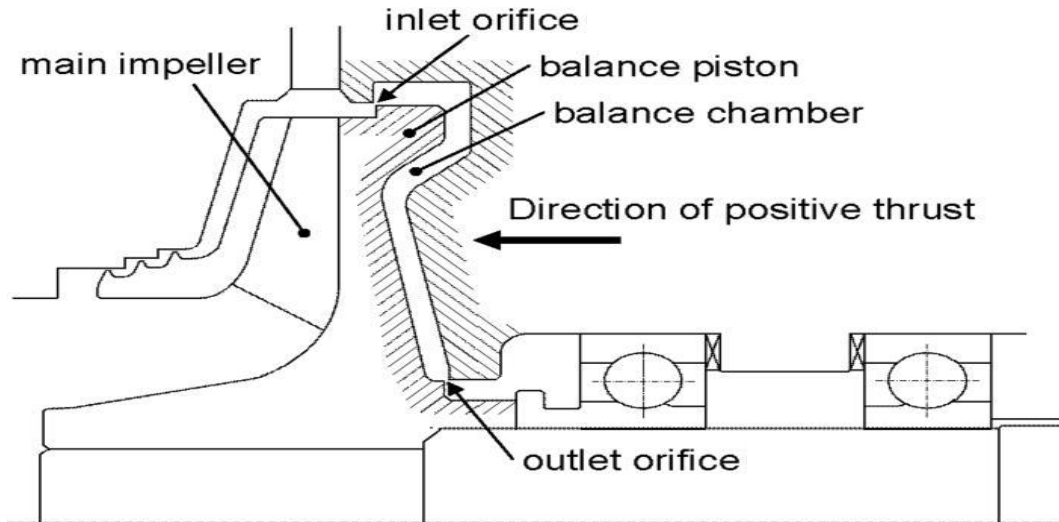


Fig. 2.11- Aeronautical balancing piston displacement



*Fig. 2.12 - centrifugal machine balancing piston displacement*

### 2.1.5 Passive clearance control

SAS air flow also enhance heat transfer in the machine, damping the thermal gradients and so the concentrated thermal stresses, that can lead the structure to an early fatigue collapse. For example the circulation of air through air passages warms and cools the rotor component from all the sides, guaranteeing rapid and more uniform temperature changes, compared to the only (mostly radial) conductive heat transfer, lower thermal stresses and a rapid approach of stationary conditions, therefore less blade rubbing and lower aerodynamic losses in radial clearances. Some concepts of F-class heavy-duty gas turbines are single-casing and single-shaft engines for which compressor and turbine sections have a common disk-type rotor held up by a pre-stressed central tie-rod. Rotor disks must be splinted together to permit the transmission of torque, in some case these disks are welded, in other radial facial serrations named as Hirth-couplings are used. The last rotor configuration permits rapid and uniform disk and tie-rod temperature changes, thanks to cooling flows and leakage air, which flows in the teeth gaps of Hirth-couplings, preventing thermal stress and rotor distortion during load changes and rapid starts.

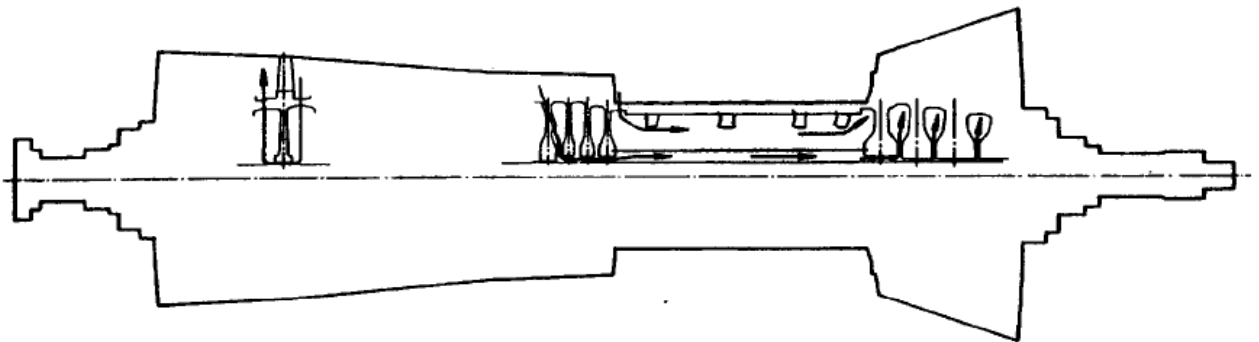


*Fig. 2.13 - Example of internal SAS line*

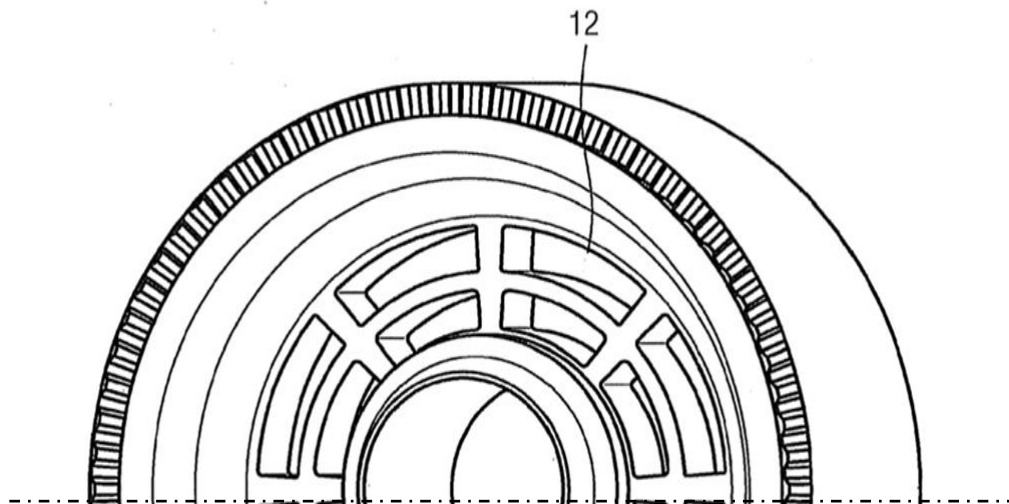


Fig. 2.14 - Example of turbine disk provided with Hirth couplings

### 2.1.6 Leakages

For production and mounting concerns every single blade is casted singularly and then assembled on a disk or a casing: the mounting inevitably will not be absolutely perfect, also to prevent any problem deriving from thermal dilatations, generating some gaps between the blade-blade couplings or between the blade-housing couplings: to minimize these gaps some mechanical devices are used, as visible in Fig. 2.15. The mass flow rate passing between these interfaces is generally called leakage and results difficult to forecast or to simulate also because the great variation of the gap values in different operating conditions.

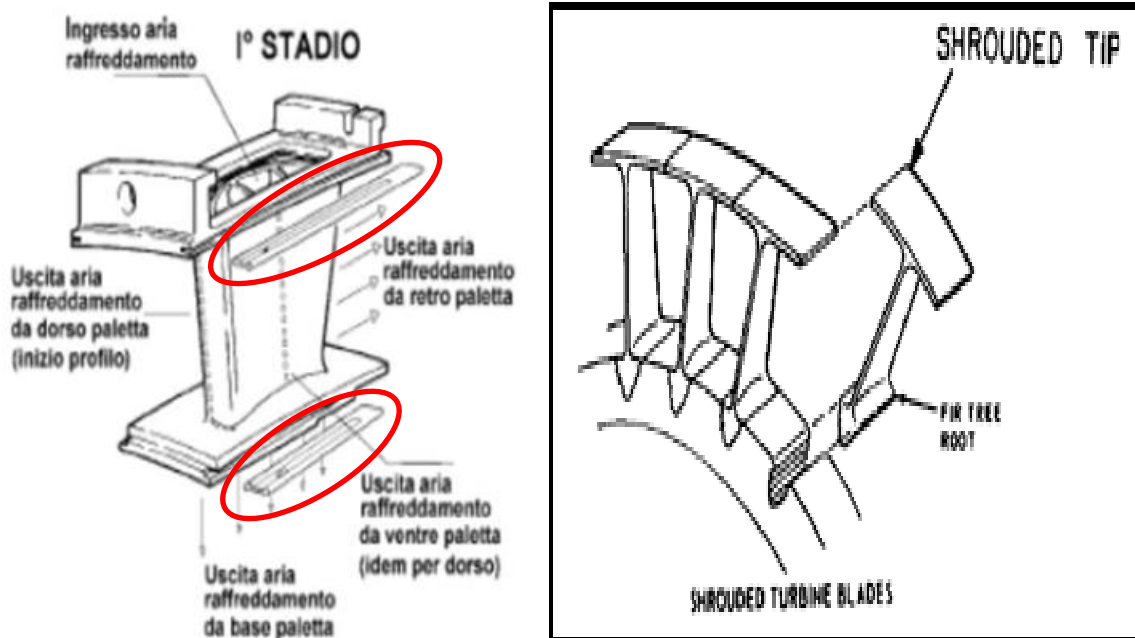


Fig. 2.15 - Details of mechanical solution for leakage reduction and blade mounting example

### 2.1.7 Optimal and robust SAS design

In the competitive modern energy market the gas turbine design cannot disregard an efficient and robust SAS implementation: the turbine will work in many different conditions and temperatures but the overall performance and safety must be always guaranteed. Many little tricks may lead to an overall efficiency increase:

- Optimization of the compressor bleeding extraction points reduces the energy losses (saving of expensive compressed air)
- The same mass flow may be used to fulfil many different SAS tasks: for example the turbine vane cooling flow may be used also to seal the cavity between vane and blades
- Adoption of Pre-swirl nozzles on the rotating circuit to decrease the pumping losses and lower the blade root total relative temperature with an increase of the cooling effectiveness
- Use of secondary air system to keep stable the flow in the combustion chamber to prevent pollutant creation: both CO at minimum load both NOx

But in the modern GT daily operating profile the efficiency must be pursued in a wide range of conditions, the design must be robust: a variation in any operational parameter must not lead to a fall in performances. To reach the robustness many design guide lines must be followed [12]:

- The turbine vanes and blades should work in the plateau zone of the cooling characteristic curve, to guarantee a fixed mass flow rate in case of pressure ratio variations and fluctuations (paragraph 4.7)
- The ratio between the turbine mass flow rate and the cooling mass flow rate should be kept constant by pressure regulation, if possible, e.g. the external lines with regulating butterfly valve
- Avoid choked pipes before the blades because the flow rate should be regulated by valves or by the blades' internal flow: compromises between the structural design and the low pressure losses must occur

The sizing of a machine must happen in the most demanding operating conditions: for the SAS circuit the operating points in Tab. 2.1 are crucial for design due to temperature level and/or the sufficient difference between tap pressure and turbine pressure to avoid backflows. The SAS circuit design is inherently linked to the compressor and turbine performances and because of this, a careful study of these components, in design and off design conditions, must be carried on to correctly project the SAS circuit.

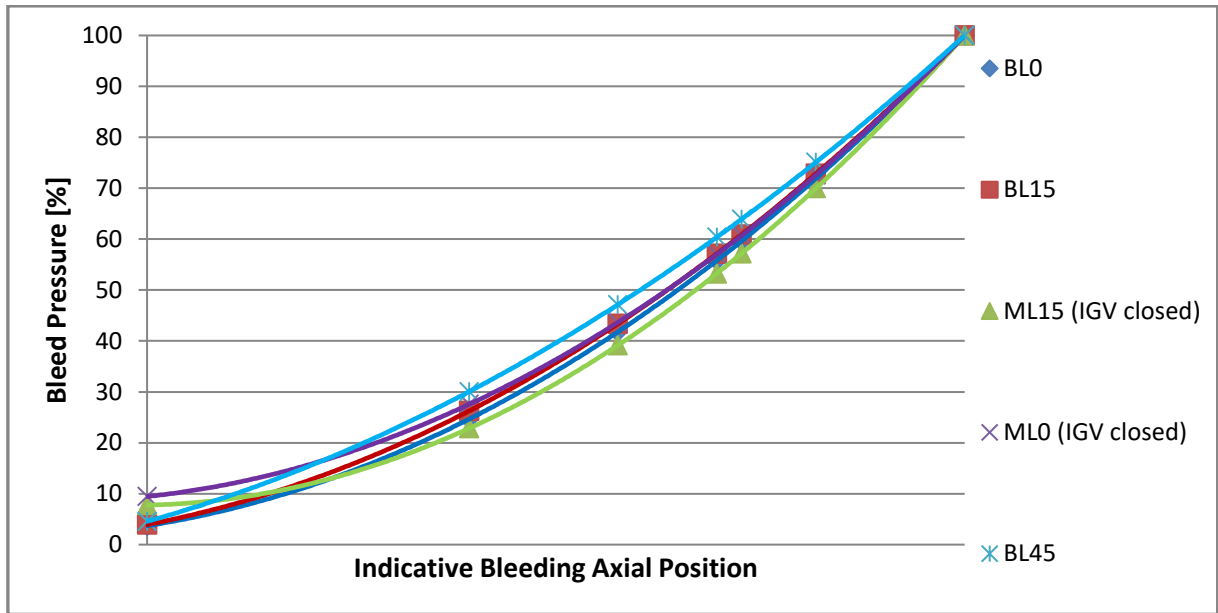


Fig. 2.16 - Compressor pressure trend along the axial direction in various working conditions

Tab. 2.1 - SAS critical conditions

-	Ambient Temperature [°C]	IGV [%]	Critical for
BL	+15	100% (load)	SAS optimization
ML	0	Closed (load)	3 <sup>rd</sup> vane, 2 <sup>nd</sup> blade
BL	0	100% (load)	Bearing casings, 4 <sup>th</sup> stage

Fig 2.16 shows an example of pressure, referred to the compressor exit pressure, at the indicative bleed points on the compressor side including the operating points on Tab. 2.1 and the standard calculations used to verify compressor operating: the nomenclature reports the operating point (base load BL or minimum load ML) followed by the ambient temperature in Celsius degrees. Note that the pressure levels at the extraction points EC2, IC1, EC3 AND IC2 suffer variations of more than 10% from part load (with fully-closed position of IGV) at low ambient temperature and base load at high temperature. Such variations can be reduced, only for vanes, by the control valves on the external lines.

From the expander analysis several effects may be observed:

- The static pressure in the turbine flow path, expressed in percent of the compressor outlet pressure, is quite constant in the entire operating range. If the cooling supply pressure remains constant, the pressure ratio across the cooling circuit and the constant reduced mass flow of cooling air will be constant
- Supply pressure of cooling system of first vane leading edge is slightly higher than compressor discharge pressure calculated at the exit of the diffuser, since cooling air is bled off just close to the exit of OGV (Fig. 2.1)
- It is clear the importance of the control system of the external bleed lines, which maintains constant the supply pressure at a given ratio of the compressor discharge pressure; whereas the rows downstream the 2<sup>nd</sup> vane suffer strong variations of cooling pressure. Such variation is negligible for the 1<sup>st</sup> stage, since it is supplied at the discharge of the compressor

## 3. Secondary Air System Numerical Integration

### 3.1 Secondary Air System network solver

The 3D CFD analysis of the entire SAS circuit is not compatible with the modern design procedure time scheduling, nor it would be justifiable because the degree of uncertainty of the boundary conditions assumptions. Generally the use of a 0D network satisfies the common design needs of evaluating many engine configurations or conditions in reasonably short time: in a market focused on the flexibility, the same time required by a complete 3D CFD study of 1 operating condition may be used to evaluate many different conditions using a 0D network giving a deeper analysis of the. In the 0D approach the SAS is schematized as a fluid network where many components are represented by as many models, in each of which the classic equations of continuity, momentum and energy conservation are solved [13]: 3D complex phenomena must be modelled with experimental correlations. Every element, or block, is linked to one or more block via a node, characterized by pressure and temperature. The modular 0D code allows modelling the bleed lines from the compressor extraction points to the hot gas section of the turbine meridian channel. Network components are graphically connected together by means of a bus data, linking their input/output ports to shape the entire cooling/sealing system of the gas turbine. Inlet boundary elements of the network model give the thermodynamic conditions (pressure and temperature from the compressor calculation) at the compressor extraction points. Outlet boundary elements are, respectively:

- modules for the leakage flows through roots
- modules for the cooling flows at stationary and rotating blades
- modules for stator-rotor cavities

Leakage and sealing flows are calculated by lumped-parameter loss-elements using as boundary condition the local static pressure calculated by CFD calculation of turbine rows. Cooling flows are calculated by a special network element CHARACTERISTIC, using as data inputs the blade root static pressure and the thermodynamic conditions of hot gas flow at the exit of cooling circuit. For this particular application the open source software CalculiX has been chosen as a base to develop a simplified 0D network solver.

### 3.2 CalculiX

CalculiX (CCX) is a free and open source finite element analysis application, developed by MTU Aero Engines which granted the publication. This software already have implemented a series of fluid network elements, which has been extended to adapt it for the gas turbine engine application. The software is based on a combination of many programming languages, to describe the element's physics, and an implementation of the root finding Newton Raphson algorithm as solver. The solver can handle linear and non-linear calculations: the applications of the software can range from the static and dynamic structural analysis to the steady thermal fluid dynamic problem. This wide pool of applications allows a Multiphysics structural-fluid dynamic approach: for example gas turbine clearances could be calculated together with the fluid dynamic analysis in a similar way to the turbine blade and vane cooling approach [14].

### 3.2.1 Newton-Raphson scheme

Newton's method, also called the Newton-Raphson method, is a root-finding algorithm that uses the first few terms of the Taylor series of a function  $f(x)$  in the vicinity of a suspected root. Newton's method is sometimes also known as Newton's iteration, although in this work the latter term is reserved to the application of Newton's method for computing square roots. Methods such as the bisection method and the false position method of finding roots of a nonlinear equation  $f(x) = 0$  require bracketing of the root by two guess values. Such methods are called bracketing methods. These methods are always convergent when a single solution exists since they are based on reducing the interval between the two guesses so as to zero in on the root of the equation. In the Newton-Raphson method, the root is not bracketed: in fact, only one initial guess of the root is needed to get the iterative process started to find the root of an equation. The method hence falls in the category of open methods. Convergence in open methods is not guaranteed but if the method does converge, it does so much faster than the bracketing methods [15].

The Taylor series of  $f(x)$  about the point  $x = x_0 + \varepsilon$  is given by

$$f(x_0 + \varepsilon) = f(x_0) + f'(x_0)\varepsilon + \frac{1}{2}f''(x_0)\varepsilon^2 + \dots \quad ((3.1))$$

Keeping terms only to first order,

$$f(x_0 + \varepsilon) \approx f(x_0) + f'(x_0)\varepsilon \quad ((3.2))$$

Equation (3.2) is the equation of the tangent line to the curve at  $(x_0, f(x_0))$ , so  $(x_1, 0)$  is the place where that tangent line intersects the  $x$ -axis. A graph can therefore give a good intuitive idea of why Newton's method works at a well-chosen starting point and why it might diverge with a poorly-chosen starting point.

This expression above can be used to estimate the amount of offset  $\varepsilon$  needed to land closer to the root starting from an initial guess  $x_0$ . Setting  $f(x_0 + \varepsilon) = 0$  and solving (3.2) for  $\varepsilon \equiv \varepsilon_0$  gives

$$\varepsilon_0 = -\frac{f(x_0)}{f'(x_0)} \quad ((3.3))$$

which is the first-order adjustment to the root's position. By letting  $x_1 = x_0 + \varepsilon_0$ , calculating a new  $\varepsilon_1$ , and so on, the process can be repeated until it converges to a fixed point (which is precisely a root) using

$$\varepsilon_n = -\frac{f(x_n)}{f'(x_n)} \quad ((3.4))$$

Unfortunately, this procedure can be unstable near a horizontal asymptote or a local extremum. However, with a good initial choice of the root's position, the algorithm can be applied iteratively to obtain

$$x_{n+1} = x_n + \Delta x_n = x_n - \frac{f(x_n)}{f'(x_n)} \quad ((3.5))$$

for  $n=1, 2, 3, \dots$ . An initial point  $x_0$  that provides safe convergence of Newton's method is called an approximate zero.

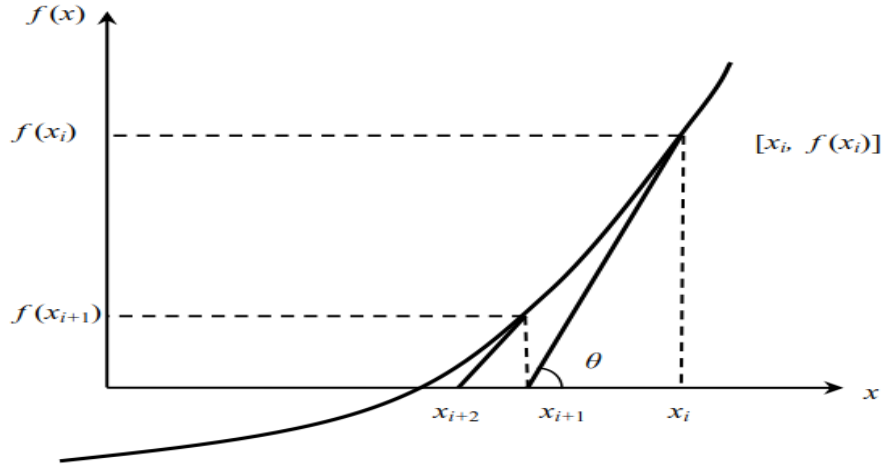


Fig. 3.1 - Newton-Raphson first iterations

Assume that Newton's iteration  $x_{k+1}$  converges toward  $x^*$  with  $f'(x^*) \neq 0$ , and define the error after the  $k^{\text{th}}$  step by

$$x_k = x^* + \varepsilon_k \quad (3.6)$$

Expanding  $f(x_k)$  about  $x^*$  gives

$$f(x_k) = f(x^*) + f'(x^*)\varepsilon_k + \frac{1}{2}f''(x^*)\varepsilon_k^2 + \dots \quad (3.7)$$

$$= f'(x^*)\varepsilon_k + \frac{1}{2}f''(x^*)\varepsilon_k^2 + \dots \quad (3.8)$$

$$f'(x_k) = f'(x^*) + f''(x^*)\varepsilon_k + \dots \quad (3.9)$$

But

$$\varepsilon_{k+1} = \varepsilon_k + (x_{k+1} - x_k) \quad (3.10)$$

$$= \varepsilon_k - \frac{f(x_k)}{f'(x_k)} \quad (3.11)$$

$$\approx \varepsilon_k - \frac{f'(x^*)\varepsilon_k + \frac{1}{2}f''(x^*)\varepsilon_k^2}{f'(x^*) + f''(x^*)\varepsilon_k} \quad (3.12)$$

Taking the second-order expansion

$$\frac{a\varepsilon + \frac{1}{2}b\varepsilon^2 + c\varepsilon^3}{a + b\varepsilon + c\varepsilon^2} \approx \varepsilon - \frac{b}{2a}\varepsilon^2 \quad (3.13)$$

gives

$$\varepsilon_{k+1} \approx \frac{f''(x^*)}{2f'(x^*)}\varepsilon_k^2 \quad (3.14)$$

Therefore, when the method converges, it does so quadratically.

The univariate Newton-Raphson discussed above can be generalized to solve an N-D multivariate equation system:

$$\begin{cases} f_1(x_1, \dots, x_N) = f_1(\mathbf{x}) = 0 \\ \dots \dots \\ f_N(x_1, \dots, x_N) = f_N(\mathbf{x}) = 0 \end{cases} \quad \text{or} \quad \mathbf{f}(\mathbf{x}) = \mathbf{0} \quad (3.15)$$

Where

$$\mathbf{x} = [x_1, \dots, x_N]^T, \quad f_i(x_1, \dots, x_N) = f_i(\mathbf{x}), \quad \mathbf{f}(\mathbf{x}) = [f_1(\mathbf{x}), \dots, f_N(\mathbf{x})]^T \quad (3.16)$$

Again, to solve this equation  $\mathbf{f}(\mathbf{x}) = \mathbf{0}$ , we first consider the Taylor series expansion of a ND function:

$$f_i(\mathbf{x}) = f_i(\mathbf{x}_0) + \sum_{j=1}^N \frac{\partial f_i(\mathbf{x}_0)}{\partial x_j} (x_j - x_{0j}) + r_i(\|\mathbf{x} - \mathbf{x}_0\|^2) \quad (i = 1, \dots, N) \quad (3.17)$$

Where  $r_i(\|\mathbf{x} - \mathbf{x}_0\|^2)$  represents second and higher order terms in the series beyond the linear term, which can be neglected if  $\|\mathbf{x} - \mathbf{x}_0\|$  is small. Now these equations can be written in vector form:

$$\begin{aligned} \mathbf{f}(\mathbf{x}) = \begin{bmatrix} f_1(\mathbf{x}) \\ \dots \\ f_N(\mathbf{x}) \end{bmatrix} &\approx \begin{bmatrix} f_1(\mathbf{x}_0) \\ \dots \\ f_N(\mathbf{x}_0) \end{bmatrix} + \begin{bmatrix} \frac{\partial f_1(\mathbf{x}_0)}{\partial x_1} & \dots & \frac{\partial f_1(\mathbf{x}_0)}{\partial x_N} \\ \vdots & \ddots & \vdots \\ \frac{\partial f_N(\mathbf{x}_0)}{\partial x_1} & \dots & \frac{\partial f_N(\mathbf{x}_0)}{\partial x_N} \end{bmatrix} \begin{bmatrix} x_1 - x_{01} \\ \dots \\ x_N - x_{0N} \end{bmatrix} \\ &= \mathbf{f}(\mathbf{x}_0) + \mathbf{J}(\mathbf{x}_0)(\mathbf{x} - \mathbf{x}_0) \end{aligned} \quad (3.18)$$

Where  $\mathbf{J}(\mathbf{x}_0)$  is an  $\mathbf{N} \times \mathbf{N}$  Jacobian matrix of  $\mathbf{f}(\mathbf{x})$  evaluated in  $\mathbf{x}_0$ .

If these functions are linear, then the second and higher order terms are zero, and the Taylor series contains only the first two terms (constant and linear terms). The approximation above becomes exact. To find the root  $\mathbf{x}^*$  at which  $\mathbf{f}(\mathbf{x}^*) = \mathbf{0}$ , we set the above function to zero  $\mathbf{f}(\mathbf{x}) = \mathbf{0}$ , and solve the resulting equation for  $\mathbf{x}$  to get

$$\mathbf{x}^* = \mathbf{x} = \mathbf{x}_0 - \mathbf{J}(\mathbf{x}_0)^{-1} \mathbf{f}(\mathbf{x}_0) \quad (3.19)$$

If the function  $\mathbf{f}(\mathbf{x})$  is not linear, the sum of the first two terms of the Taylor expansion is only an approximation of the function, and the resulting  $\mathbf{x}$  we found above is only an approximation of the root. However, we can improve this approximation iteratively from an initial value  $\mathbf{x}_0$ :

$$\mathbf{x}_{k+1} = \mathbf{x}_k - \mathbf{J}(\mathbf{x}_k)^{-1} \mathbf{f}(\mathbf{x}_k) = \mathbf{x}_k + \Delta \mathbf{x}_k \quad (3.20)$$

where:

$$\Delta \mathbf{x}_k = -\mathbf{J}(\mathbf{x}_k)^{-1} \mathbf{f}(\mathbf{x}_k) \quad (3.21)$$

is the search of Newton direction. The iteration moves  $\mathbf{x}_k$  in the ND space from an initial position  $\mathbf{x}_0$  along such a path that all functions  $f_i(\mathbf{x})$  ( $i = 1, \dots, N$ ) are reduced. Same as in the univariate case, a scaling factor  $\delta_k$  can be used to control the step size of the iteration

$$\mathbf{x}_{k+1} = \mathbf{x}_k + \delta_k \Delta \mathbf{x}_k = \mathbf{x}_k - \delta_k \mathbf{J}(\mathbf{x}_k)^{-1} \mathbf{f}(\mathbf{x}_k) \quad (3.22)$$

When  $\delta < 1$ , the step size becomes smaller and the convergence of the iterations is slower, however, we will have a better chance not to skip a solution, which may happen if  $f(x)$  is not smooth and the step size is too big.

### 3.2.2 Drawbacks of the Newton-Raphson Method

A deeper analysis of the Newton-Raphson method shows some criticalities: as expressed before, the residual (eq. 3.14) may tend to infinite when the 1<sup>st</sup> derivative tends to zero or when the 2<sup>nd</sup> derivative is very huge. When the function roots are near to maximum/minimum points ( $f'(x) = 0$ ) or great curvature points ( $f''(x) \gg 0$ ) the Newton-Raphson method may start diverging away from the root itself: it may then start converging back to the root but the iteration number necessary for converging grows rapidly, with an oscillation across the root. This sensibility to the 1<sup>st</sup> and 2<sup>nd</sup> derivative makes this algorithm very sensible to the initial root

guess, to the iterated value of the roots but also to the function's shape itself. For example, to find the root of the equation

$$f(x) = (x - 1)^3 + 0.512 = 0 \quad (3.23)$$

the Newton-Raphson method reduces to

$$x_{k+1} = x_k - \frac{(x_k^3 - 1) + 0.512}{3(x_k - 1)^2} \quad (3.24)$$

Starting with an initial guess of  $x_0 = 5$ , Tab. 3.1 shows the iterated values of the root of the equation. As you can observe, the root starts to diverge at Iteration 6 because the previous estimate of 0.92589 is close to the inflection point of  $x=1$  (the value of  $f'(x)$  is zero at the inflection point). Eventually, after 12 more iterations the root converges to the exact value of  $x = 0.2$ .

Tab. 3.1 - Example of the iteration flow of the tested function starting from  $x_0 = 5$

<i>Iteration number</i>	$x_i$	<i>Iteration number</i>	$x_i$
0	5	9	-8.2217
1	3.656	10	-5.1498
2	2.7465	11	-3.1044
3	2.1084	12	-1.7464
4	1.6	13	-0.85356
5	0.92589	14	-0.28538
6	-30.119	15	0.039784
7	-19.746	16	0.17475
8	-12.831	17	0.19924

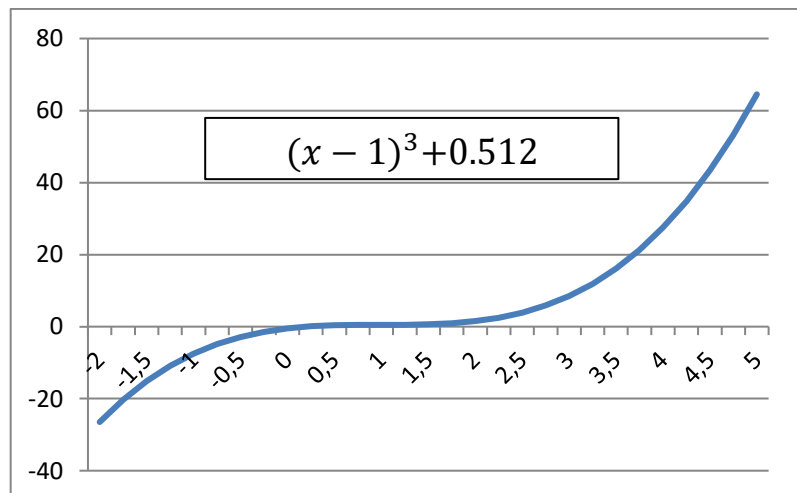


Fig. 3.2 - Plot of the tested function

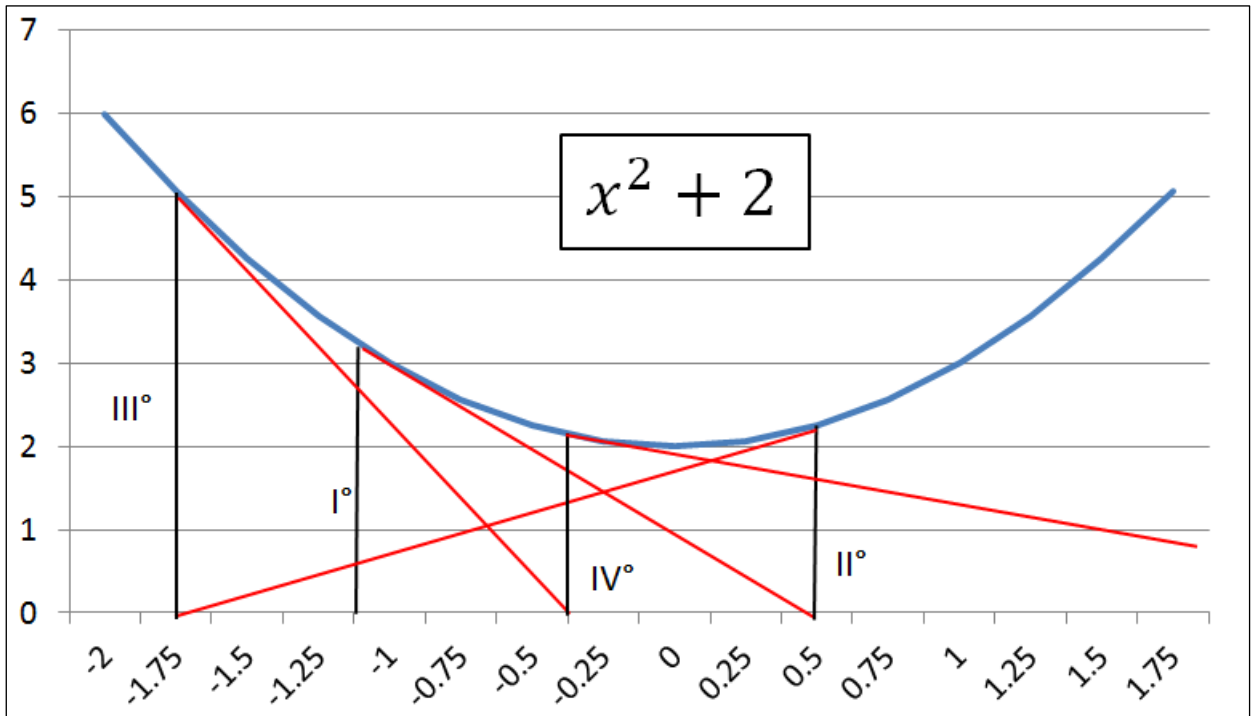


Fig. 3.3 - example of the oscillations of the Newton-Raphson method close to a stationary point

The Newton-Raphson algorithm is also prone to root jumping: in some case where the function  $f(x)$  is oscillating and has a high number of roots, it is possible to choose an initial guess close to a root but, the guesses may jump and converge to some other root. For example for solving the equation  $\sin(x) = 0$  if it is chosen  $x_0 = 2.4\pi = 7.539822$  as an initial guess, it converges to the root of  $x=0$ , as shown in Table 3 and Figure 26, skipping the root  $x = \pi$  or  $x = 2\pi$ .

Tab. 3.2 - Example of the iteration flow of the tested function  $\sin(x)$

Iteration Number	$x_i$	$f(x_i)$	$ \varepsilon_a \%$
0	7.539822	0.951	-----
1	4.462	-0.969	68.973
2	0.5499	0.5226	711.44
3	-0.06307	-0.06303	971.91
4	$8.376 \times 10^{-4}$	$8.375 \times 10^{-5}$	$7.54 \times 10^4$
5	$-1.95861 \times 10^{-13}$	$-1.95861 \times 10^{-13}$	$4.28 \times 10^{10}$

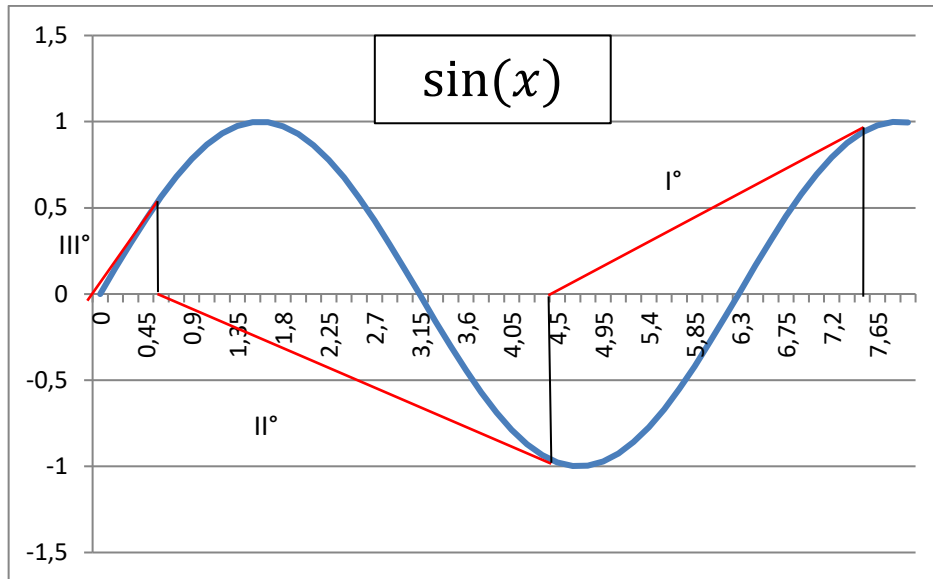


Fig. 3.4 - First 3 iterations on the test function  $\sin(x)$

For example, in this thesis application, in some element equations, the equation  $\dot{m} \propto \sqrt{\Delta p}$  has been squared ( $\dot{m}^2 \propto \Delta p$ ) to regulate the function: the square root can lead to convergence problems due to 1<sup>st</sup> derivative that is not well behaved and may cause overshooting in the root finding. The new formula avoids the overshooting problem but introduces a double solution: for very low flow rate the two solution are close to each other, with the risk of root jumping.

### 3.2.3 Implementation

To perform the characteristic curve analysis the geometry of the engine has been considered fixed, as an input for the solver, while the internal nodes temperature and pressure are the unknowns of the problem: this approach is used for the actual performance test and is different from the design approach where the mass flow rate are fixed and the geometry of the piping is the real unknown.

The original CCX implementation solved the problem respect to the mass flow rate, the total pressure and the temperature, but in this thesis application the element's equations are set to be solved for the mass flow rate, the static pressure, the total temperature and the swirl. The choice of solving for the static pressure instead of the total pressure is motivated by a physical, mathematical as well as company procedural background:

- in a 0D code a unique static pressure can be associated to the outlet of e.g. a pipe or an orifice into a plenum: the static pressure at the outlet throat of a pipe is (unless choking) the same as the static pressure inside the outlet plenum, while the total pressure is different
- Given the mass flow rate, the total temperature, the cross section and the static pressure at a given node, it is always possible to find the corresponding Mach number as the positive solution of a quadratic equation: if this solution exists, it can be found in explicit form. On the contrary, starting from the total pressure at a given section, an implicit equation (which may have no solution for high mass flow rate) is required to derive the Mach number

- Several correlations (cavity, orifice, static-to-static, zeta...) are used in the static-to-static form, to enhance the possibility of a faster matching with the static-to-static pressure drops coming from experimental data

Although the original CalculiX code solves for the total pressure by assuming that the boundary node of any network element corresponds to a large cavity, the old code is still compatible with the new practice because the static pressure at the outlet of a pipe, or a labyrinth seal into a plenum coincides with the total pressure in the downstream plenum. The special application on a gas turbine engine lead to the addition of the new variable tangential velocity, defined at the boundary nodes of each element: unlike the original CalculiX code, where the user had to specify where a rotating cavity had to take its input swirl from, this extended library is able to automatically deal with the mix and split of tangential velocities at junctions, even in presence of reverse flow, according to the network topology. Every element in CCX is made of three nodes in series: two corner nodes and 1 middle node: to every node one and only one degree of freedom is associated.

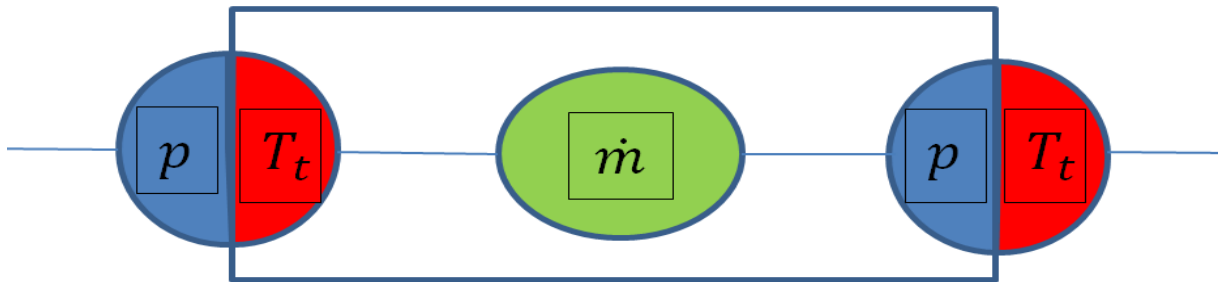


Fig. 3.4 - Example scheme of the generic element

The mass flow is not necessarily uniquely determined at the corner nodes, since more than two branches can come together. Therefore, it is logical to define the mass flow as unknown in the middle of a network element. Similarly, the total temperature or static pressure may not be known within the element, since the exact location of discontinuities (such as enlargements or orifices) is not necessarily known. Consequently, it is advantageous to define the total temperature and static pressure as unknowns in the corner nodes: the connection between elements happen on the corner node, so in the connection both total temperature and static pressure are known. The static temperature is not a basic variable: once the total temperature, mass flow and static pressure are known, the static temperature can be calculated. A field called *nactdog* is introduced for network applications: it can be viewed as a matrix with 3 rows and as many columns as there are nodes in the model. It indicates whether a specific degree of freedom in a gas node is active: if the entry is nonzero it is active, else it is inactive.

Tab. 3.3 - Degrees of freedom in fluid nodes

Degree of freedom	Corner node	Middle node
0	Total temperature	-
1	-	Mass flow rate
2	Static pressure	-

Consequently, if  $nactdog(2,328)$  is nonzero, it means that the static pressure in node 328 is an unknown in the system. Actually, the nonzero value represents the number of the degree of freedom attached to the static pressure in node 328. The number of the degree of freedom corresponds with the column number in the resulting set of equations. What  $nactdog$  is for the degrees of freedom is  $nacteq$  for the equations: it is a field of the same size of  $nactdog$  but now a nonzero entry indicates that a specific conservation equation applies to the node, in a loop over all network elements the necessary equations are determined.

Tab. 3.4 - Conservation equations in fluid nodes

Degree of freedom	Corner node	Middle node
0	Energy	-
1	-	Mass
2	Momentum	-

In a given corner node the conservation of mass equation is formulated if the mass flow in at least one of the adjacent network elements is unknown. The conservation of energy is written if the temperature in the corner node is unknown. Finally, conservation of momentum equation (also called element equation) is formulated for a middle node of a network element if not all quantities in the element equation are known. This latter check is performed in the subroutine *flux.f*. It contains on its own subroutines for several fluid section types, e.g. subroutine *orifice.f* for the fluid section of type ORIFICE. The number of unknowns relevant for the network element depends on its section type. After having identified all necessary equations in field  $nacteq$  they are numbered and the number of equations is compared with the number of unknowns. They must be equal in order to have a unique solution. Next, multiple point constraints among network nodes are taken into account.

As discussed in the section 3.1.2 the algorithm resolves for the vector

$$\Delta \mathbf{x}_k = -J(\mathbf{x}_k)^{-1} f(\mathbf{x}_k) \quad (3.28)$$

Three matrices  $(\mathbf{x}_{k=0}(p_{in}^0, p_{out}^0, T_{tin}^0, T_{tout}^0, \dot{m})$ , the unknowns matrix,  $\mathbf{U}_{k=0}(p_{in}^0, p_{out}^0, T_{tin}^0, T_{tout}^0, \dot{m})$ , the boundary conditions matrix and  $\mathbf{f}_{k=0}(p_{in}^0, p_{out}^0, T_{absin}^0, T_{absout}^0, \dot{m})$ , the results matrix), are initialized respectively by “*initialnet.f*” and “*resultnet.f*”: this is especially important for gas networks, since the initial values are taken as starting solution. Since the gas equations are very nonlinear, a good initial guess may accelerate the Newton-Raphson convergence quite a bit (or make a convergence possible in the first place). At first an initial pressure distribution is determined. To that end the pressure value for nodes with a pressure boundary condition is stored in the matrix  $U(2,i)$ , where  $i$  is the global node number. If no pressure boundary conditions applies, the minus the number of elements to which the node belongs is stored in the same field. If a node belongs to only one element, it is a boundary node and a fictitious initial pressure slightly smaller than the minimum pressure boundary condition is assigned to it: in that way, all boundary nodes are guaranteed to have a value assigned. The initial pressure in all other nodes is determined by solving for the Laplace equation in the network, i.e. the value in a node is the mean of the values in all surrounding nodes. To obtain a more realistic distribution the values are biased by an inverse tangent function, i.e. the values upstream decrease more slowly than on the downstream side of the network. The temperature initial conditions are fixed at 293 K (only for those nodes for which no temperature boundary condition applies).

In general, the temperature initial conditions are not so critical for the global convergence. Based on the total temperature and static pressure the mass flow in the elements is determined using the element equations. Finally, the static temperature is calculated for the nodes not identified as chambers based on the static pressure, total temperature and mass flow. For every block 3 equations are solved: in this special application 2 systems are solved in series, one for  $p, \dot{m}, T$ ; the other for  $p, \dot{m}, c_\theta$ . The Jacobian matrix is assembled by as many row vector gradients as the number of equations to be solved (3 per number of blocks), the exact analytical form of the gradient has been implemented in every single block element: the subroutine “*mafillnet.f*” fills the Jacobian matrix values. The linear systems obtained are solved by “*dgesv.f*” (operating a PLU factorization on the matrix (direct method with pivoting). The equations are not preconditioned with an equilibration then the resulting matrices have high condition numbers. The “*dgesv.f*” is from LAPACK 3.0 (all the subroutines originally called by “*dgesv.f*” in LAPACK are included in this file in Calculix).

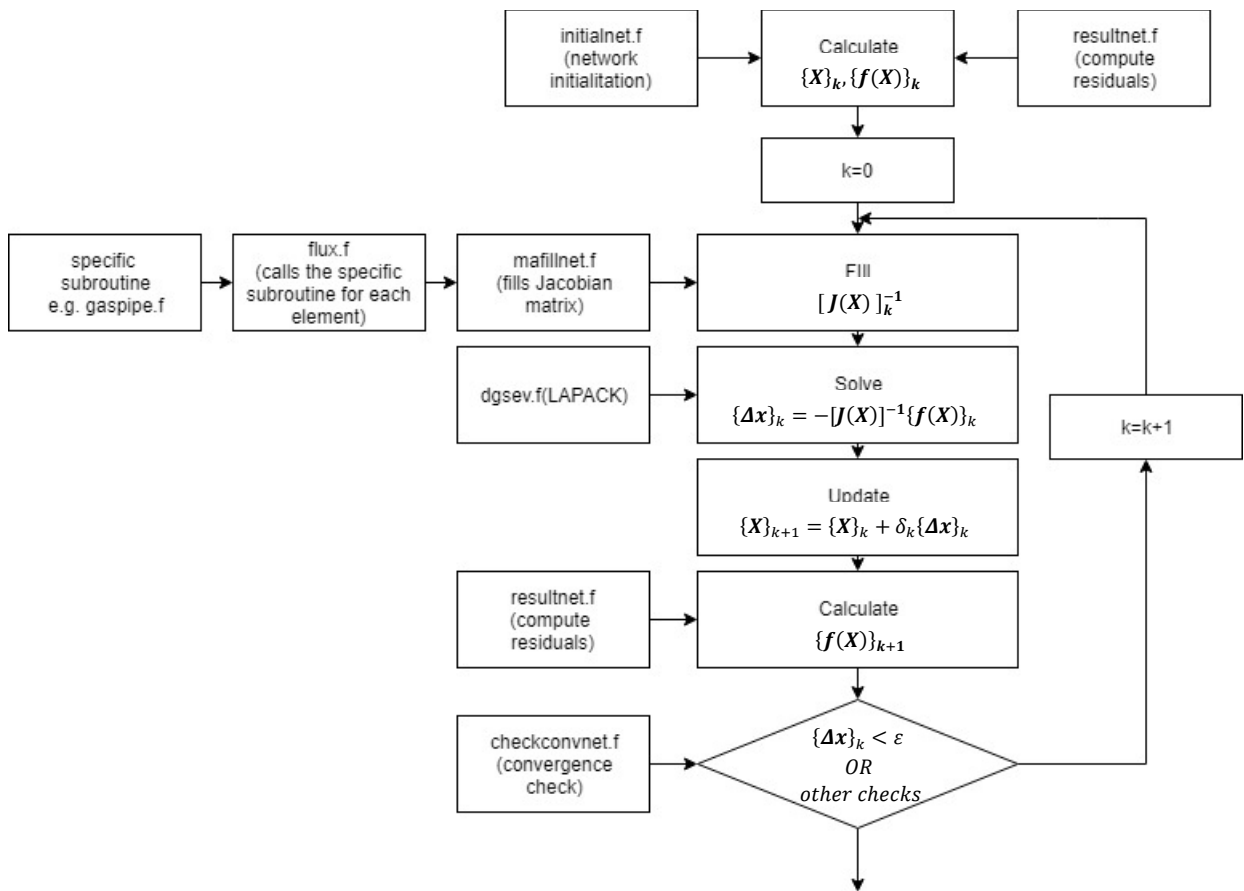


Fig. 3.5 - Modified Calculix resolution scheme

Two indexes,  $ieq$  and  $idof$ , are necessary to fill the solution matrix of the system of equations:  $ieq$  is the line index and  $idof$  is the column index. The solution matrix has the shape visible in Eq. 3.28:  $J$  is the Jacobian matrix,  $f$  is the matrix of the right hand side of all equations,  $\Delta X$  is the matrix of solution variables. For all type of elements a specific subroutine exists and it calculates the residual values and the derivatives of the momentum equation. The overall matrix  $f$  is made up of the right hand side of the governing equations and is built by the subroutine “*resultnet.f*” which has also the task to update on each loop all governing equations until Newton Raphson reach convergence. Likewise, the routine “*mafillnet.f*” builds the Jacobian

matrix. A similar matrix equation is made to solve the swirl for all elements node. To provide stability to the system a simple over-relaxation parameter has been implemented in the loop:

$$\mathbf{x}_{k+1} = \mathbf{x}_k + \delta_k \Delta \mathbf{x}_k \quad (3.29)$$

where  $\delta_k$  is the over-relaxation parameter, at the current iteration, and the value  $\delta_k \Delta \mathbf{x}_k = \delta_k \mathbf{J}(\mathbf{x}_k)^{-1} \mathbf{f}(\mathbf{x}_k)$  is the Newton-Raphson correction (*cam\**). The subroutine *radflowload.c* is the main subroutine of the solution loop. It takes into account the number of iterations, applies the Newton-Raphson method to all equations and calls the subroutine “*mafillnet.f*” and “*resultnet.f*”. There are two iteration counters, a relative iteration counter called “*iin*” and an absolute iteration counter called “*iin\_abs*”. When the relative iteration counter is set (or reset) to zero an initialization step (calling “*initialnet.f*”) is performed by *radflowload.c*. The relative iteration counter can be reset to zero after one of the following events:

- Singular matrix
- negative pressure or temperature at any node.
- *idivergence=1* in *checkconvnet.c*, meaning that either a “large” residual is detected after 80 iterations (standard value) or the maximum number of iterations ( $20*ic=320$  with  $ic=1600$ , standard values) is reached.

When the relative iteration counter is reset, the network is re-initialized with the same initial values which brought to the divergence event but this time a smaller over-relaxation parameter  $\delta_k = \delta_k df$  with  $df=0.25$  is used.

### 3.2.4 Convergence criteria

The native convergence check algorithm is embedded in the subroutine *checkconvnet.c*: it consists in a check of the current Newton Raphson correction *cam\** (*camp* for pressure, *campf* for flow, *camt* for temperature...) with the highest correction (*vam\**) ever met from the beginning of the iterations, the current must be smaller than a little fraction ( $c_2$ ) of the highest.

$$cam^* = c_{i,max}^\alpha \leq c_2 \Delta u_{i,max}^\alpha = c_2 vam^* \quad (3.30)$$

$\Delta u_{i,max}^\alpha$  the largest change in solution (in absolute value) of field  $\alpha$  since the start of the iterations, i.e. the maximum value of the difference between the solution at the end of a generic iteration  $i$  and the solution at the start of the generic iteration  $i$ .

$\Delta u_{i,max}^\alpha = \max_e \max_{n_e} \max_{k_n} |\Delta u_i^\alpha|$  where  $\Delta$  denotes the change due to the present increment with

$e = \text{number of elements,}$

$n_e = \text{all nodes belonging to the element,}$

$k_n = \text{all degrees of freedom, for a field } \alpha, \text{ belonging to a given node.}$

$c_{i,max}^\alpha$  the largest change in solution (in absolute value) of field  $\alpha$  in iteration  $i$ :  $c_{i,max}^\alpha =$

$$\max_e \max_{n_e} \max_{k_n} |\delta u_i^\alpha|$$

In the same time (AND condition) the current Newton Raphson largest residual must be less than a fraction ( $c_1$ ) of the average (*qam\**) of the largest residuals from the beginning of the iterations.

$$r_{i,max}^\alpha \leq c_1 \widetilde{q}_1^\alpha = c_1 qam^* \quad (3.31)$$

$\widetilde{q}_i^\alpha$  the iteration-average of the average flux for field  $\alpha$  of all iterations in the present increment up to but not including iteration  $i$ .

$r_{i,\max}^\alpha$  the largest residual flux (in absolute value) of field  $\alpha$  at the end of iteration  $i$ . For its calculation each degree of freedom is considered independently from all others:

$$r_{i,\max}^\alpha = \max_{\text{DOF}} |\delta q_i^\alpha| \text{ where } \delta \text{ denotes the change due to iteration } i.$$

The original algorithm above is prone to problems in case of a series of residuals convergent to zero but never being less than its average from the beginning (for instance the geometric series  $q^n$  with  $q < 1$  and  $n$  is the number of iterations): it may happen that a perfectly convergent network cannot be seen as convergent. For this reason a new convergence check algorithm, based on the simple condition that, for all the nodes and all the variables (pressure, temperature, mass flow and swirl), the relative correction must be less than a required tolerance, is added (in OR condition) to the original algorithm. The native algorithm also possess a non-convergence criterion: when the pressure (or temperature) is negative, or number of iterations is greater than a given value, or the largest correction ( $cam1^*$ ) at a given step is greater than the largest correction ( $cam2^*$ ) at the previous step, the network is detected as divergent and re-initialized with a smaller over-relaxation parameter. The network is deemed convergent when the Newton-Raphson relative correction (i.e. the ratio residual/variable) for all the nodes and all the variables is less than the specified tolerance (0.00001 in this case). This algorithm is in OR with the original check on the history of corrections from the beginning of iterations. Both criteria are important: a convergent solution with divergent residuals points to a local minimum, convergent residuals with a divergent solution point to a singular equation system.

### 3.2.5 User interface

For the user interface a system of connections and nodes is implemented. The nodes are objects that show the values of pressure, total temperature, radius and swirl in that specific location and can be both static (blue squares), rotating (blue circles) or boundary (green circles); the connections are objects used to link the nodes and show the values of mass flow rate, a schematic icon recalls the element simulated. The set of two nodes and a connection forms an element. A system of nomenclature, chosen by the user, is used to recall rapidly a certain node or connection: for this elaborated nodes are called with a progressive number, while connections are called with the letter B followed by a progressive number. For boundaries a more exhaustive nomenclature is used to explained what component that node simulates.

## 4. Dimensional analysis on Secondary Air System

### 4.1 Dimensional analysis for Gas Turbines

Within the strongly competitive energy market the possibility of an integrated, reliable and fast converging performance software allows to give the client a personalized commercial offer in very short time: to pursue this target it's possible to develop a structured routine between the main components of the gas turbine by the application of the dimensional analysis on the engine: the routine would ask for the "behavioural curve" of every component in various load and room temperature conditions and then would match them together to form the characteristic curve of the entire engine. Every component curve will be interpolated from a limited set of points producing, inherently, an interpolation error, but this error has been proved on the field to be small and negligible, compared to the velocity of routine itself: in a market based on fast decisions and commercial offers this work methodology might substitute some slower but more accurate methodologies.

### 4.2 Dimensional analysis

In fluid mechanics the purely mechanic quantities are dimensionally expressible via 3 dimensions, that constitute a triad of base fundamental physical variables [16] [17]. A dimension is a measure of physical quantity (without numerical values), while unit is a way to assign a number to that dimension. The dimensions are quantities that can be expressed with the product of a pure number per a number of measurement. Such unit is a sample chosen between the quantities with the same nature, or can be derived from other units via formulas that define the quantity considered in function of those assumed as fundamental. For example, length is a dimension that is measured in units such as microns ( $\mu\text{m}$ ), centimeters (cm), meters (m), kilometres (km) etc. In fluid dynamics it is usual to regard the three dimensions: mass (m), length (l), and time (t) as fundamental dimension which can be used to express dimension of another mechanical quantities, like velocity  $[V] = \frac{l}{t}$ , acceleration  $[a] = \frac{l}{t^2}$ , force  $[F] = \frac{ml}{t^2}$ , pressure  $[p] = \frac{[F]}{l^2} = \frac{m}{lt^2}$ , density  $[\rho] = \frac{m}{l^3}$ , where square brackets indicate "dimension of". The dimension of the other quantities in fluid dynamics, e.g. the coefficient of viscosity  $\mu$ , must be derived from the definition: Shear stress  $\tau = \frac{\mu dv}{dy}$

so that

$$\frac{m}{lt^2} = \frac{[\mu]}{t} \quad (4.1)$$

and hence

$$[\mu] = \frac{m}{lt} \quad (4.2)$$

It follows that

$$[v] = \frac{[\mu]}{[\rho]} = \frac{l^2}{t} \quad (4.3)$$

Dimension of further quantities arising in fluid dynamics can be evaluated in a similar manner. It is not hard to note that dimension of all the quantities discussed so far are in the form of monomial powers

$$m^{\alpha_1} l^{\alpha_2} t^{\alpha_3} \quad (4.4)$$

This property is true for all physical quantities.

In some problem resolutions can be convenient substitute the fundamental triad with another one. The substitution is legitimate if the new quantities assumed as fundamental are dimensionally independent, namely if the determinant, built with the dimensions that these quantities present in respect to the base ones, is different from zero. The equations that rule the physical phenomena are homogeneous (namely if their 2 members present the same dimensions) and can be attributable to equations between dimensionless terms (pure numbers) as it has emerged from  $\Pi$  theorem. This theorem establish that if a physical phenomenon involves  $m+1$  dimensional quantities with  $k$  base dimensions ( $k=3$  in mechanical phenomena), the  $m+1$  quantities can be grouped between themselves in  $m+1-k$  dimensionless terms. The function that correlates these terms, that is characteristic of the phenomenon in exam, doesn't result however identified: for its determination it is necessary to use theoretical analysis or experimental observations. The most important pure numbers that intervene ( in general not at the same time) in fluid mechanics phenomena are: the Newton Number  $Ne$ , the Reynolds number  $Re$ , the Froude number  $Fr$ , the Mach number  $Ma$ , the Weber number  $We$ , that respectively contain the effect of viscosity, of acceleration, of gravity, of compressibility and of surface tension; other specific pure numbers, bound to particular behaviour; parameters that describe the system geometrical shape.

$$\text{Reynolds number (viscous flows) } Re = \frac{\rho UL}{\mu} = \frac{\text{inertial force}}{\text{viscous force}} \quad (4.5)$$

$$\text{Froude number (free-surface flows) } Fr = \frac{U}{\sqrt{gL}} = \sqrt{\frac{\text{inertial force}}{\text{gravitational force}}} \quad (4.6)$$

$$\text{Weber number (surface tension) } We = \frac{\rho U^2 L}{\sigma} = \frac{\text{inertial force}}{\text{surface tension}} \quad (4.7)$$

$$\text{Mach number (compressible flows) } Ma = \frac{U}{c} = \sqrt{\frac{\text{inertial force}}{\text{compressibility force}}} \quad (4.8)$$

Assumed as fundamental quantities the mass  $m$ , the length  $l$  and the time  $t$ , whose unit of measurement are fixed in a conventional way, a mechanical quantity  $Q$  has dimensions  $\alpha, \beta, \gamma$  respect to the mass  $m$ , the length  $l$ , the time  $t$ , so:

$$[Q] = m^{\alpha} l^{\beta} t^{\gamma} \quad (4.9)$$

if we multiply the unit of measure of  $m, l, t$  by the quantities  $\mu, \lambda, \tau$  respectively, the unit of measurement of  $Q$  results multiplied by the quantity

$$q = \mu^{\alpha} \lambda^{\beta} \tau^{\gamma} \quad (4.10)$$

If  $\alpha, \beta, \gamma$  are all null the unit of measure of  $Q$  remains unchanged at the change of the unit of measure of the fundamental quantities, therefore it constitutes a dimensionless quantity, namely a pure number.

The homogeneity criterion establishes that the equations that rule the physical phenomena must be dimensionally homogeneous, namely is assumed that must appear quantities and pure numbers so that their 2 members present the same dimensions.

Three mechanical dimensions, called generically  $Q_1, Q_2, Q_3$ , can be assumed as fundamental quantities in place of  $m, l, t$  if they are suitable to define dimensionally whichever mechanical quantity and, in particular, the quantities  $m, l, t$ .

To characterize the condition, that must be satisfied, this procedure is followed:

- (a)  $Q_1, Q_2, Q_3$  are expressed dimensionally, as functions of  $m, l, t$  and 3 numerical equations (as 4.10) are reached:

$$q_1 = \mu^{\alpha_{11}} \lambda^{\alpha_{12}} \tau^{\alpha_{13}}; q_2 = \mu^{\alpha_{21}} \lambda^{\alpha_{22}} \tau^{\alpha_{23}}; q_3 = \mu^{\alpha_{31}} \lambda^{\alpha_{32}} \tau^{\alpha_{33}} \quad (4.11)$$

Equivalent to

$$\log(q_1) = \alpha_{11} \log(\mu) + \alpha_{12} \log(\lambda) + \alpha_{13} \log(\tau) \quad (4.12)$$

$$\log(q_2) = \alpha_{21} \log(\mu) + \alpha_{22} \log(\lambda) + \alpha_{23} \log(\tau) \quad (4.13)$$

$$\log(q_3) = \alpha_{31} \log(\mu) + \alpha_{32} \log(\lambda) + \alpha_{33} \log(\tau) \quad (4.14)$$

- (b) The last system is solved respect to  $\log(\mu), \log(\lambda), \log(\tau)$ . This system admits non trivial solutions if the coefficient matrix determinant is non zero

$$|\alpha_{ij}| \neq 0 \quad (4.15)$$

If this condition is satisfied results

$$\log(\mu) = \beta_{11} \log(q_1) + \beta_{12} \log(q_2) + \beta_{13} \log(q_3) \quad (4.16)$$

$$\log(\lambda) = \beta_{21} \log(q_1) + \beta_{22} \log(q_2) + \beta_{23} \log(q_3) \quad (4.17)$$

$$\log(\tau) = \beta_{31} \log(q_1) + \beta_{32} \log(q_2) + \beta_{33} \log(q_3) \quad (4.18)$$

where

$$\beta_{ij} = \frac{1}{|\alpha_{ij}|} (-1)^{i+j} M_{ij} \quad (4.19)$$

being  $M_{ij}$  are the minors extracted from the coefficient matrix. The following numerical equations

$$\mu = q_1^{\beta_{11}} q_2^{\beta_{12}} q_3^{\beta_{13}}; \lambda = q_1^{\beta_{21}} q_2^{\beta_{22}} q_3^{\beta_{23}}; \tau = q_1^{\beta_{31}} q_2^{\beta_{32}} q_3^{\beta_{33}} \quad (4.20)$$

and their relative symbolic equations are reached

$$[m] = Q_1^{\beta_{11}} Q_2^{\beta_{12}} Q_3^{\beta_{13}}; [l] = Q_1^{\beta_{21}} Q_2^{\beta_{22}} Q_3^{\beta_{23}}; [t] = Q_1^{\beta_{31}} Q_2^{\beta_{32}} Q_3^{\beta_{33}} \quad (4.21)$$

That express dimensionally  $m, l, t$  as functions of  $Q_1, Q_2, Q_3$ .

Every other quantity  $Q_n$ , since it is expressible as function of  $m, l, t$ , results expressible as function of  $Q_1, Q_2, Q_3$ . In general, if  $[Q_n] = m^{\alpha_{n1}} l^{\alpha_{n2}} t^{\alpha_{n3}}$ , results:

$$[Q_n] = Q_1^{\beta_{n1}} Q_2^{\beta_{n2}} Q_3^{\beta_{n3}} \text{ with } \beta_{nj} = \beta_{ij} \alpha_{ni} \quad i = 1, 2, 3 \quad (4.22)$$

Finally, to assume  $Q_1, Q_2, Q_3$  as fundamental quantities it's necessary and sufficient that the condition 4.15 is verified that ensure the dimensional independence of these quantities, namely the impossibility to build by them a 0 order polynomial, that would represent a dimensionless quantity.

### 4.2.1 II Theorem

The equations that rule the physical phenomena must be leadable to equations between dimensionless terms. To achieve this objective one of the most frequently employed method is the one using the  $\Pi$  theorem, known also as Riabouchinsky-Buckingham theorem, previously stated by Vaschy. It's supposed that in the physical phenomenon study, on the basis of the elementary laws that intervene in the phenomenon or experimental observations, that the following general formulation has been achieved:

$$Q_0 = f_0(Q_1, Q_2, Q_3, \dots, \dots, Q_m, r_i) \quad (4.23)$$

That express, without specifying it, the dependence of the dimensional parameter  $Q_0$  from the dimensional parameters  $Q_1, Q_2, Q_3, \dots, \dots, Q_m$  and from the dimensionless terms  $r_i$  (ratios between quantities with the same dimensions, for example roughness and shape coefficients, etc..).

If the phenomenon is mechanic, assumed  $Q_1, Q_2, Q_3$  as fundamental quantities, it's possible to rewrite the eq. 4.22 in the shape as

$$\frac{Q_0}{Q_1^{\beta_{01}} Q_2^{\beta_{02}} Q_3^{\beta_{03}}} = f^*(Q_1, Q_2, Q_3, \frac{Q_4}{Q_1^{\beta_{41}} Q_2^{\beta_{42}} Q_3^{\beta_{43}}}, \dots, \dots, \frac{Q_m}{Q_1^{\beta_{m1}} Q_2^{\beta_{m2}} Q_3^{\beta_{m3}}}, r_i) \quad (4.24)$$

and to use the eq. 4.22 to determine the exponents of the parameters that appear in the monomial at denominator of every ratios, so that this result as a dimensionless term, that is indicated with  $\pi$ . It results, therefore:

$$[Q_0] = Q_1^{\beta_{01}} Q_2^{\beta_{02}} Q_3^{\beta_{03}}; [Q_1] = Q_1^{\beta_{11}} Q_2^{\beta_{12}} Q_3^{\beta_{13}}; \dots; \dots; [Q_m] \\ = Q_1^{\beta_{m1}} Q_2^{\beta_{m2}} Q_3^{\beta_{m3}} \quad (4.25)$$

$$\pi_0 = \frac{Q_0}{Q_1^{\beta_{01}} Q_2^{\beta_{02}} Q_3^{\beta_{03}}}; \pi_1 = \frac{Q_1}{Q_1^{\beta_{11}} Q_2^{\beta_{12}} Q_3^{\beta_{13}}}; \dots; \dots; \pi_m \\ = \frac{Q_m}{Q_1^{\beta_{m1}} Q_2^{\beta_{m2}} Q_3^{\beta_{m3}}} \quad (4.26)$$

Introducing the eq. 4.26 in the eq. 4.25 it's achieved

$$\pi_0 = f(Q_1, Q_2, Q_3, \pi_4, \dots, \dots, \pi_m, r_i) \quad ((4.27)$$

Changing the unit of measurement of  $Q_1$ , the 1<sup>st</sup> member of the eq. 4.27 remains unchanged, because is a pure number, while the 2<sup>nd</sup> member all the arguments of the function  $f$  remain unchanged except  $Q_1$ . In fact remain unchanged both the  $\pi_i, r_i$  terms, because they are pure numbers, and  $Q_2, Q_3$ , because they don't depend from  $Q_1$ . The conclusion is that, if the  $f$  function must remain unchanged (because the 1<sup>st</sup> member doesn't change) it cannot depend from  $Q_1$ . In a similar way it's verified that  $f$  cannot depend from  $Q_2, Q_3$ .

The eq. 4.27 must be substituted by

$$\pi_0 = f(\pi_4, \dots, \dots, \pi_m, r_i) \quad ((4.28)$$

Or by the equivalent equations, in an implicit form,

$$f_i(\pi_0, \pi_4, \dots, \dots, \pi_m, r_i) = 0 \quad ((4.29)$$

The  $\pi$  theorem transforms a functional relation such as eq. 4.23 in an equation with the structure of eq. 4.29. The application of the  $\pi$  theorem allows to write a relation between the only dimensionless terms, that result in being in a smaller number than the dimensional parameters (dimensional parameter number  $m+1$ , dimensionless parameter number  $m+1-3$ ) but it doesn't

specify the type of dependency. To obtain the shape of the function  $f$  it's necessary to use theoretical analyses that use the mechanic general principles or the experimental investigations.

### 4.3 $\Pi$ theorem applications

The theorem described has many useful applications:

- Increasing insight about key parameters
- Decreasing number of parameters in the problem (easier communication, fewer experiments and simulations)
- Possibility of easier result extrapolations in untested conditions

The reduction of parameter count is potentially a huge simplification. Considering, for example, a problem with 5 parameters: one dependent and 4 independent: a full test matrix with 5 data points for each independent parameter would require  $5^4 = 625$  experiments. If it's possible to reduce to 2 non-dimensional parameter, the number of independent parameters is reduced from 4 to 1, which results in  $5^1 = 5$  experiments against the original 625.

Dimensional analysis provides a similarity law for the phenomenon under consideration: similarity, in this context, implies a certain equivalence between two physical phenomena that are actually different. Dimensional analysis makes possible to predict prototype performance from experimental results obtained using a scaled model. The scaling may happen to every parameter of the problem: some applications are the wind gallery scaled models or the combustor/turbine cold flow test rigs. The application of  $\Pi$  theorem is important in those test rigs that have to replicate very extreme conditions such as very high working temperature (combustor and turbine flows, blade cooling): the scaled model will work at low temperature and the results will be scaled for the real operating temperatures with a great saving in terms of rig costs and complications; in addition the use of a reduced length model is a very effective way to reduce money and space cost.

The main application of the  $\Pi$  theorem, in this thesis, is the non-dimensional scaled problem independence from the dimensional boundary conditions applied: for example the scaled problem of the flow rate across a scaled pipe won't be a function of the local values of pressure at the inlet and outlet but only of the dimensionless parameter driving pressure ratio. Given the results for one value pressure ratio, they can be used for many different boundary pressure conditions, that respect the same pressure ratio. Because of this theorem, the design of a gas turbine main components may be carried on separately and then the results can be matched to find the global machine operating point: once a reasonable adimensionalization for every components' parameters is chosen, the solution of the components' matching equations through the only non-dimensional values becomes possible.

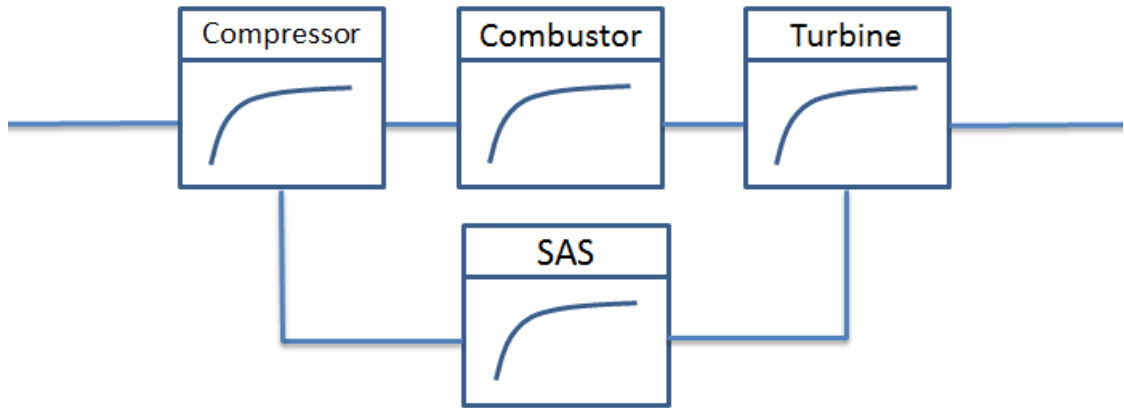


Fig. 4.1 - Turbine schematization

For this particular thesis application, the only focus was on the secondary air system characteristic modelling.

#### 4.4 II theorem application to Secondary Air System

The application of the dimensional analysis to the SAS network has been the main target of this thesis: SAS branches, with some simplifications, can be described as a thermomechanical system. The major simplifications adopted are the absence of thermal interaction between the structural and the fluid dynamic components of the gas turbine and the steady state fluid dynamic solution. To perform the dimensional analysis on a thermomechanical system, as the SAS one, the dependence of the temperature cannot be neglected while the time dependency, in this steady state treatment, is neglected. The adimensionalization of the SAS circuit is similar to the adimensionalization of any thermal machine such as compressor and turbine but the work contribution, not negligible for compressor and turbine, it is for the SAS circuits: the enthalpy variation alongside the SAS equivalent pipe, attributable to pumping and friction works doesn't affect the treatment of mass flow rate and pressure drop. The SAS circuit can be describe by the following system:

$$f(r, \dot{m}, p_1, p_2, RT_1, RT_2, k, \varepsilon, \mu) = 0 \Rightarrow 9 \text{ unknowns} \quad (4.30)$$

$$\text{mass, length, temperature} \Rightarrow 3 \text{ fundamental units} \quad (4.31)$$

Where  $r$  is a radius,  $\dot{m}$  is the mass flow rate,  $p_1$  is the start line pressure,  $p_2$  is the end line pressure,  $RT_1$  is the start line temperature time the gas specific constant,  $RT_2$  is the end line temperature time the gas specific constant,  $k$  is the gas specific heats ratio,  $\varepsilon$  is the pipe roughness,  $\mu$  is the dynamic viscosity of the fluid. Applying the II theorem on this problem we reach the following solution:

$$f\left(1, \frac{\dot{m}\sqrt{RT_2}}{r^2 p_2}, \beta, 1, \frac{RT_1}{RT_2}, 1, k, \frac{\varepsilon}{r}, Re\right) = 0 \quad (4.32)$$

Where the 9 unknowns of the original problem are reduced to

$$9 (\text{unknowns}) - 3 (\text{fundamental units}) = 6 \text{ non-dimensional parameters.}$$

$$\frac{\dot{m}\sqrt{RT_2}}{r^2 p_2} \text{ is the non-dimensional mass flow rate}$$

$\beta$  is the driving pressure ratio

$\frac{RT_1}{RT_2}$  is the thermodynamic efficiency  
 $\frac{\varepsilon}{r}$  is the non-dimensional roughness  
 $Re$  is the Reynolds number

Further simplifications may occur:

- The geometry is considered fixed in every conditions
- The Reynolds number is considered very high and the problem results independent of it
- The temperature ratio is quite constant in every conditions
- $k$  is constant because inside the SAS circuit only air circulates

These assumptions simplify further the problem:

$$f\left(\frac{\dot{m}\sqrt{RT_2}}{p_2}, \beta\right) = 0 \quad (4.33)$$

The exact values of  $T_2$ ,  $p_2$ ,  $p_1$  chosen for every line will be discussed later (Par. 4.6).

Due to the thermodynamic nature of the processes involved in this thesis, the definition of stagnation quantities is here recalled: these quantities are the sum of the static and the kinetic components of a certain quantity or the static component measured after an adiabatic and isentropic process that nulls the fluid speed.

The static enthalpy,  $h$ , and the kinetic energy,  $\frac{c^2}{2}$  are combined and the result is called the stagnation or total enthalpy,  $h^0 = h + \frac{c^2}{2}$ . The stagnation enthalpy is constant in a flow process that does not involve a work transfer or a heat transfer even though irreversible processes may be present. If the fluid is a perfect gas, then  $h = c_p T$ , where  $c_p = \frac{k}{k-1} R$ , so that the stagnation temperature can be defined as

$$T^0 = T + \frac{c^2}{2c_p} \quad (4.34)$$

$$\frac{T^0}{T} = 1 + \frac{k-1}{2} \frac{c^2}{kRT} = 1 + \frac{k-1}{2} M^2 \quad (4.35)$$

where  $M$  is the Mach number,  $Ma = \frac{c}{a} = \frac{c}{\sqrt{kRT}}$ .

The Gibbs' relation, derived from the 2<sup>nd</sup> Law of Thermodynamics, is

$$Tds = dh - \frac{dp}{\rho} \quad (4.36)$$

If the flow is brought to rest both adiabatically and isentropically, then, using the above Gibbs' relation

$$dh = c_p dT = \frac{dp}{\rho} RT \quad (4.37)$$

so that

$$\frac{dp}{p} = \frac{c_p dT}{RT} = \frac{k}{k-1} \frac{dT}{T} \quad (4.38)$$

integrating

$$\ln p = \ln constant + \frac{k}{k-1} \ln T \quad (4.39)$$

and so

$$\frac{p^0}{p} = \left(\frac{T^0}{T}\right)^{\frac{k}{k-1}} = \left(1 + \frac{k-1}{2} M^2\right)^{\frac{k}{k-1}} \quad (4.40)$$

from the perfect gas law, density is given as  $\rho = \frac{p}{RT}$  and hence

$$\frac{\rho^0}{\rho} = \left(\frac{p^0}{p}\right) \left(\frac{T}{T^0}\right) = \left(\frac{T^0}{T}\right)^{\frac{1}{k-1}} = \left(1 + \frac{k-1}{2} M^2\right)^{\frac{1}{k-1}} \quad (4.41)$$

because the strong dependence of the velocity.

The stagnation quantities are the conditions the fluid would reach if it were brought to zero speed relative to some reference frame, via a steady, adiabatic and isentropic process with no external work: this lead to a great dependence of the stagnation properties from the reference frame chosen. For gas turbine applications 2 reference frames are used: the absolute frame and the relative frame, that spins around the undeformed machine axis jointly with the machine itself, implying the use of the relative velocity  $\vec{w} = \vec{c} - \vec{u}$  instead of the absolute velocity  $\vec{c}$ . The difference will be remarked with the subscript *abs* and *rel*.

Another quantity that will be used in this application is the rothalpy:

$$I = h + \frac{c^2}{2} - uc_\theta \quad (4.42)$$

The name rothalpy comes from the contraction of the rotational stagnation enthalpy, and is a fluid mechanical property of some importance in the study of relative flows in rotating systems: for a steady flow can be deduced that this quantity must be constant along the flow lines, or along a 0D elements chain, as in this thesis application.

#### 4.5 Application of Blade and Vane Characteristic Curves

The turbine vane and blade cooling design hasn't been directly part of this thesis project work but, because the blade internal flow is often in choked condition, it has the effect of regulation of the entire upstream SAS circuit: a characteristic curve of this flow must be implemented within the SAS network solver. This happens via a black box element called CHARACTERISTIC that implements the polynomial fittings of the blade/vane characteristic curve and use the driving pressure ratio across the upstream and downstream pressure nodes to interrogate the flow function. Characteristic curves can be calculated by means of a procedure based on 3D CFD or on specific self-standing fluid network solver, shaped to model the internal cooling circuits of turbine blades and vanes. The general form of the characteristic curve is gives by Eq. 4.43.

$$\dot{m}_c \frac{\sqrt{T_c^0}}{p_c^0} = f\left(Ma_{2s}, \frac{p_{out}^0}{p_c^0}, Re_c\right) \quad (4.43)$$

Where the subscript *c* stands for coolant.

The procedure is based on a Design of Experiments analysis of several thermal calculation runs of the model chosen. It allows calculating the coefficients that multiply the independent groups of thermodynamic variables. Coefficients and shape of curves depend on several aspects, such as the cooling system, type and thickness of the surface coating, the location on the aerofoil of the outlets of cooling air flows, etc...

The influence of these parameters depends mainly from the cooling method adopted for the blade:

$$\text{Film Cooling} \quad \dot{m}_c \frac{\sqrt{T_c^0}}{p_c^0} = f\left(\frac{p_{out}}{p_c^0}, Re_c\right) \quad (4.44)$$

$$\text{Trailing edge Cooling} \quad \dot{m}_c \frac{\sqrt{T_c^0}}{p_c^0} = f\left(\frac{p_{out}}{p_c^0}, Re_c\right) \quad (4.45)$$

$$\text{Tip Cooling} \quad \dot{m}_c \frac{\sqrt{T_c^0}}{p_c^0} = f\left(\frac{p_{out}}{p_c^0}, Re_c\right) \quad (4.46)$$

In this case, film-cooling flow is influenced by the cooling system pressure ratio that is given by the relative total pressure of air at the blade root,  $p_{br}^0 = p_c^0$ , and the relative total pressure of hot gas at the row flow path axial position,  $p_{HOTGAS}^0 = p_{out}^0$ . Trailing edge and tip cooling flows depend also on the outlet Mach number of mainstream and the characteristics of the thermal barrier coating. From Eq. 4.44, 4.45 and 4.46 it's also understandable how the dimensional analysis may influence the experimental campaign on the blade cooling: the experimental data, collected in a cold flow test with a  $T_{c_{model}}^0$  lower than the real application one, can be scaled to obtain the hot flow ones.

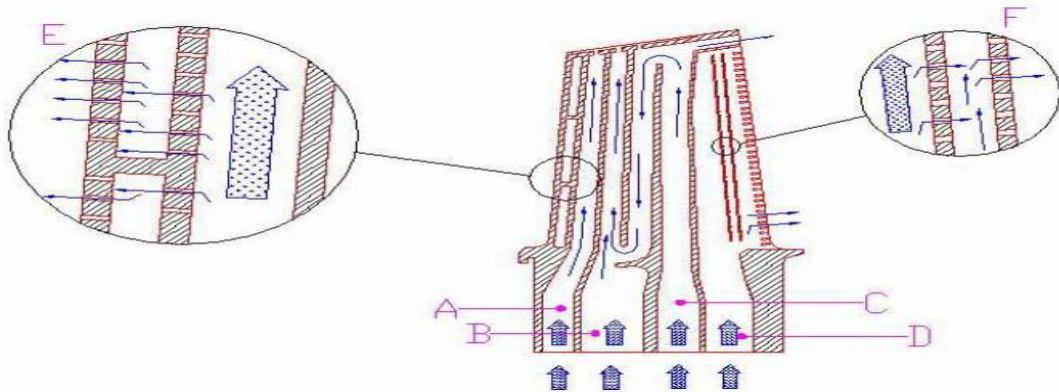
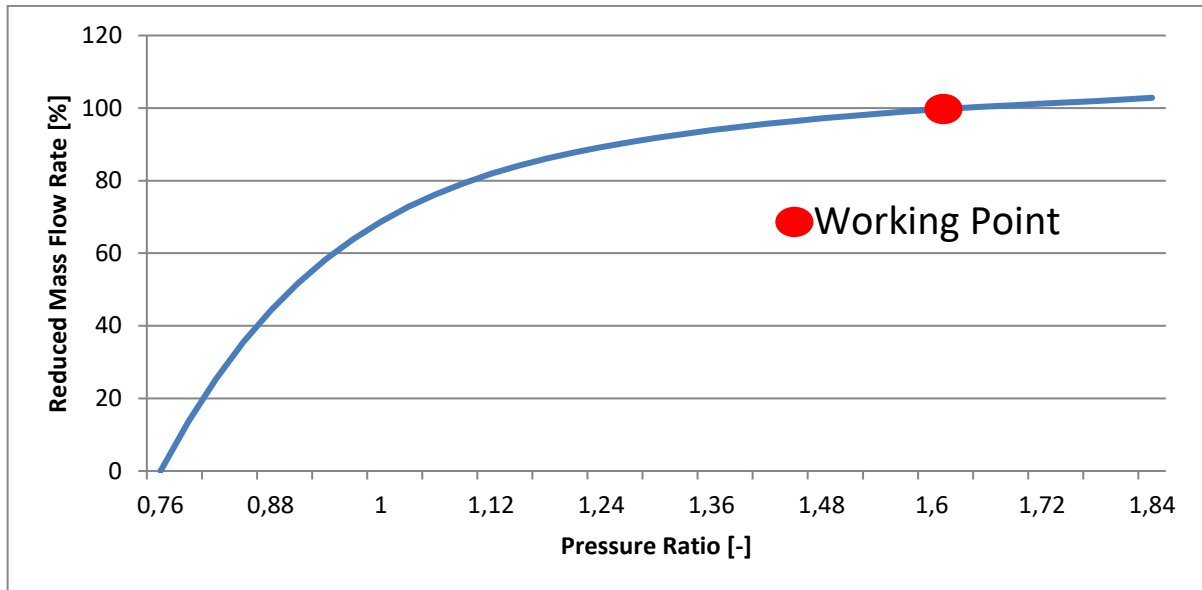


Fig. 4.2 - Blade internal cooling channels

The sum of the three cooling fractions calculated by Eqs. 4.44-4.45-4.46 gives the total consumption of air for a single blade, which is plotted as reduced mass flow,  $\dot{m}_c \frac{\sqrt{T_c^0}}{p_c^0}$ , in function of the cooling system pressure ratio,  $\frac{p_{out}^0}{p_c^0}$ . To derive the example trend shown in Fig. 4.3 from Eq. 4.43, design values for thermal barrier coating thickness and conductivity and base load conditions for Mach number and Reynolds of coolant are applied. The mark shows an example of the blade working point at base load (BL15)



*Fig. 4.3 - Blade cooling flow characteristic curve*

As discussed before the best working point for the blade/vane characteristic curve is in the plateau region, to guarantee the blade integrity also in a strong off-design condition: also a large variation in the blade driving pressure ratio, would generate only a negligible variation in the reduced mass flow rate value or, in approximation, in the unscaled mass flow rate, guaranteeing, in every conditions, the needed coolant flow rate. From this figure is also possible to understand how the blades that work with a very low pressure ratio (1<sup>st</sup> stage) are in critical conditions.

#### **4.6 Characteristic curves matching**

The simplest example of characteristic curves matching is the steady, compressor-turbine matching, neglecting the secondary air system flow rate, that is here briefly recalled: the matching happens by 3 balances (balance of continuity, balance of work on the connecting/linking shaft, balance of rotational speed) [18] [19]

- The 1<sup>st</sup> balance comes from the respect of the continuity equation: the mass flow rate elaborated by the compressor, plus the fuel mass flow rate, must be elaborated from the expander.
- The 2<sup>nd</sup> balance comes from the respect of the shaft rotational speed: the component speed, multiplied for its transmission ratio must match the shaft velocity, moreover in this simplified example, the system is considered steady, with no transient velocity changes
- The 3<sup>rd</sup> balance comes from the conservation of energy applied on the linking shaft, neglecting heat transfer and transient effects, the net power on the shaft must be zero: the algebraic sum of the power of the components connected on the shaft (compressor, turbine and electric generator) net of the friction losses must be zero

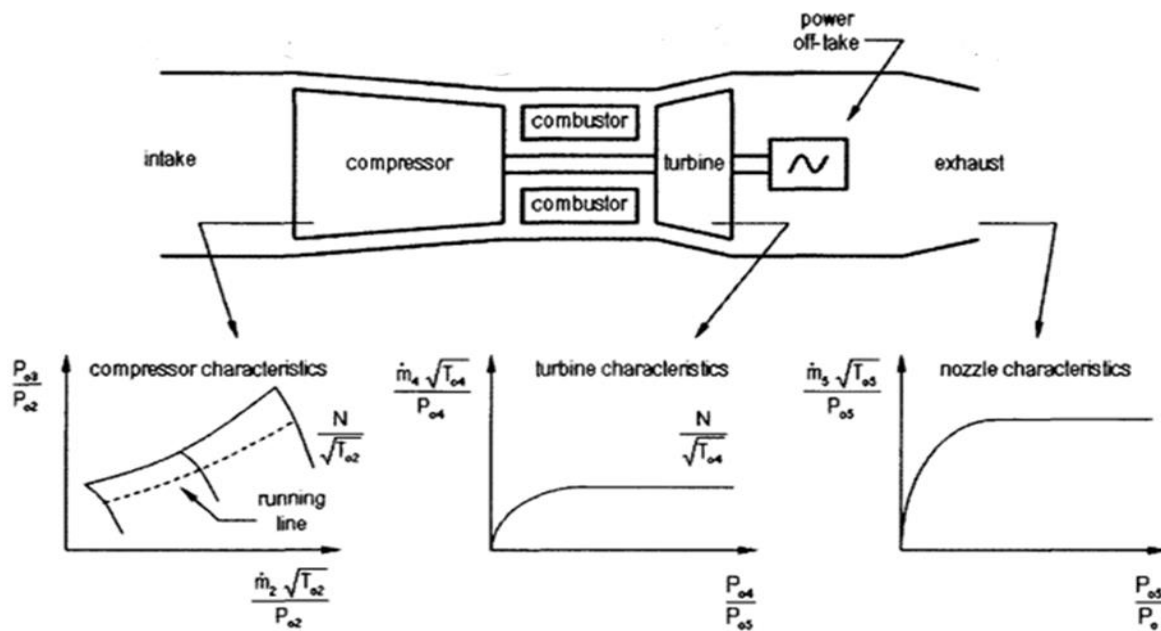


Fig. 4.4 - GT engine characteristic curves

These balances, expressed in terms of dimensional unknowns, must be modified to be functions of the non-dimensional parameters of the components: if an adequate non-dimensionalization of the components has been chosen, all the unknowns can be obtained from the characteristic curves. Usually the matching follows an iterative scheme, assuming an initial guess values of the compressor pressure ratio and corrected speed: with these two terms fixed the corrected mass flow rate and the component efficiency is fixed and then, the corresponding point on the turbine characteristic is obtained from consideration of compatibility of rotational speed and flow. The matching with the SAS component is quite similar: the same balances of the compressor-turbine matching are applied, with the added constraints of the bled and injected mass flow rates in the mass balance and the friction and pumping work contributions in the work balance. The effect of the SAS bleedings on the compressor flow path is quite small, instead the effect of the injected flow rate on the turbine characteristic is quite big: these effects may be seen on the component non-dimensional map, in fact the typical compressor working point is quite insensible to variation of reduced mass flow rate, while the turbine working point is heavily influenced from it. The matching process convergence speed is heavily dependent of the initial guess working point on the characteristic flow curve: in an industrial reality the use of an older engine model or a literature data to obtain a realistic working point as initial guess of the process could be a very effective way to improve the calculation timing.

#### 4.7 Secondary Air System characteristic curves production

The SAS network solver solves one operating condition at a time and it produces the data of temperature, pressure, swirl and mass flow rate for all the nodes: to generate the SAS characteristic curve it is necessary to process a set of operating conditions. For this thesis project, the choice of the 6 testing points has been kept quite simple: from an hypothetical, but realistic, base condition the values of compressor and turbine pressures have been scaled by simple constant coefficients to provide an homogeneous overview of the circuit pressure ratio values, inside the permissible range. To automatize this procedure a custom excel file and a

macroinstruction have been implemented: the system needs only the engine's values of temperature and pressure at the base condition. From the boundary pressures and temperatures the SAS network solves for the mass flow rate and the swirl, as described before: from the flow rate values the reduced mass flow is calculated: to uniform the design of the different GT components (compressor, SAS, combustor, turbine) the definition of reduced mass flow rate and pressure ratio are described as follow. The static and rotating branches of the SAS circuit are extremely different and also the governing equations differ, an homogeneous representation is impossible because the systems' dependencies are different: the reduced flow characteristics are defined versus a driving pressure ratio, that is specified for each SAS line individually and referred always to the total pressure at the turbine inlet. It is convenient to choose the turbine inlet total pressure as pressure reference value of the entire GT because:

- It's representative of the operating conditions of all the components
- It's strongly correlated with the turbine stage pressures over a wide load range (last stage has the poorest correlation but also the lowest cooling flow)
- It is independent of the combustor pressure loss (which may change over the course of a design phase)
- It's closer to the turbine control volume boundary, so should be a simpler characteristic with wider validity range
- It is closely correlated with the measured value of outlet pressure

As a general rule the mass flow rate passing for the cooling holes is called cooling flow rate, the remaining one (passing for the slits, clearances, etc...) is called leakage flow. Also in a simple turbine flow model, 0D or 1D, the injection locations must be known with a good resolution to have a valid solution: to reach this level of resolution a further subdivision of the characteristic has been established. The nomenclature of every characteristics is based on:

- The extraction line from which the flow is bled (IC1, IC2, EC1, EC2)
- The vane/blade that is fed with the flow
- The type of flow (cooling or leakage)
- The injection location respect to the row throat (upstream or downstream)
- The radial injection position (hub, mid or tip)

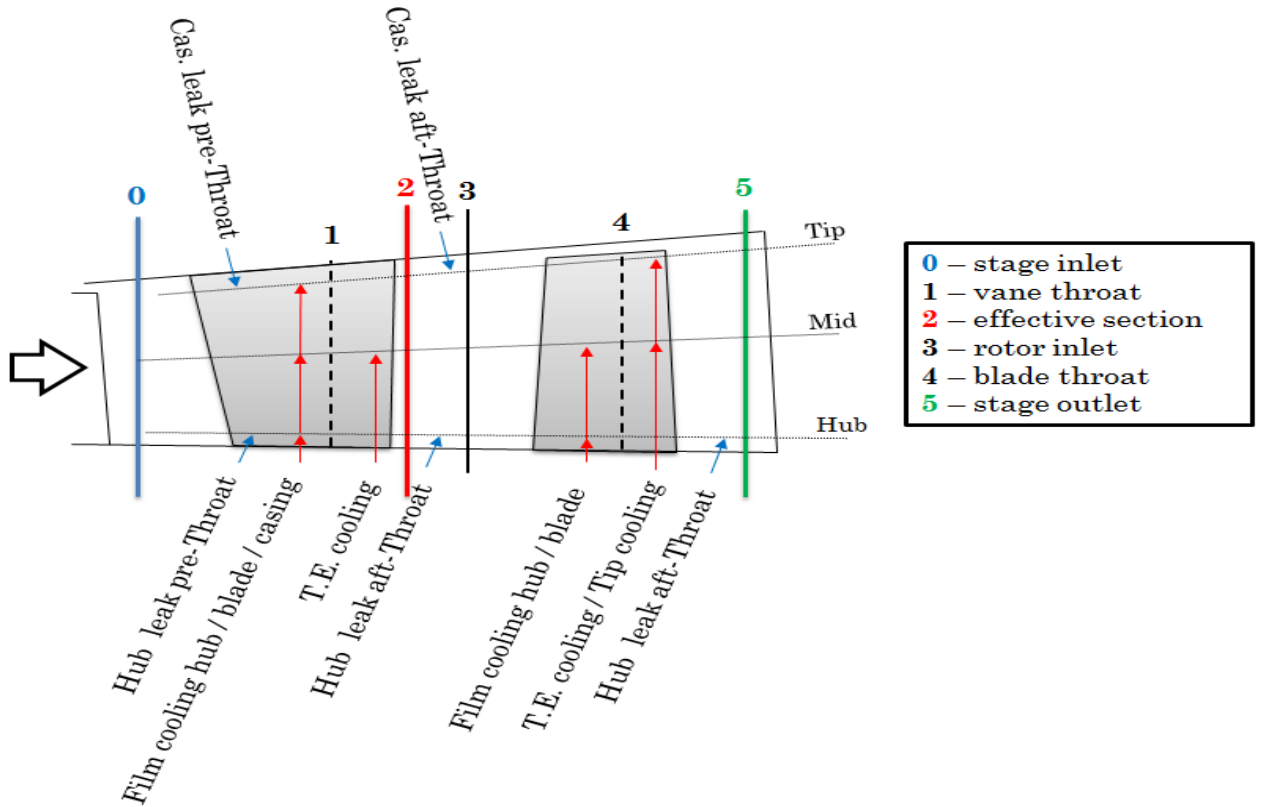


Fig. 4.5 - Scheme of the SAS injections and nomenclature

#### 4.7.1 Internal lines

The characteristic curve of an internal line could be given as with no explicit dependence on the swirl:

$$\dot{m}_{red\,int} = f(\beta_i) = f\left(\frac{p_{rel\,id\,end\,line}^0}{p_{abs\,turb\,inlet}^0}\right) \quad (4.47)$$

$$\dot{m}_{red\,int} \equiv \frac{\dot{m}}{p_{rel\,id\,end\,line}^0} \sqrt{RT_{rel\,end\,line}^0} \quad (4.48)$$

Where  $p_{rel\,id\,end\,line}^0$  is the ideal total relative pressure calculated at the end of a SAS circuit and  $p_{abs\,turb\,inlet}^0$  the total absolute pressure at the turbine inlet: it will be demonstrated that, thanks to this reduction choice, the reduced mass flow rate results independent from the swirl values for a given geometry of the piping in which the fluid flows.

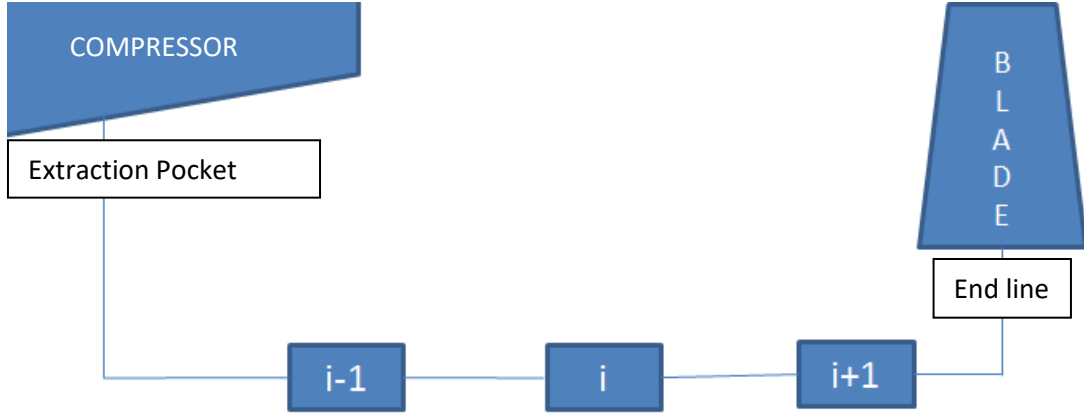


Fig. 4.6 - Scheme of a SAS internal line

The  $p_{rel\,id\,end\,line}^0$  is defined as

$$p_{rel\,id\,end\,line}^0 = p_{abs\,extr\,pocket}^0 \left( \frac{T_{rel\,end\,line}^0}{T_{abs\,extr\,pocket}^0} \right)^{\frac{k}{k-1}} \quad (4.49)$$

and does not depend on the geometric detail of the SAS circuit but only on the inlet total pressure and temperature at the extraction location and the total relative temperature at the end of a line. From the rothalpy conservation (Par. 4.4) and recalling the definition of total enthalpy:

$$\begin{aligned} h_{abs\,end\,line}^0 &= h_{abs\,extr\,pocket}^0 - c_{\theta\,extr\,pocket} u_{extr\,pocket} + c_{\theta\,end\,line} u_{end\,line} = \\ &= h_{abs\,extr\,pocket}^0 - sw_{extr\,pocket} u_{extr\,pocket}^2 + sw_{end\,line} u_{end\,line}^2 \end{aligned} \quad (4.50)$$

where  $sw = \frac{c_{\theta}}{u}$  is the swirl ratio. Hence:

$$\begin{aligned} h_{rel\,end\,line}^0 &= h_{abs\,end\,line}^0 + u_{end\,line}^2 \left( \frac{1}{2} - sw_{end\,line} \right) = \\ &= h_{abs\,extr\,pocket}^0 - sw_{extr\,pocket} u_{extr\,pocket}^2 + sw_{end\,line} u_{end\,line}^2 \\ &\quad + u_{end\,line}^2 \left( \frac{1}{2} - sw_{end\,line} \right) = \\ &= h_{abs\,extr\,pocket}^0 + \frac{u_{end\,line}^2}{2} - sw_{extr\,pocket} u_{extr\,pocket}^2 = \\ h_{rel\,end\,line}^0 &= h_{rel\,extr\,pocket}^0 + \frac{u_{end\,line}^2}{2} - \frac{u_{extr\,pocket}^2}{2} \end{aligned} \quad (4.51)$$

From  $h_{rel\,end\,line}^0$ , in the hypothesis of calorically perfect gas,  $h_{rel\,end\,line}^0 = c_p T_{rel\,end\,line}^0$ . It can be seen from 4.51 that the value  $h_{rel\,end\,line}^0$  depends on  $h_{abs\,extr\,pocket}^0$  through the inlet swirl  $sw_{extr\,pocket}$ : in other words the knowledge of  $h_{abs\,extr\,pocket}^0$  alone does not define alone the outlet total relative enthalpy. But the inlet total relative enthalpy does define alone the outlet relative enthalpy for a given geometry, with no additional dependence on the swirl. This consideration can be applied also to the ideal total relative pressure  $p_{rel\,id\,end\,line}^0$ : its independence from the extraction pocket swirl ratio  $sw_{extr\,pocket}$  will allow to write the

reduced mass flow rate as function only of the driving pressure ratio  $\beta = \frac{p_{rel\,id\,end\,line}^0}{p_{abs\,turb\,inlet}^0}$  reducing further the number of variables of the problem, as we will see below. Starting from the assumptions:

$$\dot{m}_{red} = \frac{\dot{m}}{p_{rel\,end\,line}^0} \sqrt{RT_{rel\,end\,line}^0} = f \left( \frac{p_{rel\,end\,line}^0}{p_{HOTGAS_x}} \right) \quad (A)$$

where  $x$  may be the leading edge (LE) or the trailing edge (TE) of the blade considered and

$$\frac{\dot{m}}{p_{rel\,i+1}^0} \sqrt{RT_{rel\,i+1}^0} = f_i \left( \frac{p_{rel\,i+1}^0}{p_{rel\,id\,i+1}^0} \right) \quad (B)$$

where A is the reduced mass flow rate of the blade (defined as in 4.43-4.44-4.45) and B is the reduced mass flow rate of an internal line generic element (see Fig. 4.6). Since the blade flow function is applied to the blade root, where the tangential velocity matches the blade velocity in every condition, the dependence of (A) from the swirl ratio falls. The assumed independence of (B) from the swirl is acceptable for almost all the elements implemented in this thesis: actually, for the element “rotating pipe inlet”, the discharge coefficient and the consequent pressure loss does depends on the value of the inlet relative swirl  $sw_{rel} = \frac{w_\theta}{u}$ , but the impact on the pressure drop is an higher order correction relative to the impact of the mass flow variation.

$p_{rel\,id\,i+1}^0$  appearing in equation (B) is defined as:

$$p_{rel\,id\,i+1}^0 \equiv p_{rel\,i}^0 \left( \frac{T_{rel\,i+1}^0}{T_{rel\,i}^0} \right)^{\frac{k}{k-1}} \quad (4.52)$$

Applying the conservation of rothalpy the equation above can be written as:

$$p_{rel\,id\,i+1}^0 = p_{rel\,i}^0 \left( \frac{T_{rel\,i}^0 \left( 1 + \frac{\Delta u_{i,i+1}^2}{2c_p T_{rel\,i}^0} \right)}{T_{rel\,i}^0} \right)^{\frac{k}{k-1}} = p_{rel\,i}^0 \left( 1 + \frac{\Delta u_{i,i+1}^2}{2c_p T_{rel\,i}^0} \right)^{\frac{k}{k-1}} \quad (4.53)$$

where

$$\Delta u_{i,i+1}^2 = u_{i+1}^2 - u_i^2 \quad (4.54)$$

that, for a given  $i$ , is constant for every working condition.

It is observed that the  $\frac{\Delta u_{i,i+1}^2}{2c_p T_{rel\,i}^0}$  term is small (typically of the order of 5%) and depends only on the radius (for  $\Delta u_{i,i+1}^2$ ) and  $T_{rel\,i}^0$ : even a huge 100K variation of  $T_{rel\,i}^0$  with the operating condition impacts for 1% or less on  $1 + \frac{\Delta u_{i,i+1}^2}{2c_p T_{rel\,i}^0}$ , hence we can neglect the dependence on this

term. Hence  $p_{rel_{id_{i+1}}}^0$  is proportional to  $p_{rel_i}^0$  times a geometric factor independent of the operating condition.

$$p_{rel_{id_{i+1}}}^0 = p_{rel_i}^0 (1 + constant(i))^{k-1} \quad (4.55)$$

It will be showed that the reduced mass flow in the SAS branch can be expressed as a function of the pressure ratio  $\frac{p_{rel_{id_{end\ line}}^0}}{p_{HOTGAS_x}}$  alone with no additional dependence on swirl:

$$\frac{\dot{m}}{p_{rel_{id_{end\ line}}^0}} \sqrt{RT_{rel_{end\ line}}^0} = h \left( \frac{p_{rel_{id_{end\ line}}^0}}{p_{HOTGAS_x}} \right) \quad (T)$$

Applying 4.55 to  $p_{rel_{id_{end\ line}}^0}$  it can then be written the demonstration thesis, Eq. T, that still has to be proven, as:

$$\frac{\dot{m}}{p_{rel_{extr\ pocket}}^0} \sqrt{RT_{rel_{end\ line}}^0} = h \left( \frac{p_{rel_{extr\ pocket}}^0}{p_{HOTGAS_x}} \right) \quad (4.56)$$

dropping all the unessential geometric factors.

Equation 4.56 can be written as

$$\frac{p_{rel_1}^0}{p_{rel_{extr\ pocket}}^0} \frac{p_{rel_2}^0}{p_{rel_1}^0} \dots \frac{\dot{m}}{p_{rel_{end\ line}}^0} \sqrt{RT_{rel_{end\ line}}^0} = h \left( \frac{p_{rel_{extr\ pocket}}^0}{p_{rel_1}^0} \frac{p_{rel_1}^0}{p_{rel_2}^0} \dots \frac{p_{rel_{end\ line}}^0}{p_{HOTGAS_x}} \right) \quad (4.57)$$

Now will be showed, by induction, that any pressure ratio  $\frac{p_{rel_{i+1}}^0}{p_{rel_i}^0}$  can be expressed as a function

of the reduced mass flow rate  $\frac{\dot{m}}{p_{rel_{end\ line}}^0} \sqrt{RT_{rel_{end\ line}}^0}$ .

For the principle of mathematical induction, a relationship that is true for the last couple of elements of the SAS line is also true for any other couple belonging to the SAS line itself, assuming that is true for its downstream couple: going from the last element, the blade flow function, to the first element, the compressor bleeding, it's possible to define a relationship between pressure ratio across the generic element and the mass flow rate reduced with the thermodynamic conditions of the end line element.

First  $\frac{p_{rel_{end\ line}}^0}{p_{rel_{end\ line-1}}^0} = f_{end\ line}^{-1} \left( \frac{\dot{m}}{p_{rel_{end\ line}}^0} \sqrt{RT_{rel_{end\ line}}^0} \right)$  for the last couple of elements is true for hypothesis B, after the drop of the unessential geometric factors. Here and in the following invertibility of all the  $f_i$  follows from the absence of any choking element before the blade root (physical design rule). Then we check:

$$\frac{p_{rel_i}^0}{p_{rel_{i-1}}^0} = f_{i-1}^{-1} \left( \frac{\dot{m}}{p_{rel_i}^0} \sqrt{RT_{rel_i}^0} \right) = f_{i-1}^{-1} \left( \frac{\dot{m}}{p_{rel_{i+1}}^0} \sqrt{RT_{rel_{i+1}}^0} \frac{p_{rel_{i+1}}^0}{p_{rel_i}^0} \right) \quad (4.58)$$

Where in the last step we assumed that  $T_{rel_{i+1}}^0$  is equal to  $T_{rel_i}^0$  times an unessential geometric factor from the rothalpy conservation, as visible from Eq. 4.53.

But for induction hypothesis  $\frac{p_{rel_{i+1}}^0}{p_{rel_i}^0}$  can be expressed as a function  $F_i$  of the reduced mass flow

rate  $\dot{m}_{red} = \frac{\dot{m}}{p_{rel_{end\ line}}^0} \sqrt{RT_{rel_{end\ line}}^0}$ . Hence it is obtained:

$$\frac{p_{rel_i}^0}{p_{rel_{i-1}}^0} = f_{i-1}^{-1}(f_{i-1}^{-1}(F_i(\dot{m}_{red})) F_i(\dot{m}_{red})) \quad (4.59)$$

It can be seen from eq. 4.59 that the pressure ratio across any generic element can be expressed as a function  $G_i$  of  $\dot{m}_{red} = \frac{\dot{m}}{p_{rel_{end\ line}}^0} \sqrt{RT_{rel_{end\ line}}^0}$  alone. Hence it can be written (Eq. T and 4.57) as:

$$G_1(\dot{m}_{red}) G_2(\dot{m}_{red}) \dots \dot{m}_{red} = h \left( \frac{1}{G_1(\dot{m}_{red})} \frac{1}{G_2(\dot{m}_{red})} \dots f^{-1}(\dot{m}_{red}) \right) \quad (4.60)$$

that can be made true for an appropriate choice of the function  $h$ .

Then the proved equation T holds, i.e. that the characteristic reduced mass flow rate of the

rotating branch can be expressed as a function of the pressure ratio  $\frac{p_{rel_{id\ end\ line}}^0}{p_{HOTGAS_x}}$  alone, with no additional dependence on swirl.

Furthermore it is assumed a single-valued functional relation between every  $p_{HOTGAS_x}$  and  $p_{abs_{turb\ inlet}}^0$  for what has been written in paragraph 2.1.7: the ratio of pressure in the turbine flow path on the turbine inlet absolute total pressure, has negligible variations in every working conditions of the gas turbine. More precisely, for a fixed turbine geometry and a given gas composition, the ratio  $\frac{p_{HOTGAS_x}}{p_{abs_{turb\ inlet}}^0}$  may depend on non-dimensional variables only, such as the

inlet reduced mass flow rate (or, alternatively, on the inlet Mach number which is just another way to write the same variable): this is the only relevant non-dimensional variable. For a set of conditions where turbine is nearly choked the inlet Mach number does not change too much.

Hence the ratio  $\frac{p_{HOTGAS_x}}{p_{abs_{turb\ inlet}}^0}$  (which depends only on the inlet Mach number) stays (almost) constant and the eq. (T) becomes:

$$\frac{\dot{m}}{p_{rel_{id\ end\ line}}^0} \sqrt{RT_{rel_{end\ line}}^0} = h \left( \frac{p_{rel_{id\ end\ line}}^0}{p_{HOTGAS_x}} \right) = i \left( \frac{p_{rel_{id\ end\ line}}^0}{p_{abs_{turb\ inlet}}^0} \right) \quad (4.61)$$

As conclusion, the choice of  $p_{rel_{id\ end\ line}}^0$  and  $T_{rel_{end\ line}}^0$  as normalization values for the rotating line characteristic allows to get the SAS network calculation results aligned along a single characteristic, which is a function only of a single pressure ratio: the basilar assumptions made in the development of this procedure have led to an uncontested simplification of the routine. The use of absolute total pressure as reference would lead to a cloud of points difficult to correlate with a single characteristic: unlike  $u_{extr\ pocket}$  and  $u_{end\ line}$ , the tangential velocity  $c_{\theta_{extr\ pocket}}$  is not the same for every operating point. Thus the couples  $p_{abs_{extr\ pocket}}^0$  and  $T_{abs_{extr\ pocket}}^0$ , are not enough to fix  $p_{rel_{id\ end\ line}}^0$  and  $T_{rel_{end\ line}}^0$  and hence the reduced mass

flow rate. It's easy to figure out, for example, two points with the same  $p_{abs\,extr\,pocket}^0$  and  $T_{abs\,extr\,pocket}^0$ , thus the same pressure ratio according to this definition of reduced mass flow rate using absolute pressures and temperatures at the extraction pockets, but with different tangential speeds  $c_{\theta\,extr\,pocket}$ , thus different reduced mass flow rates for the same pressure ratio. Due to the wide variations in the compressor velocity triangle, the “work” contribution

$$\frac{u_{end\,line}^2 - 2u_{extr\,pocket}c_{\theta\,extr\,pocket}}{2c_p} \quad (4.62)$$

must be calculated and subtracted specifically for each working point and cannot be included in the characteristics as a constant term for all the points. With the assumed definition relying on  $p_{rel\,id\,end\,line}^0$  and  $T_{rel\,end\,line}^0$  the “pumping effects” are already included and do not bring to an additional degree of freedom.

#### 4.7.2 External lines

The characteristic curve of an external line uses the following definitions:

$$\dot{m}_{red\,ext} = f(\beta_e) = f\left(\frac{p_{supply}^0}{p_{turb\,inlet}^0}\right) \quad (4.69)$$

$$\dot{m}_{red\,ext} \equiv \frac{\dot{m}_{ext}}{p_{supply}^0} \sqrt{RT_{supply}^0} \quad (4.70)$$

The considering supply pressure and temperature are the total pressure and total temperature of the turbine casing plenum downstream the regulating valves (Fig. 2.1).

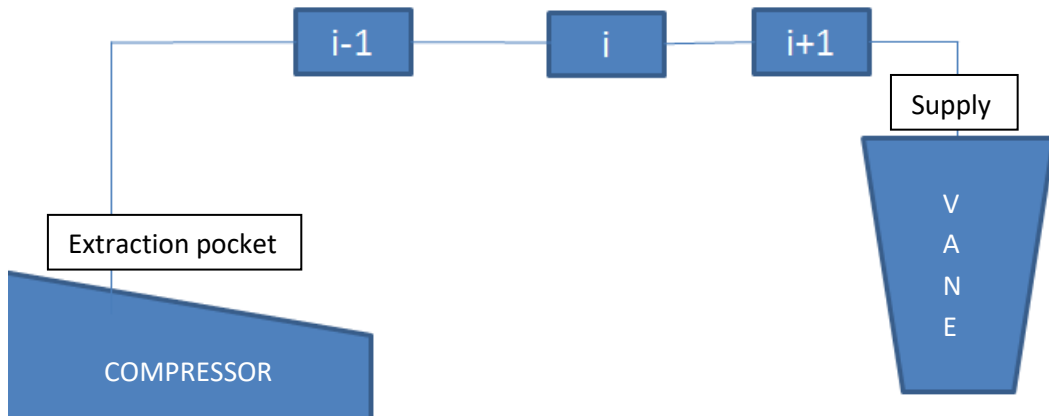


Fig. 4.7 - Scheme of a SAS external line

The pressure ratio is consequently made by the supply total pressure of the line over the total pressure at the turbine inlet. The external line characteristic may be seen as particular case of an internal line case with the blade speed  $\vec{u} = 0$ .

### 4.7.3 Pumping work

For the rotating lines the pumping work made on the fluid by entrainment can be computed apart in the work balance on the main shaft. This power consumption, at blade foot, can be estimated for the  $i^{\text{th}}$ -blade by:

$$P_{pumping_{SAS_i}} = \dot{m}_{extr\ blade_i} (h_{abs\ end\ line_i}^0 - h_{abs\ extr\ pocket_i}^0) \quad (4.71)$$

$$h_{abs\ end\ line_i}^0 = h_{abs\ extr\ pocket_i}^0 - swirl_{extr\ pocket_i} u_{extr\ pocket_i}^2 + swirl_{end\ line_i} u_{end\ line_i}^2 \quad (4.72)$$

$$P_{pumping_{SAS_i}} = \dot{m}_{extr\ blade_i} (swirl_{end\ line_i} u_{end\ line_i}^2 - swirl_{extr\ pocket_i} u_{extr\ pocket_i}^2) \quad (4.73)$$

This quantity will be used in the matching procedure inside the work balance on the turbine control volume

$$Turbine\ net\ power = Turbine\ gross\ power - \sum_{i=1}^{n_{blade}} P_{pumping_{SAS_i}} \quad (4.74)$$

### 4.7.4 Design of Experiments

As reported before, for this thesis project, every working condition thermodynamic values are derived from a base gas turbine engine simulation: in a real GT engine the values of pressure can be very variable, while the temperature values stay quite constant in every situations; because of this, the base working point temperatures are kept constant in every point simulated while the pressure one are modified. By design, in the turbine early stages, because of the choking conditions, the ratio between the turbine inlet pressure and the pressure measured at the stage flow path stays quite constant inside the possible working range: this behaviour allows the adoption of a constant ratio between the  $p_{turb\ inlet}^0$  and every boundary pressure for the turbine stages. A similar assumption will be used for the compressor pressure line, with an error greater than the turbine one as described in paragraph 2.1.7, but, for the early stages of the turbine, always acceptable: the pressure at the bleeding points will be considered linearly proportional to the compressor exit total pressure  $p_{comp\ outlet}^0$ . With these assumptions made, the two control factors for this simplified application are the two values of  $p_{comp\ outlet}^0$  and  $p_{turb\ inlet}^0$ : from these two pressure values a design of experiments has been tuned to explore the range of pressure ratio in which a real GT engine would lie, six different test points are tested following the test matrix here below that report the values of the coefficients used to scale  $p_{comp\ outlet}^0$  and  $p_{turb\ inlet}^0$

Tab. 4.1- Test matrix coefficients

	TP1	TP2	TP3	TP4	TP5	TP6
$p_{comp\ outlet}^0$	1x	1.05x	1x	0.9x	0.7x	0.65x
$p_{turb\ inlet}^0$	1x	1.05x	0.9x	0.8x	0.6x	0.4x

The first working point (TP1) is the base point, in which every values of pressure and temperature are known in both the compressor and turbine flow paths: from this working point, the ratios between the  $p_{comp\ outlet}^0$  and  $p_{turb\ inlet}^0$  and every other boundary conditions are derived. The number of working points (6) has been chosen after a sensitivity analysis, evaluating the time required and the tolerance requested.

#### 4.7.5 Characteristic Curves Post Processing

To generate the characteristic curves an excel file is used: the 6 conditions' results ( $\dot{m}, p, T, c_\theta$ ) are imported and a macroinstruction associates the elements' values to the corresponding characteristics. Then the reduced mass flow rates and driving pressure ratios are computed. For an easy data transmission a 5<sup>th</sup> order polynomial fitting curve is used to interpolate the flow function: this curve will be interrogated during the matching procedure.

$$\dot{m}_{red} = A_0 + A_1(\beta_x) + A_2(\beta_x)^2 + A_3(\beta_x)^3 + A_4(\beta_x)^4 + A_5(\beta_x)^5 \quad (4.75)$$

$$\beta_x = \begin{cases} \beta_{external} \\ \beta_{internal} \end{cases} \quad (4.76)$$

## 5. Fluid Network Assembly

In the following chapter the building procedure of the SAS fluid network of an imaginary Gas Turbine engine, developed for this thesis application and not based on any real GT engine, and of its characteristic curves will be discussed: because the method applied is the same for all the vane and blade rows only the assembling of the 2<sup>nd</sup> turbine stage SAS lines will be analysed. Almost all the element correlations used for this project, according to the best SAS design guide lines, use empirical experiments for incompressible flow: for low Ma number flows the compressibility effects are negligible and the incompressible flow resolution results much easier than the compressible one. The correlations implemented inside the elements will be described in the present chapter: the terms inlet and outlet will here be used to define the first and the last node of the three nodes element.

### 5.1 Internal line assembling

Starting from the example of Fig. 2.1 the internal rotating line that supplies the 2<sup>nd</sup> Turbine blade row is called Internal Circuit 2 (IC2): the bleeding is located in the last stages of the compressor to ensure the proper pressure gradient between the compressor and the turbine. The boundary element IC2 simulates the static pressure and total temperature at the bleeding point, while a dedicated CT element (B202) simulates the tangential velocity at the bleeding point through a swirl coefficient, that is kept constant for every working conditions here tested.

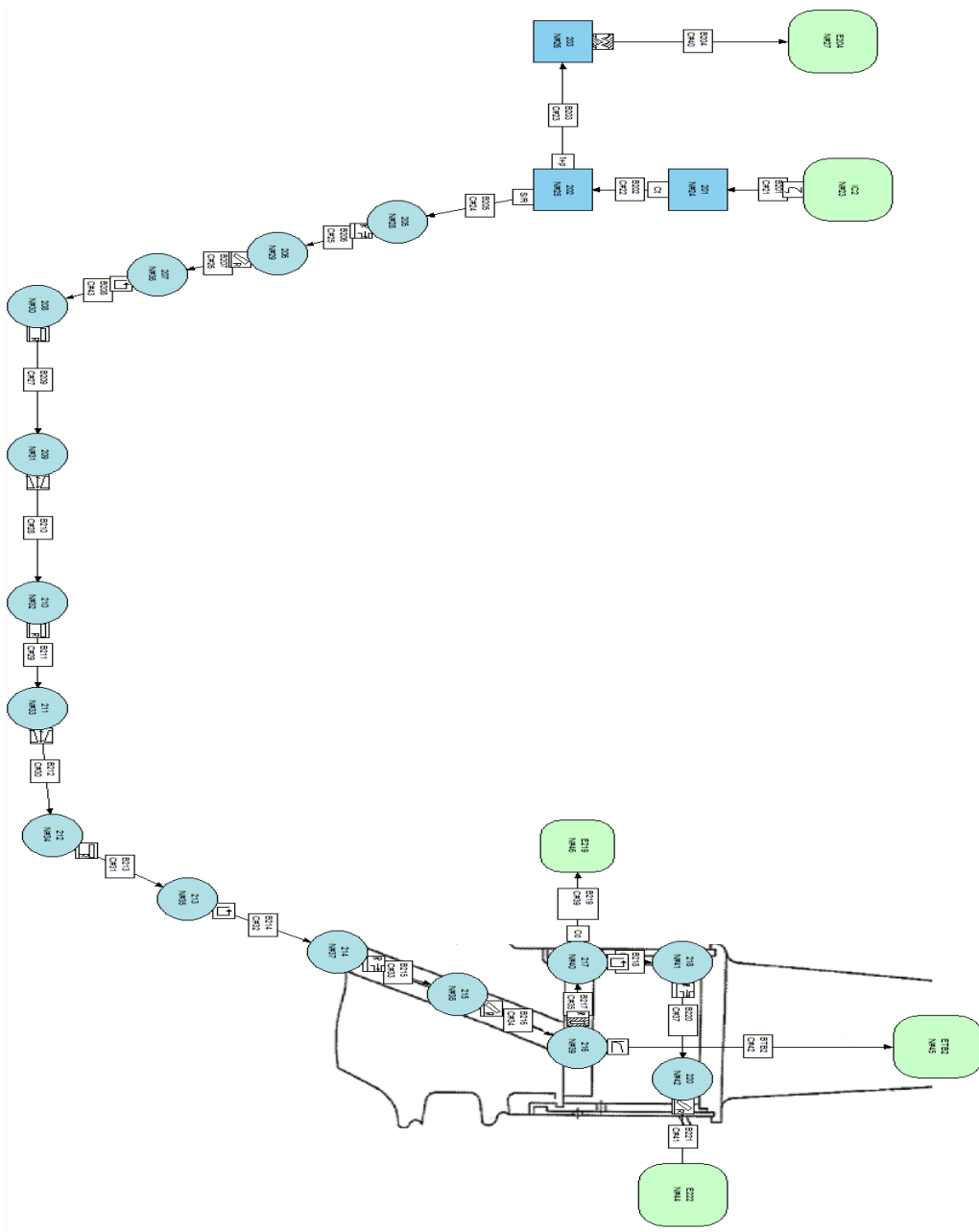
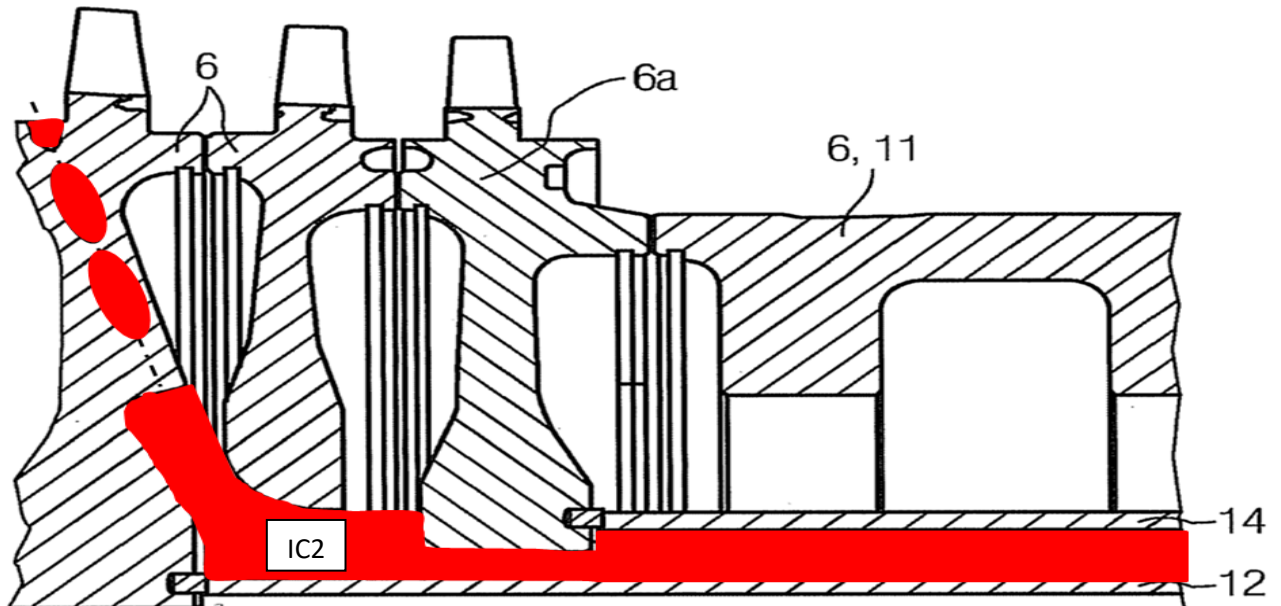


Fig. 5.1 - Detail of the internal line fluid network



*Fig. 5.2 - Detail of an internal line extraction*

The example engine is characterized with the bleeding point placed in the rotor part of the compressor, after a compressor vane trailing edge, to achieve the highest value of static pressure in the row (Fig. 5.2): because of this specific example engine design, the sealing flow between the compressor vane and the rotating disk must be modelled because the pressure gradient between the compressor vane leading and trailing edge is not negligible. This leakage is here limited by a labyrinth seal, that in this fluid net is modelled in the block B204. Successively the air enters in specific channels drilled in the rotating disk: the reference frame must pass from the absolute to the relative one and this happens inside the Absolute To Relative (Stator/Rotor) element. The Absolute To Relative (S/R) element operates maintaining unchanged between the inlet and the outlet both the mass flow rate, the static pressure and the swirl ratio but changing the total temperature from the absolute to the relative one:

$$T_{rel\,outlet}^0 = T_{abs\,inlet}^0 - \frac{u^2}{2c_p} + \frac{u^2 \, sw_{inlet}}{c_p} \quad (5.1)$$

The channels, drilled in the rotating disks upstream a cavity between the central rotating shaft and the disk are modelled as rotating inlets and pipes: in the simplest cases these channel are oriented alongside the radial direction but, for this application, the channels also have a radial angle to minimize the relative velocity between the cooling flow and the central shaft tangential speed, because a great mismatch between the cooling flow and the central shaft tangential velocities may lead to heavy pressure losses, turbulence and unwanted vibrations of the mechanical components.

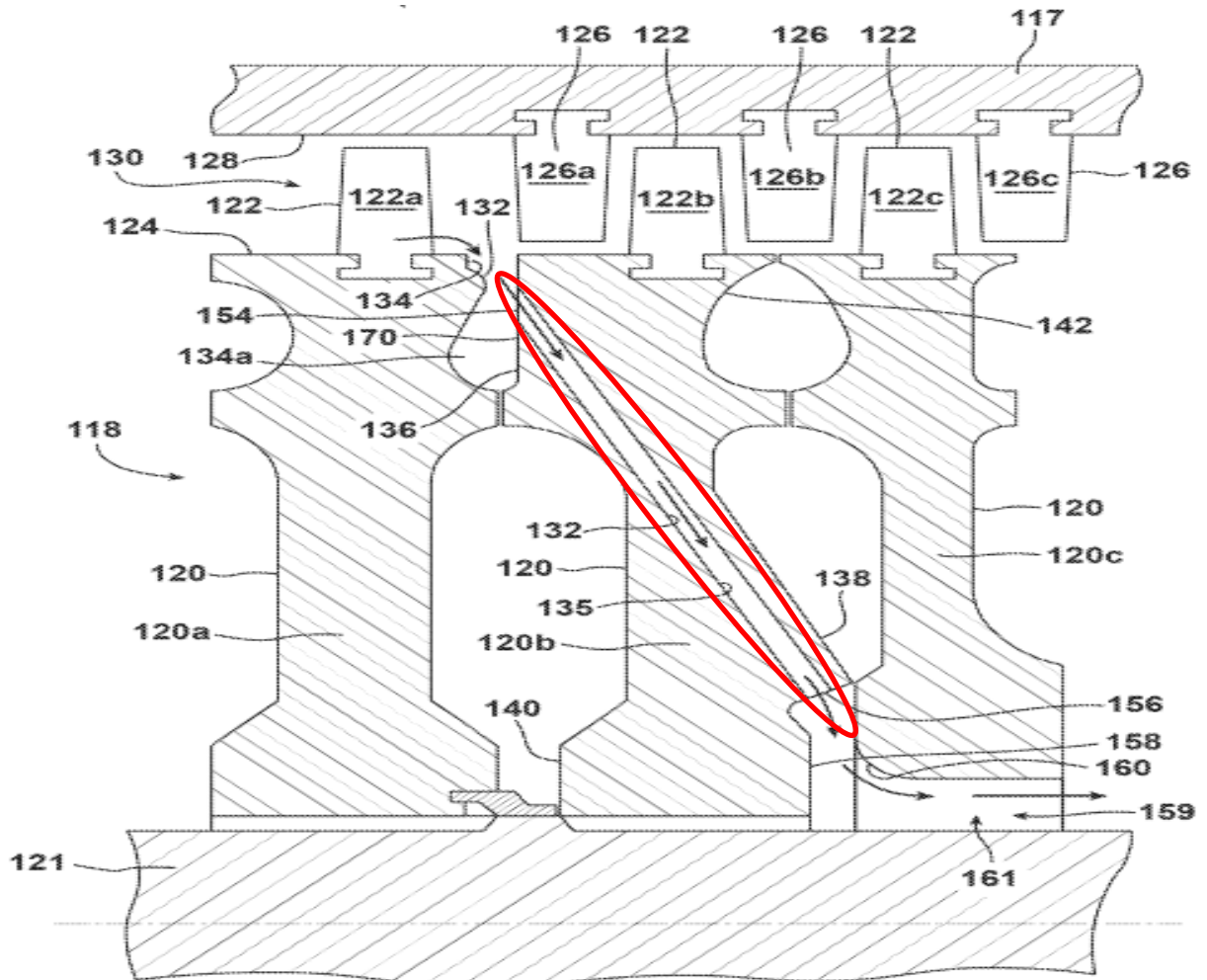


*Fig. 5.3 - Detail of a compressor extraction pocket*

The element rotating inlet is based on correlations proposed by McGreehan and Schotsch [20]: the correlations takes in account various different effect on the discharge coefficient of the rotating inlet such as the inlet fillet radius, the Reynolds number, the axial extension of the bore and the relative tangential component of velocity. The element rotating pipe uses correlations proposed by Reichert, Brillert and Simon [21]: these correlations consider various effects such as circumferential velocity component, friction, flow separation and geometrical effects. The rotation of a passage typically used in a gas turbine SAS has two main effects: firstly there is generally a not symmetric inlet flow pattern at the passage inlets, this has pronounced effect on the entrance losses; secondly strong bending forces are required to give the flow the circumferential velocity of the bores, these forces result in a change of total pressure as a function of the work transmitted to the fluid. For typical applications in Secondary air systems of a gas turbines, the effects of secondary flow patterns in bores are supposed to play a minor role in terms of the generation of total pressure losses. The flow bending forces at the entrance of the bore on the one hand lead to a large pressure difference across the entrance cross section: this bending of the flow occurs if the circumferential velocities of the flow and of the bores differ significantly. Common use piping inside the rotating disks are characterised with exit

strong velocity asymmetries in comparison of a fully developed velocity profile in a long piping: these flow distortions lead to total pressure loss in addition to the separation and friction ones that need to be considered.

$$p_{rel_{id_{outlet}}}^0 - p_{rel_{outlet}}^0 = p_{rel_{inlet}}^0 \left( 1 + \frac{u_{outlet}^2 - u_{inlet}^2}{2c_p T_{rel_{inlet}}^0} \right)^{\frac{k}{k-1}} - p_{rel_{outlet}}^0 = \zeta \frac{|\dot{m}|\dot{m}}{2\rho_2 N^2 S^2} \quad (5.2)$$

$$sw_{outlet} = 1 + \frac{c_{u_{outlet}}}{u} \frac{\dot{m}}{\rho NS} \quad (5.3)$$

$$T_{rel_{outlet}}^0 = T_{rel_{inlet}}^0 + \frac{u_{outlet}^2 - u_{inlet}^2}{2c_p} \quad (5.4)$$

Where  $N$  is the number of elements in parallel,  $S$  is the single element cross sectional area and  $c_u$  is the circumferential projection of the pipe directional unit vector: the last value is used when the rotating pipe is not oriented along the radial or the axial directions.

$$D_{hydro} = \sqrt{\frac{4Area}{perimeter}} \quad (5.5)$$

$$Re_D = \frac{D_h \dot{m}}{NS0.6\mu} \quad (5.6)$$

$$\lambda_f^{[24]} = \left( -\frac{1.8 \ln \left[ \left( \frac{\varepsilon}{3.7D_h} \right)^{1.11} + \frac{6.9}{Re_D} \right]}{\ln 10} \right)^{-2} \quad (5.7)$$

$$f_{v,D} = \min \left[ \max \left[ \frac{(\sqrt{\lambda_f} + 2)(\sqrt{\lambda_f} + 1)}{2}, 0 \right], 4 \right] \quad (5.8)$$

$$f_{p,D} = \min \left[ \max \left[ f_{v,D}^3 \frac{2}{(3\sqrt{\lambda_f} + 2)(3\sqrt{\lambda_f} + 1)}, 0 \right], 4 \right] \quad (5.9)$$

$$\zeta = \frac{\lambda_f L}{D_h} + f_{p,D} \quad (5.10)$$

For this thesis project, the tangential velocity distribution inside the cavity has been modelled as a free vortex distribution: this simplifying assumption comes from the fluid analysis. The fluid motion inside these cavities is heavily dominated from the radial through-flow velocity condition, therefore the entrainment of the fluid from the rotating walls can be neglected: the neglecting of any pumping work inside these cavities lead to a fluid motion that can be approximated, with a very small error, to a free vortex distribution of tangential velocity

$$c_{\theta}r = \text{constant} \quad (5.11)$$

The element CAVITY implements a radial equilibrium based on the integration of the Euler equation, neglecting viscosity and radial velocity: the differential equation is integrated with the simplifying assumption of constant total temperature, that is considered to be the sum of the static temperature and the tangential kinetic energy contribution (incompressible flow), and polytropic flow.

$$\frac{dp}{dr} = \frac{\rho c_{\theta}^2}{r} \quad (5.12)$$

At the end of the cavity the flow enters in a rotating circular crown shaped pipe: this geometry is a trade-off compromise to fulfil both the structural requisites both the aerodynamic requisites. The inlet and the outlet of this duct are associated with a sudden enlargement and a sudden restriction leading to concentrated total pressure losses that must be evaluated by the element CONTRACTION-ENLARGEMENT (B210 and B212) that model both the contraction both the enlargement: this element includes a concentrated total pressure drop (Eqs. 5.13-5.14) based on Idel’Cik [22] correlations, a correction of the outlet swirl coefficient based on the mean radius change between inlet and outlet (5.15), and the conservation of rothalpy to evaluate the outlet total temperature (Eq. 5.16).

$$p_{rel\,id\,outlet}^0 - p_{rel\,outlet}^0 = p_{rel\,inlet}^0 \left( 1 + \frac{u_{outlet}^2 - u_{inlet}^2}{2c_p T_{rel\,inlet}^0} \right)^{\frac{k}{k-1}} - p_{rel\,outlet}^0 = \zeta \frac{|\dot{m}| \dot{m}}{2\rho_2 N^2 S^2} \quad (5.13)$$

$$\zeta = \left( 1 + 0.707 \sqrt{1 - \frac{A_0}{A_1} - \frac{A_0}{A_2}} \right)^2 \quad (5.14)$$

$$sw_{outlet} = \frac{sw_{inlet} r_{inlet}}{r_{outlet}} \quad (5.15)$$

$$T_{rel\,outlet}^0 = T_{rel\,inlet}^0 + \frac{u_{outlet}^2 - u_{inlet}^2}{2c_p} \quad (5.16)$$

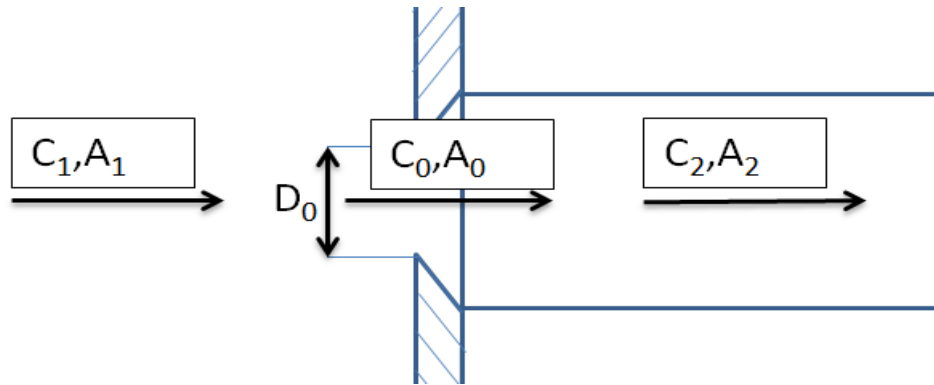


Fig. 5.4 - Scheme of a thin plate sharp edged orifice geometry

After this duct the flow is forced in the radial direction toward the external by centrifugal forces inside the cavity and the channels obtained in the turbine disks, similarly to the compressor ones: these ducts reach a specific plenum obtained from the blade root and, from this plenum, the cooling and the sealing flows are injected in the turbine main flow. Because of this ‘symmetry’ the modelling of the cavity and of the channels is done with the same compressor disk elements (B214-B215-B216), with the corrected geometrical data, that are different.

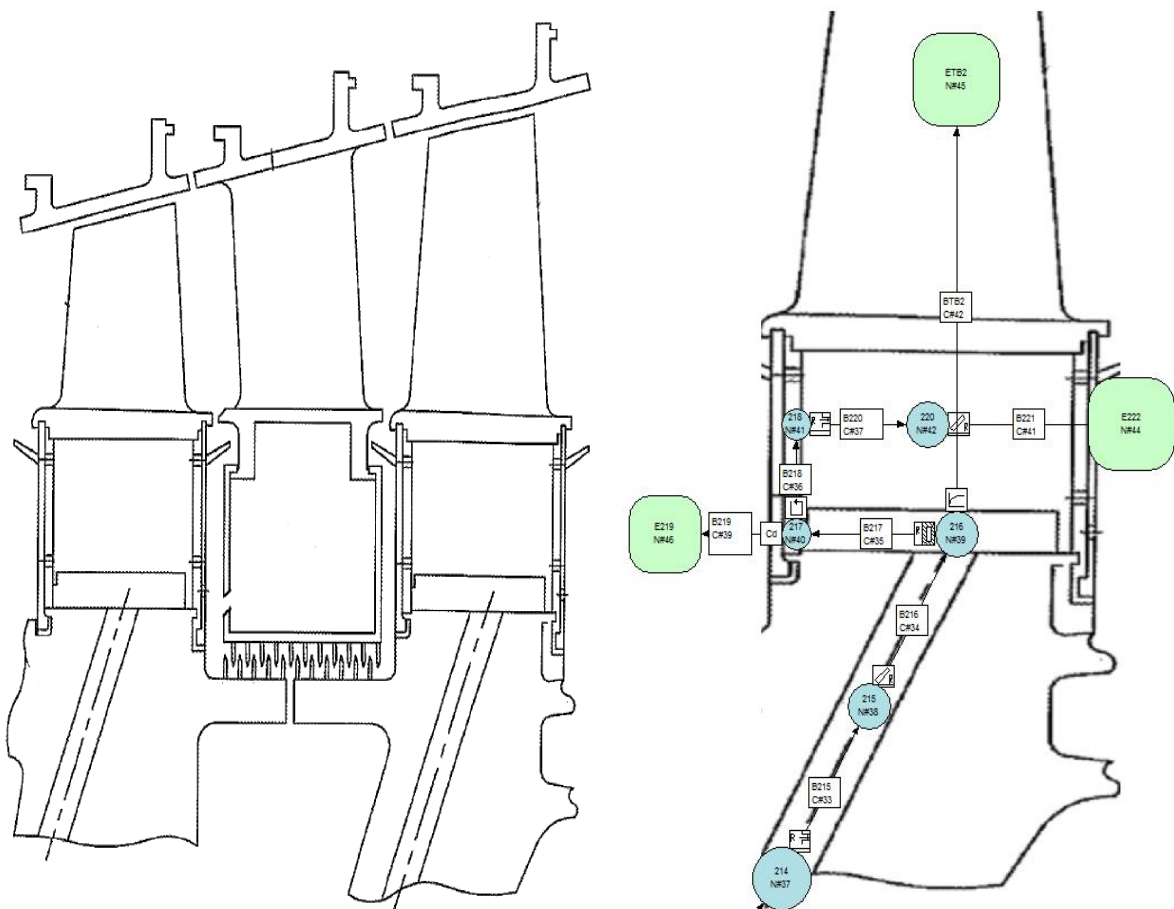


Fig. 5.5 - Blade cooling channel scheme and fluid network modelling

From the blade root plenum the major part of the SAS line flow rate is driven through the blade internal cooling channel: as described before the blade is modelled as a flow function of the ratio between the total pressure of the blade root, that in the plenum is considered equal to the static one, and the total pressure of the turbine main flow. This flow function is implemented in the FLOWFUNCTION element (BTB2): values of swirl coefficient and Total relative temperature are considered constant along the element while the mass flow rate is calculated from the reduced mass flow rate that is function of the pressure ratio. Once this single value of cooling mass flow rate is calculated, according to the nomenclature illustrated in paragraph 4.7 and according to the blade cooling channel outlet bore locations, 2 constant split coefficients are used to split this mass flow rate value in 2 specific contributes: IC2\_TB2\_COOL\_PRE\_MID and IC2\_TB2\_COOL\_POST\_MID; for this thesis application the 2 values used are

$$\frac{IC2\_TB2\_COOL\_PRE\_MID}{IC2\_TB2\_COOL} = \frac{1}{5} \quad (5.17)$$

$$\frac{IC2\_TB2\_COOL\_POST\_MID}{IC2\_TB2\_COOL} = \frac{4}{5} \quad (5.18)$$

The remaining flow rate, that will be briefly called leakage flow, passes in an equivalent SAS circuit schematised in Fig. 5.5. For construction issues the front part of the blade, near the hub region, has an open gap, from which the leakage air flows: this opening in a rotating frame may be seen has a concentrated pressure loss or as a thin rotating orifice. The solution, in this thesis, is to use an element called ROTATINGSLIT that implements the correlations for a compressible flow in a thin orifice using the inlet total relative pressure, instead of the static pressure, as an input: therefore the equations implemented in the element are the same as the CD element, that will be analysed in detail in the next chapter of this document, with the only change in the pressure inlet value. After the rotating slit the flow experiences a split: to simulate the leakage flow below the sealing element in Fig. 5.5 a CD element (B219) with the discharge coefficient  $C_d$  equal to 0.6 has been used, as discussed in the next chapter: this flow, according to the nomenclature procedure illustrated in paragraph 4.7, will be called IC2\_TB2\_LEAK\_PRE\_HUB. The remaining leakage flow rate passes through a rotating cavity (B218), between the blade root and the sealing element: this flow has been simulated, according to the previous practice, with a free vortex tangential velocity distribution, with a total relative pressure recovery due to pumping work. The air is then lead through the fir tree gaps (Fig. 5.6): these gaps, because their important axial extension and their strong 3 dimensionality flow effects, can't be easily modelled as thin orifices because the usage of a CD element would request a validation campaign to determine the exact  $C_d$  value to be implemented. For this thesis application, the rotating inlets and rotating pipes elements (B220 and B221) have been used to simulate this leakage flow that will be called IC2\_TB2\_LEAK\_POST\_HUB: known the cross sectional area, the inclination of the disk mounting and the bore length an equivalent rotating pipe is generated and the element equations are calculated.

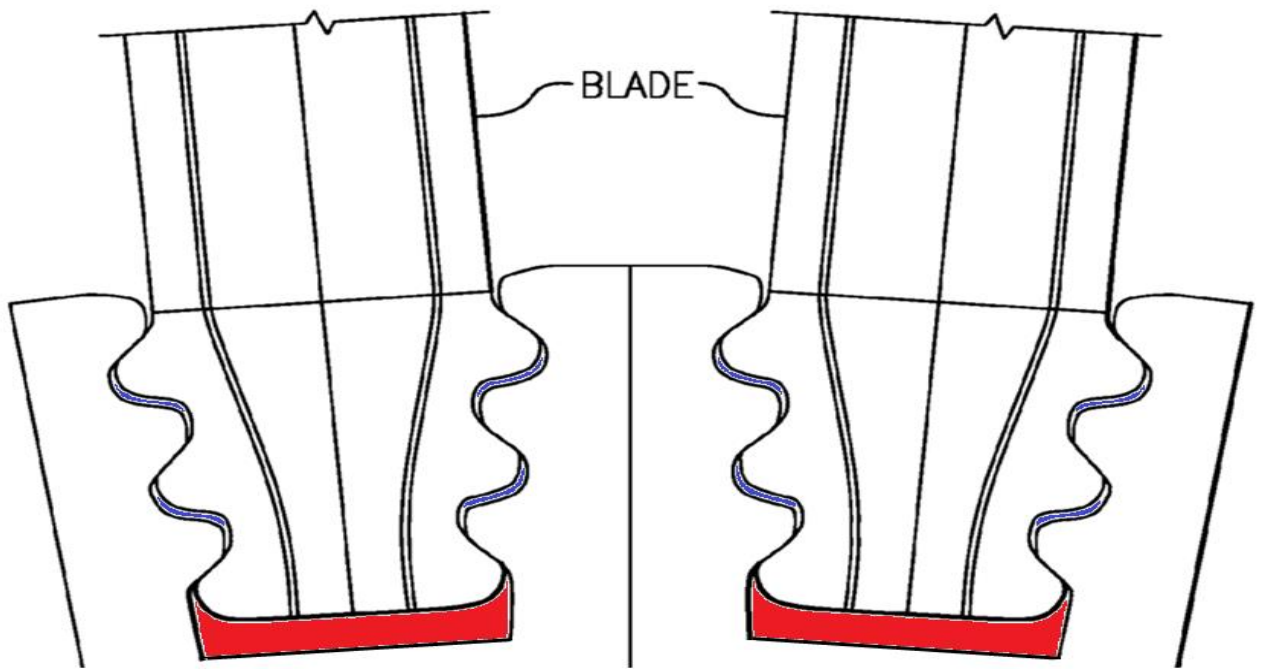


*Fig. 5.6 - Blade mounting with rotating slit (red) and fir tree area (blue)*

## **5.2 External line assembling**

The external line design of a GT engine's SAS, due to the lack of strict structural constraints, relatively to the internal line's, is oriented to the efficiency and to the control of the flow rate bled from the operating machine: the essential component of the 2<sup>nd</sup> vane row supply line is the regulating valve that reduces the variations of the pressure ratio seen by the vane cooling channel. The external line for the 2<sup>nd</sup> turbine row (EC3) starts from a dedicated plenum obtained in the compressor outer casing: from here 2 equal pipes exit from the casing and lead the flow to the turbine stages. In the external lines the choice of the piping diameters are lead from cost and safety criteria: standard UNI pipes are used for all the first part of this line. For this particular thesis application the pipe diameter of choice for EC3 was an 8 inches diameter stainless steel pipe: two additional 90° bends, made with the same 8" diameter pipe used for the rest of the line, are installed to direct the flow radially in the turbine casing.

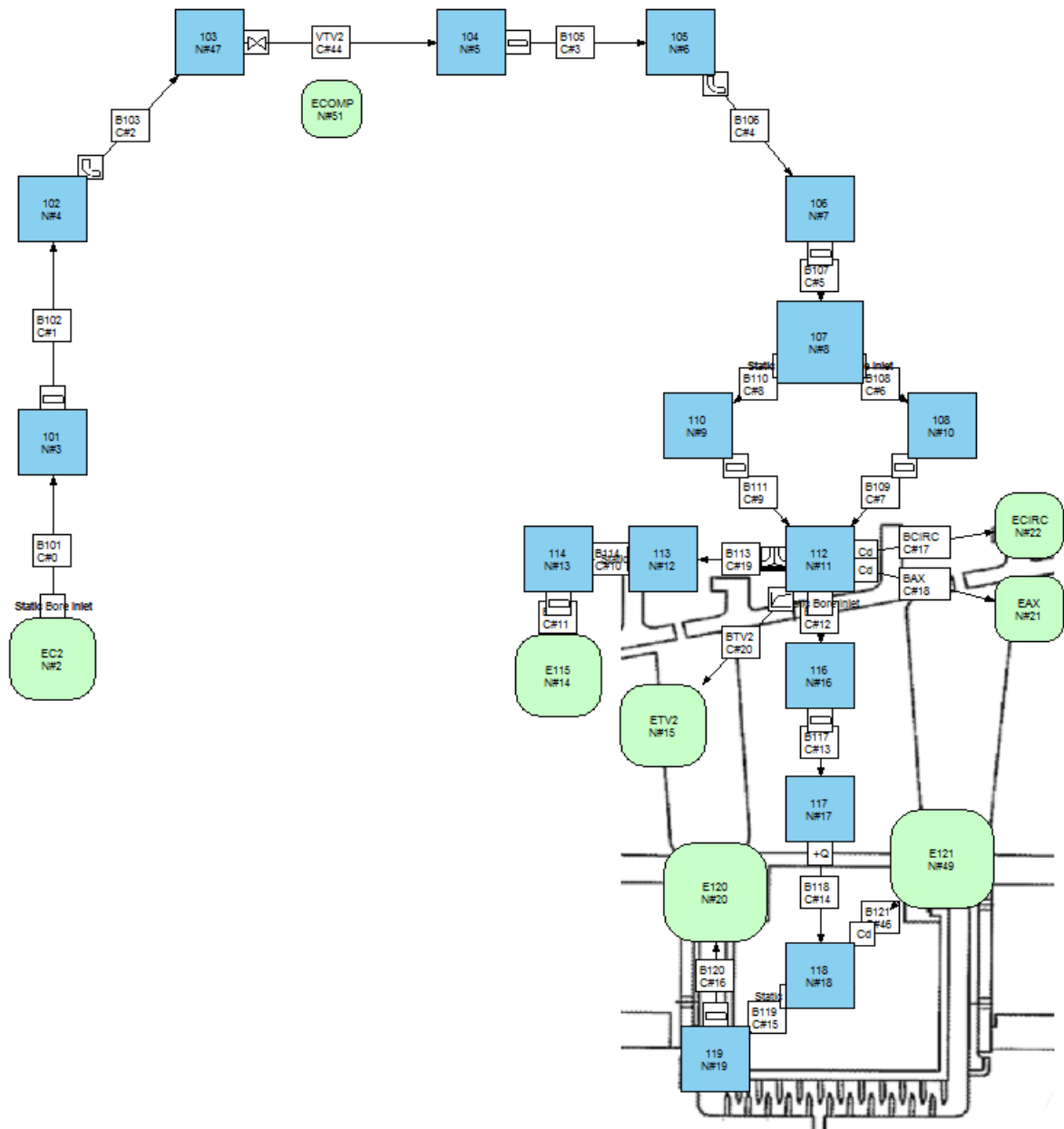


Fig. 5.7 - Detail of the external line fluid network

The elements used to simulate the pipe are the element StaticBoreInlet (B101) and the element PIPE (B102, B105 and B107), while the bend is modelled by the element BEND (B103 and B106): all these elements have implemented correlations for pressure losses based on incompressible flow, every compressibility effects, that in the internal line may be present due to the necessary structural compromises, in the external lines are absent. Some empirical corrections are applied to this elements following the correlations proposed by Idel’Cik [22]: for the StaticBoreInlet the inlet flow is assumed to be still, with the static inlet pressure equal to the inlet total pressure

$$p_{abs_{inlet}}^0 - p_{abs_{outlet}}^0 = p_{inlet} - p_{abs_{outlet}}^0 = \zeta \frac{|\dot{m}|\dot{m}}{2\rho_2 N^2 S^2} \quad (5.19)$$

$$SW_{outlet} = SW_{inlet} \quad (5.20)$$

$$T_{outlet}^0 = T_{inlet}^0 \quad (5.21)$$

With  $\zeta$  the Idel'Cik [22] correction factor defined as the sum of two correction contributes given by the inclination of the bore and by the inlet fillet radius

$$\zeta = \zeta_{angle} + \zeta_{fillet} \quad (5.22)$$

$$\zeta_{angle} = 0.5 + 0.3 \cos\delta + 0.2 \cos^2 \delta \quad (5.23)$$

$$\zeta_{fillet} = 1.0185 - 16.578 \frac{r}{D} + 97.044 \left(\frac{r}{D}\right)^2 - 193.99 \left(\frac{r}{D}\right)^3 \quad (5.24)$$

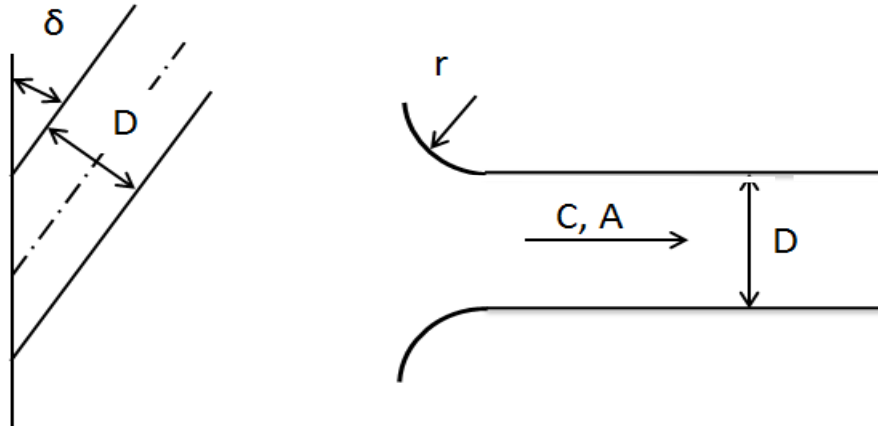


Fig. 5.8 - Pipe geometry schematization

A similar model is applied for the element PIPE:

$$p_{abs_{inlet}}^0 - p_{abs_{outlet}}^0 = (\zeta_{distr} + \zeta_{conc}) \frac{|\dot{m}|\dot{m}}{2\rho_2 N^2 S^2} \quad (5.25)$$

$$SW_{outlet} = SW_{inlet} \quad (5.26)$$

$$T_{outlet}^0 = T_{inlet}^0 \quad (5.27)$$

Where  $\zeta_{conc}$  and  $\zeta_{distr}$  are obtained respectively from Idel'Cik's and Moody's correlations [22] [23] for exit concentrated losses and distributed losses for turbulent flows

$$\zeta_{conc} = \frac{(2m + 1)^3 (m + 1)^3}{4m^4 (2m + 3) (m + 3)} \quad (5.28)$$

$$\zeta_{distr} = \frac{f_D L}{D} \quad (5.29)$$

$$f_D^{[25]} = \frac{1.325}{\left[ \ln \left( \frac{\varepsilon}{3.7D} + \frac{5.74}{Re^{0.9}} \right) \right]^2} \quad (5.30)$$

For this thesis the standard value for m used is 5 so

$$\zeta_{conc} = 1.105754 \quad (5.31)$$

The element BEND uses the same distributed losses of the element PIPE, the Darcy factor approach, and a concentrated loss coefficient provided by Idel’Cik [22]

$$p_{abs_{inlet}}^0 - p_{abs_{outlet}}^0 = (\zeta_{distr} + \zeta_{conc}) \frac{|\dot{m}|\dot{m}}{2\rho_2 N^2 S^2} \quad (5.32)$$

$$SW_{outlet} = SW_{inlet} \quad (5.33)$$

$$T_{outlet}^0 = T_{inlet}^0 \quad (5.34)$$

$$\zeta_{conc} = 2\zeta_M + \zeta_f \quad (5.35)$$

$$\zeta_M = \frac{0.21}{\sqrt{\frac{Re_D}{D_h}}} \quad (5.36)$$

$$\zeta_f = \frac{0.0175 \lambda Re}{D_h} \quad (5.37)$$

$$\lambda = \frac{1}{(1.8 \ln Re - 1.64)^2} \quad (5.38)$$

After the 1<sup>st</sup> bend the regulating valve is placed in position: this element (VTV2) is used to impose the pressure at a chosen node. The element uses a characteristic curve for the valve capacity ( $K_v$ ) in terms of the valve opening angle ( $\alpha$ ) that is supplied from the valve manufacturer: when the valve position is within the range 0-100%, the element sets the static pressure at a given node to a value which is a given percentage of the static pressure at a given reference node. When the valve is at full range the boundary nodes are set the same static pressure.

$$p_{set\ node} = f_{\%} p_{reference\ node} \quad (5.39)$$

$$K_v = 10 \frac{\dot{m}}{\sqrt{\rho(p_{inlet} - p_{outlet})}} 3600 \quad (5.40)$$

$$\alpha = f(K_v) \quad (5.41)$$

$$SW_{outlet} = SW_{inlet} \quad (5.42)$$

$$T_{outlet}^0 = T_{inlet}^0 \quad (5.43)$$

For this thesis application the pressure set node has been imposed as the node 107 that models the turbine outer casing pocket: this choice comes from the relative easiness of placing, in a real plant application, a pressure sensor in this location that is not interested by pressure fluctuations or by high temperature values. The reference node is set in an auxiliary node (ECOMP) that mimics the compressor exit values in all the 6 test conditions, while the percentage of static pressure  $f\%$  is fixed at 60%. From this outer casing plenum (B107) the air is driven through the inner casing inside 2 separate channels: these 2 channels, that are modelled with 2 StaticBoreInlet (B108 and B110) and 2 pipes (B109 and B111) elements, have cooling effects on the metallic casing, that are not considered in this fluid net. The 2 flow rates mix in a plenum located just above the turbine vane.

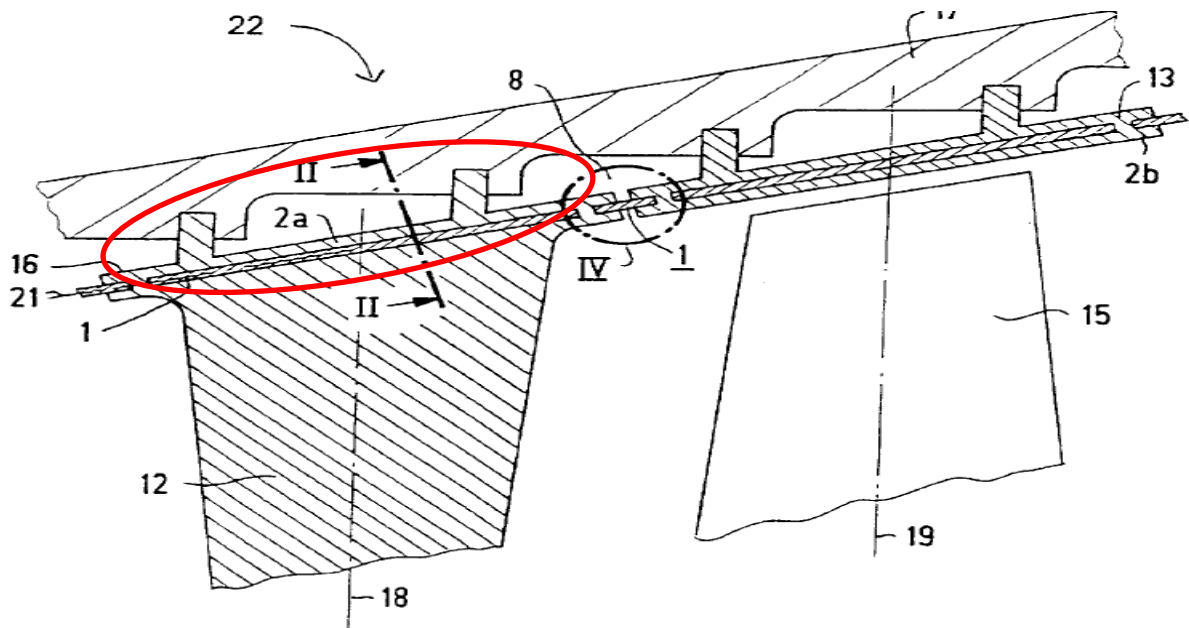
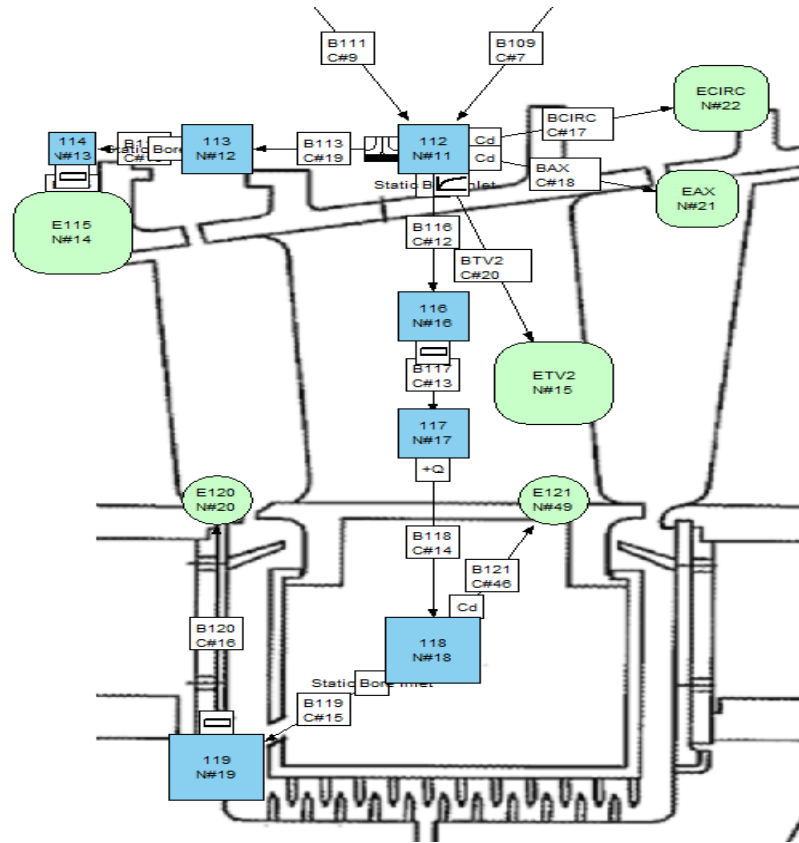
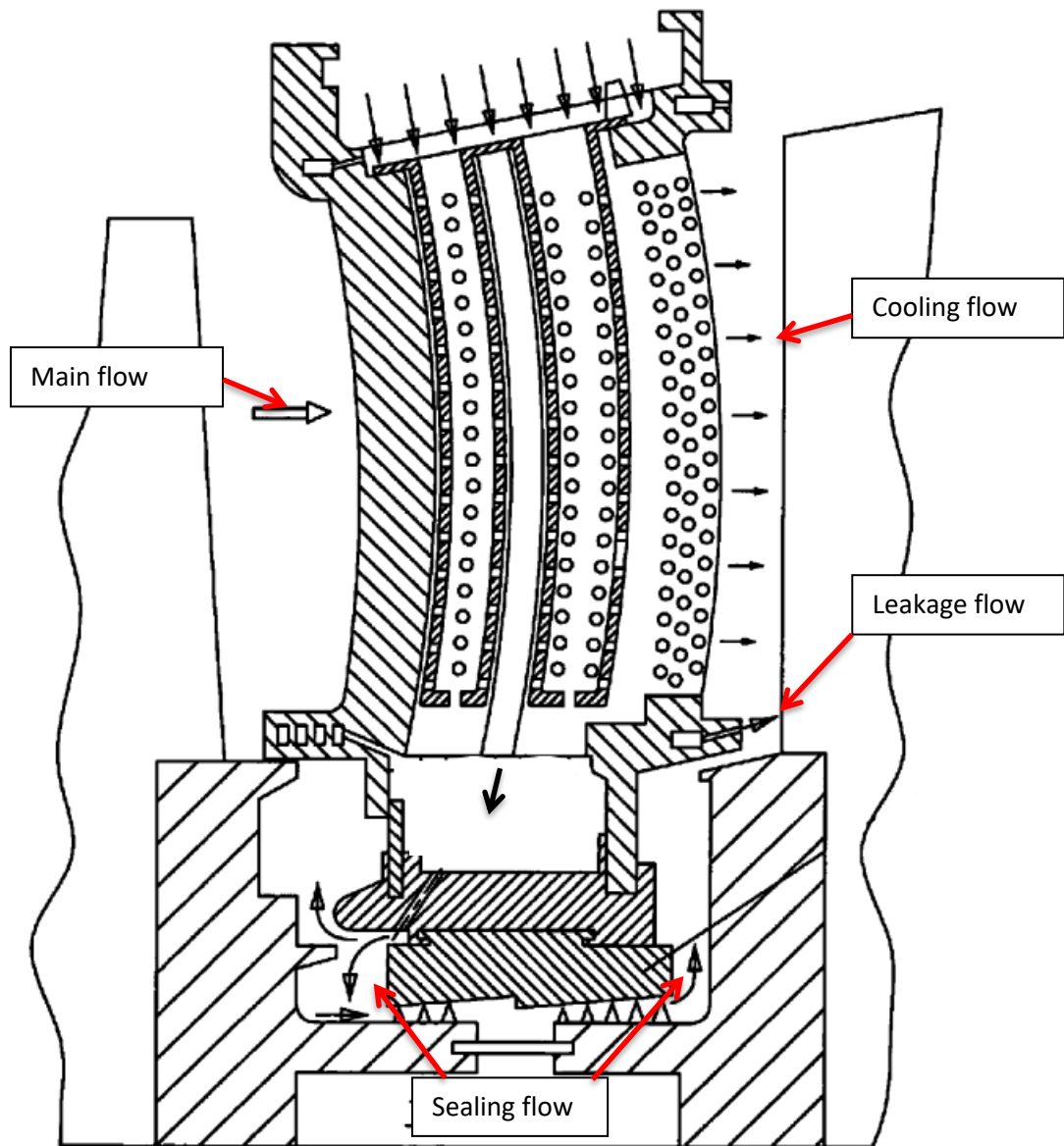


Fig. 5.9 - Detail of the vane tip plenum



*Fig. 5.10 - Fluid network vane schematization*

From this plenum (112) 5 flow rates are simulated: 1 for the vane shroud cooling, 1 for the vane cooling, 2 for tip leakage flows and 2 for the hub leakage flows. According to the blade modelling, the vane cooling flow rate is simulated with a FLOWFUNCTION element (BTV2) that expresses the cooling reduced mass flow rate in terms of the driving pressure ratio. The turbine vane however is designed differently from the turbine blade: the vane presents a structural element at the hub region called vane box in which a flow rate coming from the tip plenum, after the passage inside the vane cooling channel, is redirected to seal the rotor-stator cavities upstream and downstream.



*Fig. 5.11 - Example of turbine vane and SAS flows*

The portion of vane channel that lead the flow to the vane box is represented, according to the previous modelling, as the series of a StaticBoreInlet (B116) and a pipe element (B117). As described in 4.7, for this application, only the flow rate that passes through the cooling bores is called cooling flow rate and the remaining is called leakage flow rate, but the flow rate that passes through the vane cooling channel and reaches the vane box also contributes to the cooling effect, incurring in a temperature increase that is not negligible: a specific element called HeatConnection is implemented to impose a given temperature pick up.

$$T_{abs\,outlet}^0 = T_{abs\,inlet}^0 + \Delta T \quad (5.44)$$

From the vane box 2 flows are modelled: a sealing flow that leaves the box through a designed bore in the box upstream wall and a leakage flow that leaves the box by some clearance gaps. The box bore is modelled by the elements StaticBoreInlet (B119) and pipe (B120), while the flow between the clearance gaps is modelled by a CD element. The sealing flow, as visible in Fig. 5.11, is divided in a contribute upstream the vane and a contribute downstream: for the characteristic curves production this behaviour implies the use of 2 coefficients that split the flow rate passing in the vane box bore in 2 different flow rates located one upstream the vane throat and one downstream the throat; these split values (0.2 per the upstream flow and 0.8 for the downstream), kept constant for all the working conditions, are an approximation and need to be tuned with CFD studies or with experimental data. The element  $C_d$ , that is used to model 3 different leakage flows in the vane region and another leakage flow in the blade region, implements correlations for the adiabatic compressible flow through an orifice [26]: considering the mass flow rate and the total temperature constant and an upstream isentropic flow ( $\frac{p}{\rho^k} = constant$ ) it is possible to write the next equation:

$$\frac{\dot{m} \sqrt{RT_{absinlet}^0}}{C_d A p_{absinlet}^0 \sqrt{k}} = \sqrt{\frac{2}{(k-1)} \left( \frac{p_{absoutlet}^0}{p_{absinlet}^0} \right)^{\frac{2}{k}} \left( 1 - \left( \frac{p_{absoutlet}^0}{p_{absinlet}^0} \right)^{\frac{k-1}{k}} \right)} \quad (5.45)$$

Assuming that  $\frac{p_{absoutlet}^0}{p_{absinlet}^0}$  is being decreased starting from the unitary value: the above equation will result in an increasing mass flow rate up to a maximum for

$$\frac{p_{absoutlet}^0}{p_{absinlet}^0} = \left( \frac{2}{k+1} \right)^{\frac{k}{k-1}} \quad (5.46)$$

after which the mass flow rate starts to decrease. In reality, the decrease does not happen and the mass flow rate remains constant: indeed at the maximum of reduced flow rate sonic conditions are reached.

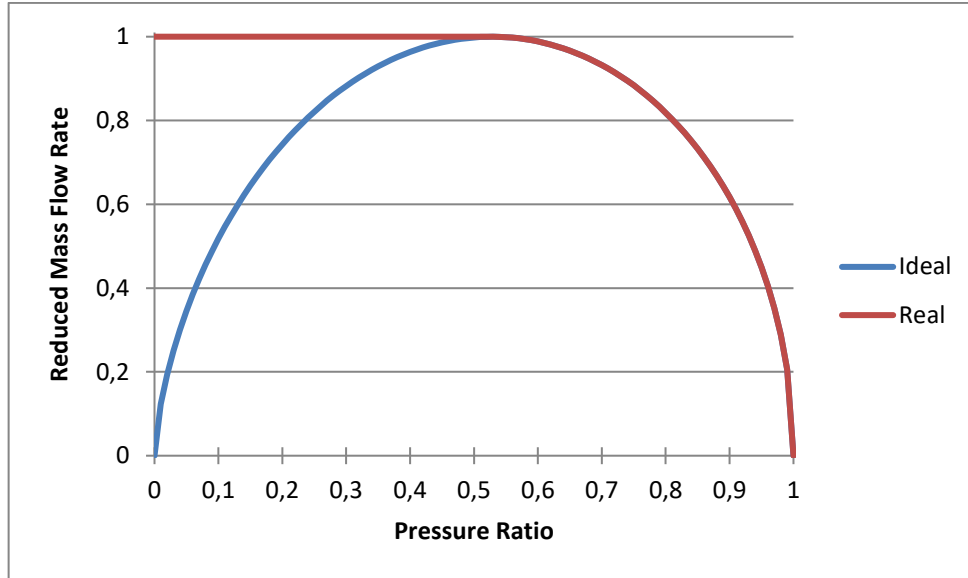


Fig. 5.12 - Compressible orifice ideal (blue) and real reduced mass flow rates (red)

For lower values of  $\frac{p_{abs\,outlet}^0}{p_{abs\,inlet}^0}$  the flow is supersonic, which means that waves cannot travel upstream; therefore, the information that the pressure ratio has decreased below the critical ratio cannot travel upstream and the critical reduced mass flow rate persists throughout.

Consequently, for  $\frac{p_{abs\,outlet}^0}{p_{abs\,inlet}^0} \leq \left(\frac{2}{k+1}\right)^{\frac{k}{k-1}}$  the equation (5.46) is replaced by:

$$\frac{\dot{m} \sqrt{RT_{abs\,inlet}^0}}{C_d A p_{abs\,inlet}^0 \sqrt{k}} = \sqrt{\left(\frac{k+1}{2}\right)^{\frac{k+1}{k-1}}} \quad (5.47)$$

From known values of  $C_d$  and cross sectional area  $A$ , the dimensional mass flow rate is function only of the inlet node thermodynamics values ( $R, T_{abs\,inlet}^0, p_{abs\,inlet}^0$ ) and of the type of fluid ( $k$ ): because of the small gaps that the leakage flows cross, and the consequent high values of velocity and Mach number, the hypothesis of incompressible flow would lead, for this element, to great relative errors and, therefore it can't be accepted. Three different contributes of the vane are modelled with  $C_d$  elements: two "axial" leakage and a "circumferential" one. These leakages are generated by the gaps from the vane hub and tip platforms that, for construction, need a tolerance gap between each other: both are approximated as orifices with thin sharp edges. Many literature data, for this specific type of geometry, converge on a  $C_d$  value equal to 0.6 so many  $C_d$  element with this  $C_d$  value and different passage areas are implemented. The axial leakage flows pass through the side gaps between the platforms, while the circumferential passes through the downstream gap between the platform of the row and the next one. The axial leakage, both at the tip and at the hub, use an equivalent area obtained multiplying the axial extension of the vane platform for the gap present between two contiguous platforms; the circumferential leakage, present in the tip region, instead in the hub region is already considered

inside the sealing flow rate, and is obtained using an equivalent area calculated multiplying the circumference, described by the platforms, for the gap between the current row platform and the next one.

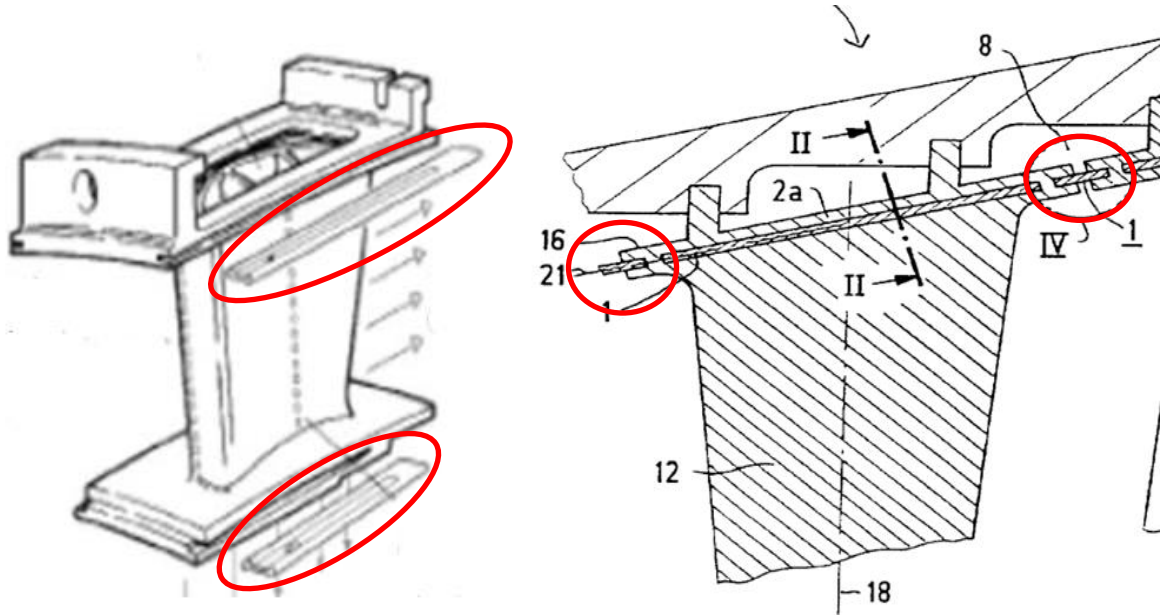


Fig. 5.13 - Details of mechanical gap reducers

The last COOLING contribution comes from the tip plenum and it is used to cool the 2<sup>nd</sup> turbine row shroud. This cooling action is achieved thanks to an impingement plate: because the cooling parameters are not interesting to this kind of SAS simulation, an incompressible flow model is implemented to evaluate the pressure drop across the holes which are simulated as an array of small orifices. The correlations, proposed by Idel’Cik [22], implemented in the IMPINGEMENT element are:

$$p_{abs_{inlet}}^0 - p_{abs_{outlet}}^0 = \zeta \frac{|\dot{m}| \dot{m}}{2\rho_2 N^2 S^2} \quad (5.48)$$

$$SW_{outlet} = SW_{inlet} \quad (5.49)$$

$$T_{outlet}^0 = T_{inlet}^0 \quad (5.50)$$

$$\zeta = 2.85 \quad (5.51)$$

After having cooled the 2<sup>nd</sup> row shroud the air is injected in the turbine flow path through a large number of small bores that are modelled with an element StaticBoreInlet (B114) and pipe (B115). Recalling the convention used for this thesis, because this flow travel through the shroud cooling holes, is classified as a cooling flow. The nomenclature convention explained in the previous chapters has been applied to this line: the vane channel cooling, because the specific design of this row vane, the flow rate has been equally split in two halves: one half is injected upstream the vane throat (EC3\_TV2\_COOL\_PRE\_MID), the other one downstream

the vane throat (EC3\_TV2\_COOL\_POST\_MID). The shroud cooling flow rate, because its location in the throat upstream region is named EC3\_TV2\_COOL\_PRE\_TIP. In the hub region the axial leakage flow and 1/5 of the sealing glow are unified in the EC3\_TV2\_LEAK\_PRE\_HUB contribute while the remaining 4/5 of the sealing flow is named EC3\_TV2\_LEAK\_POST\_HUB; the circumferential and the axial flows located in the tip region are unified un a single contribute named EC3\_TV2\_LEAK\_POST\_TIP.

## 6. Characteristic Curves Production

As discussed in paragraph 4 starting from the base working point all the other working conditions are calculated by fixed coefficient, in hypothesis of linear behaviour: for the base working point the compressor discharge total pressure has been fixed at 21 bar and the turbine inlet total pressure has been fixed to 20.3 bar. Recalling the test matrix (Tab. 4.1), the 5 derived hypothetical operative conditions are obtained multiplying the two independent variable for the coefficients reported in the matrix: in Tab. 6.1 the dimensional values, for all the tested points, are reported. Thanks to the  $\Pi$  theorem application the effects of the compressor and turbine inlet temperature variation, that are not directly considered in the fluid network simulations, will be integrated inside the characteristic curves. The effective test matrix with the applied values of boundary pressure is reported below.

*Tab. 6.1 - Test matrix boundary pressure values*

	TP1	TP2	TP3	TP4	TP5	TP6
$p_{comp\ outlet}^0$ [Bar]	21	22.05	21	18.9	14.7	13.65
$p_{turb\ inlet}^0$ [Bar]	20.3	21.315	18.27	16.24	14.21	13.195

The temperature values, applied only in the 2 boundary elements that simulate the compressor bleeding points are set, for all the tested configurations, equal to 670 K for the external bleeding EC2 and 660 K for the internal bleeding IC2. For this thesis application the relative tolerance of the Newton-Raphson scheme has been fixed to  $10^{-7}$ . The turbine flow path pressure distribution of the base configuration has been divided for the turbine inlet pressure value: the ratios obtained in this way have been kept constant for all the simulated conditions to generate a fictitious field of pressure starting from the scaled turbine inlet pressure. The characteristic curve generation routine has been launched and the resulting curves are here proposed.

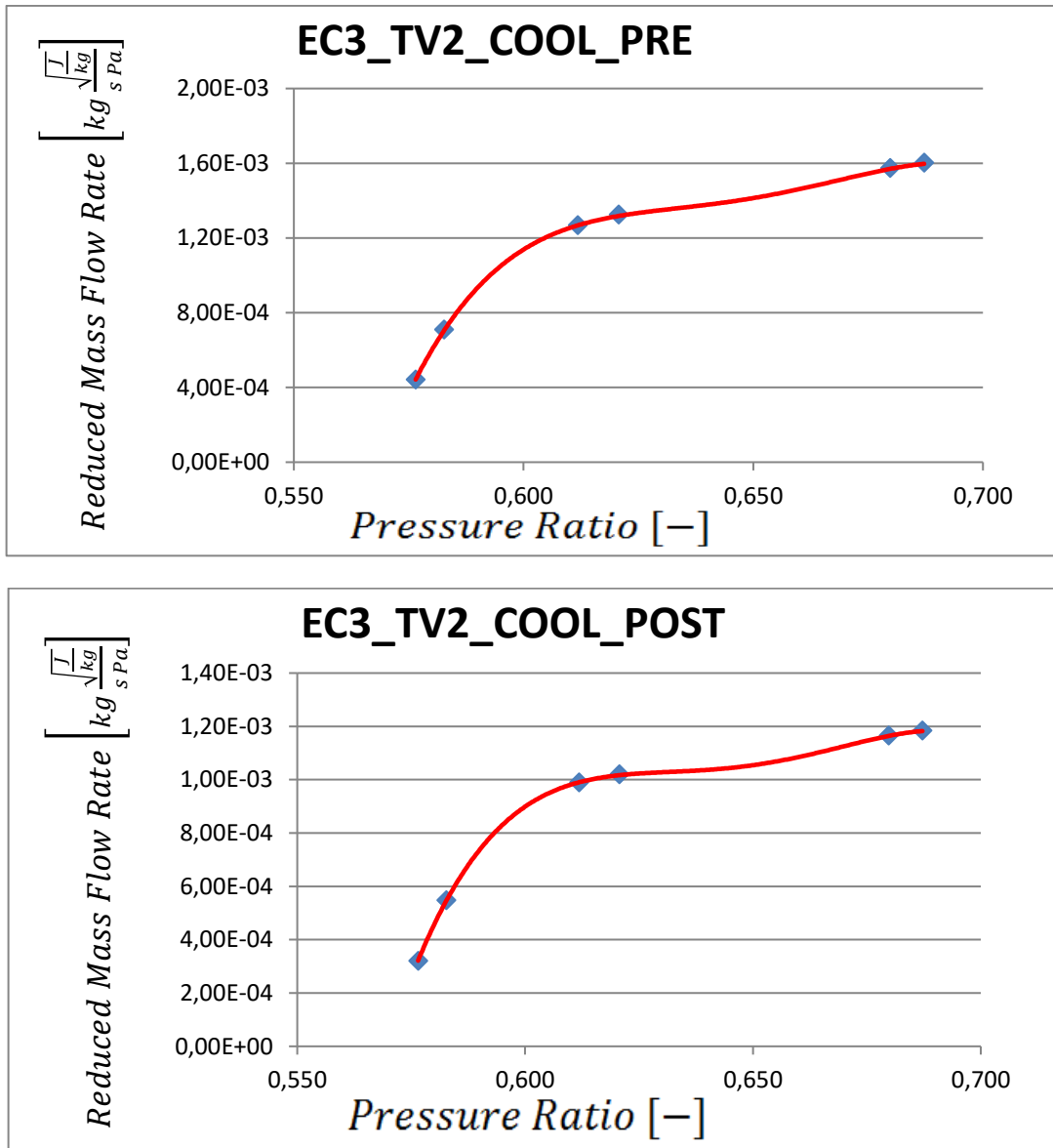


Fig. 6.1 - Cooling characteristic curves for 2<sup>nd</sup> turbine vane row

The previous 2 graphs, reporting the reduced mass flow rate of the cooling flow are quite interesting because show the strong dependence of the vane cooling flow characteristic curve. The behaviour shown in the graphs is way similar to the behaviour of the vane flow function: this can be easily justified.

$$\beta_{int} = \frac{p_{supply}^0}{p_{turb\ inlet}^0} = \frac{p_{supply}^0}{p_{flowpath}^0} \frac{p_{flowpath}^0}{p_{turb\ inlet}^0} = \beta_{vane\ cooling\ constant} \quad (6.1)$$

For this application the ratio  $\frac{p_{flowpath}^0}{p_{turb\ inlet}^0}$  is kept constant by DoE construction so the  $\beta_{int}$  is proportional to  $\beta_{vane}$ ; the EC3\_TV2\_COOL\_POST flow is composed only by the flow function element of the vane so the flow rate is directly proportional to the flow function implemented

in the element. The same approach could be applied to the EC3\_TV2\_COOL\_PRE because the contribution of the vane cooling flow is always greater than the shroud cooling flow, in quite almost the tested condition. Because of this the cooling flow characteristic curves are very similar to a stretched form of the vane flow function.

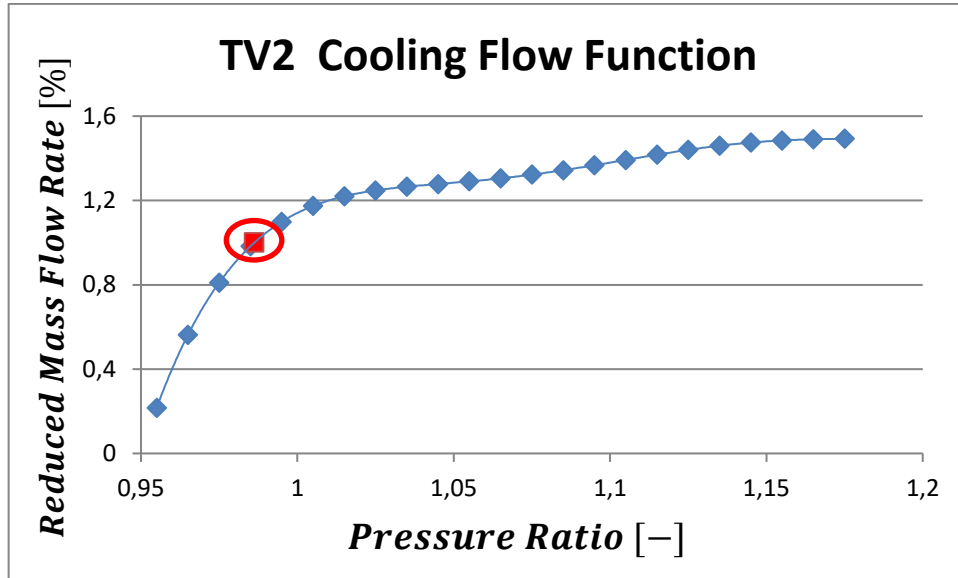


Fig. 6.2 - 2<sup>nd</sup> turbine vane row cooling flow characteristic curve (blue) and base working point (red)

The DoE, for the vane cooling contributes, has been adequate: for the lowest pressure ratios the descent in the flow function is appreciable; the working conditions with the lowest reduced mass flow rate would need a deeper analysis to ensure the lifing of the component, but this type of deepening would not be demanded to this kind of analysis. The validity of the polynomial fitting, described in paragraph 4.7, has been checked, with an additional 7<sup>th</sup> test point, in a condition with a pressure ratio different from the 1<sup>st</sup> six ( $p_{turb\ inlet}^0 = 19.6\ Bar$  and  $p_{comp\ outlet}^0 = 21$ ), Here after the data of the checked point :

Tab. 6.2 - Reduced mass flow rate errors due to the characteristic curves' interpolation

	$p_{absid\ end\ line}^0$ [Bar]	$\beta_{int}$ [-]	$\dot{m}$ [kg/s]	$\dot{m}_{red}$ [-]	$\dot{m}_{red\ poly}$ [-]	$\varepsilon$ [%]
EC3_TV2_COOL_PRE	12.420	0.6118	3.7431	$1.28 * 10^{-3}$	$1.268 * 10^{-3}$	1.115
EC3_TV2_COOL_POST			2.9597	$1.01 * 10^{-3}$	$0.99 * 10^{-3}$	2.31

where

$$\varepsilon [\%] = \frac{\dot{m}_{red} - \dot{m}_{poly}(\beta_{test})}{\dot{m}_{red}} * 100 \quad (6.2)$$

In a condition near the rapid decrease in the characteristic curve, where a small variation in the pressure ratio value may lead to a great variation in the reduced mass flow rate, the polynomial fitting showed its limitations: if the EC3\_TV2\_COOL\_PRE characteristic curve, with a percentage error of 1.115%, might be acceptable, the EC3\_TV2\_COOL\_POST would need a deeper analysis, or an additional test point located in the critical zone.

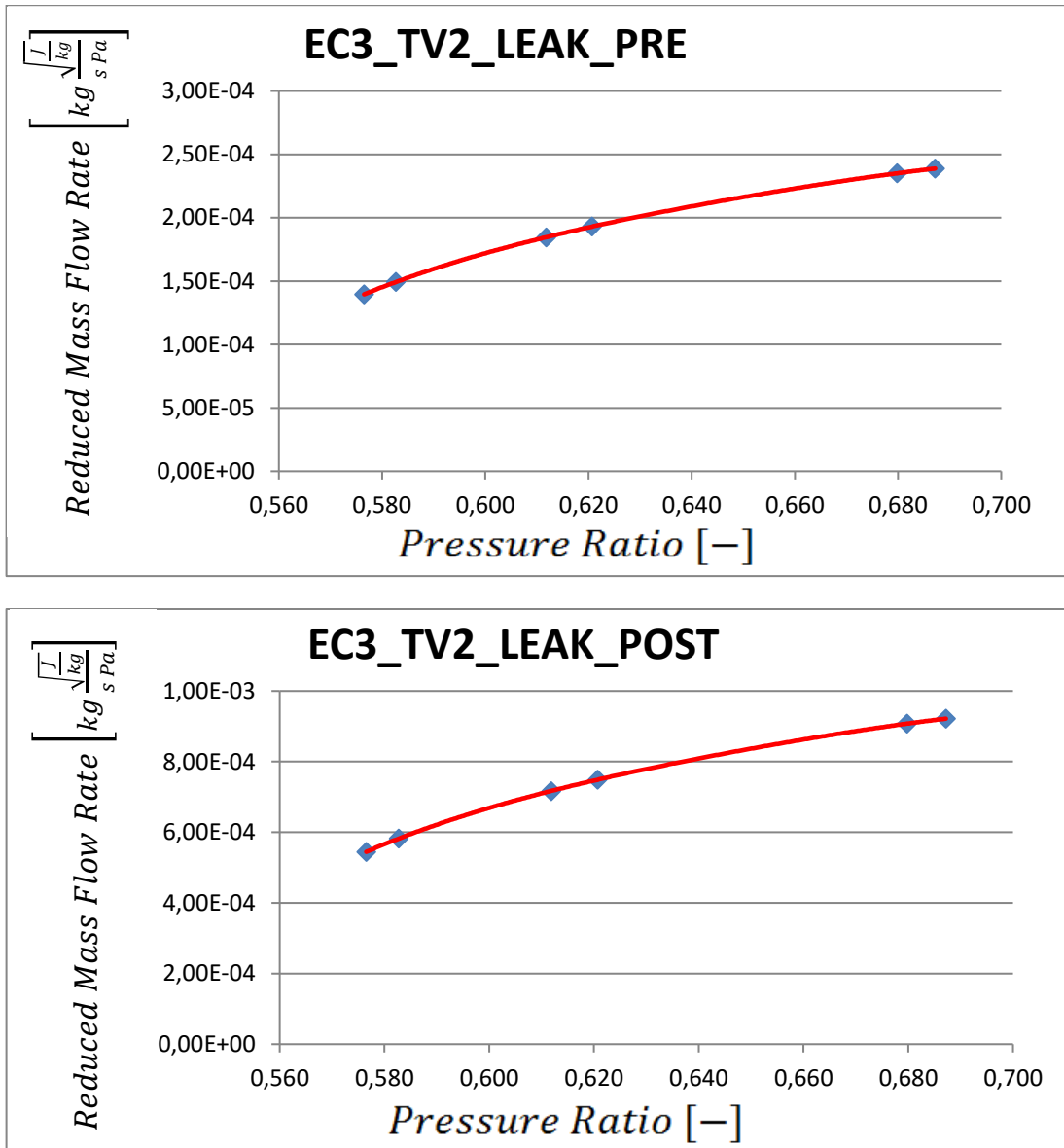


Fig. 6.3 - Leakage characteristic curves for 2<sup>nd</sup> turbine vane row

As predictable the trends of the leakage flows are increasing with the pressure ratio: also if the 1<sup>st</sup> derivative of the curve decreases with the pressure ratio, it remains positive: this trend could be influenced from the incompressible flow correlations implemented in the elements StaticBoreInlet and PIPE used to model the vane box bores. Mach number inside this bores has been checked and reaches its maximum in the TP4 with a value of  $Ma = 0.384$ : because all the other TPs' Mach numbers are below this value, compressibility effects can be neglected and

the approximation of incompressible flow is good and acceptable. However the trend shown in this thesis can't be extended for higher values of pressure ratios without a deeper analysis.

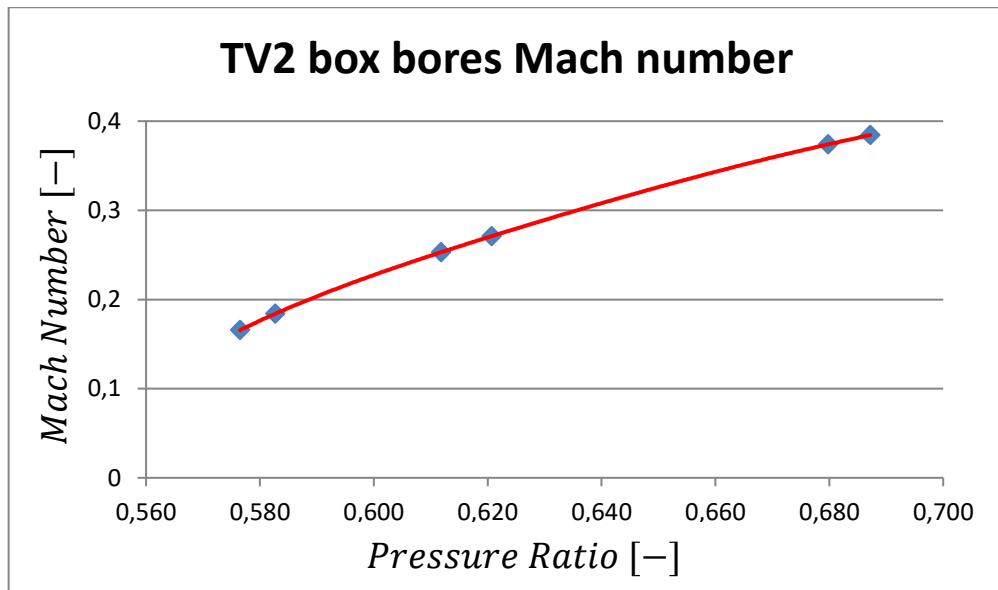


Fig. 6.4 - TV2 box bores Mach number trend in the 6 test operative conditions

From this simple verification, the importance of limiting the pressure ratio is demonstrated: the pressure ratio can be set, for an external and valve equipped lines, by the regulating valve or by the design of the compressor extraction point location and optimisation of this parameter can save up to the 59% in terms of dimensional air consumption. An interesting analysis may come from the observation of the split obtained from EC3\_TV2\_LEAK\_POST (Fig. 6.3b) in the tip and hub region:

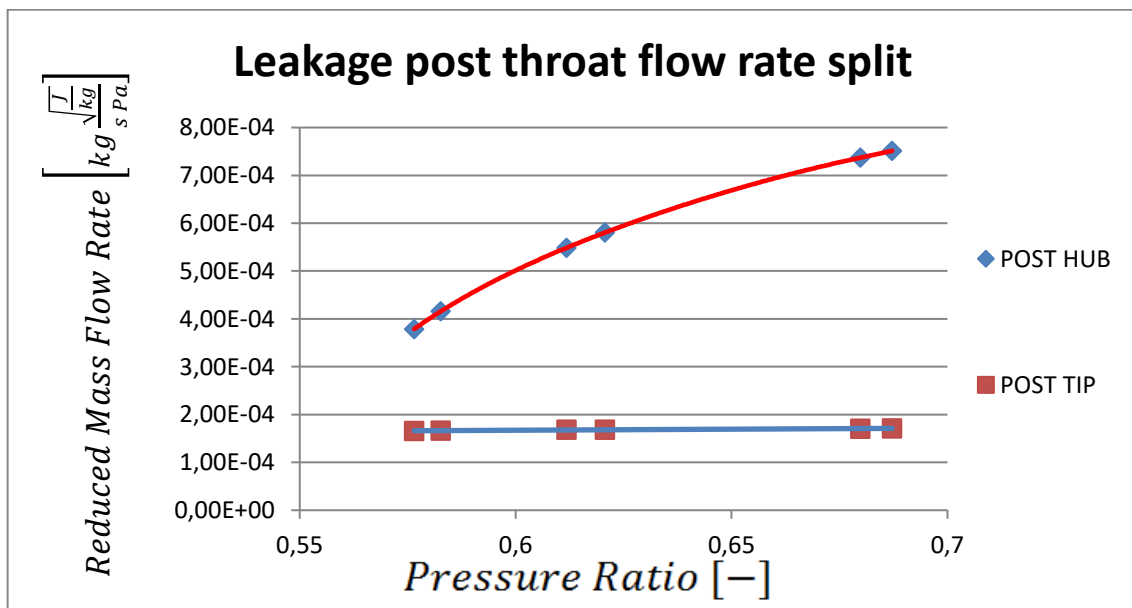
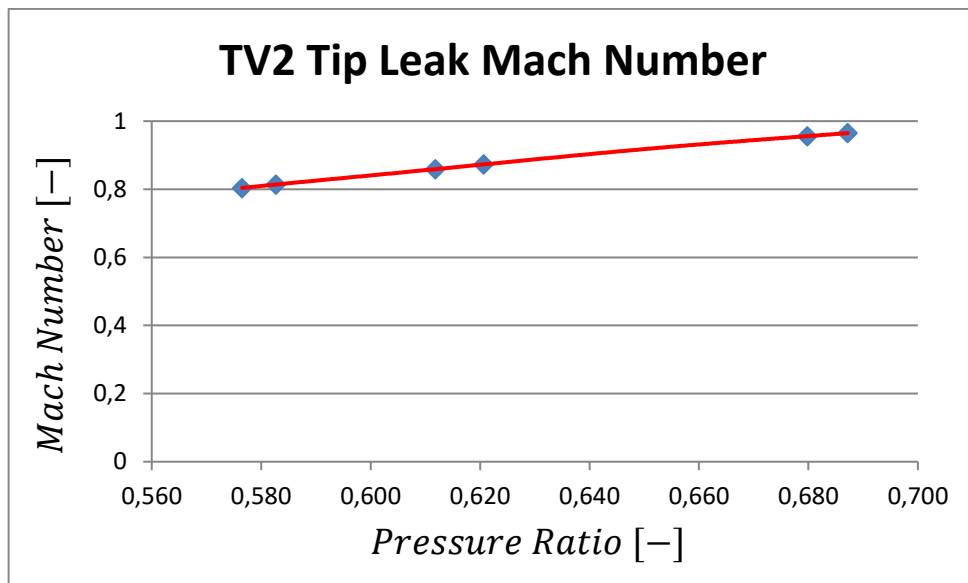


Fig. 6.5 - Detail of the hub and tip region leakage flows

The contribute of the tip leakage (2 CD elements that simulate both the axial and the circumferential leakages BAX and BCIRC) doesn't vary sensibly, while the contribute in the hub region (vane root sealing and axial leakage) has a visible increasing with the pressure ratio: this trend's cause may be found in the different modelling and flow conditions in the 2 regions. At the tip region the leakages are modelled with CD elements, that simulate compressible flow, because the Mach number of this flow is slightly lower than the unit: for these values of Mach number the compressibility effects must not be neglected. The figure below reports the Mach number of the tip leakages CD elements: the 2 different blocks have the same Ma because they are modelled with the real orifice equations, that are functions only of the pressure ratio, that the 2 blocks share.



*Fig. 6.6 - TV2 tip leakages Mach number trend in the 6 test operative conditions*

These behaviours can also be exploited in a design condition; in fact small increasing in the supply pressure, with a consequent increasing of the pressure ratio, will induce a noticeable increasing in the leakage mass flow rate only in the hub region: in case of small request of mass flow rate increasing in the hub sealing, the increasing of the pressure ratio could be a good way to operate, without any geometrical change required and without any appreciable penalty for the tip leakage flows. These statement could be applied only for small variations of the pressure ratio because for pressure ratios values above the discussed ones compressibility effects could not be neglected in the hub region.

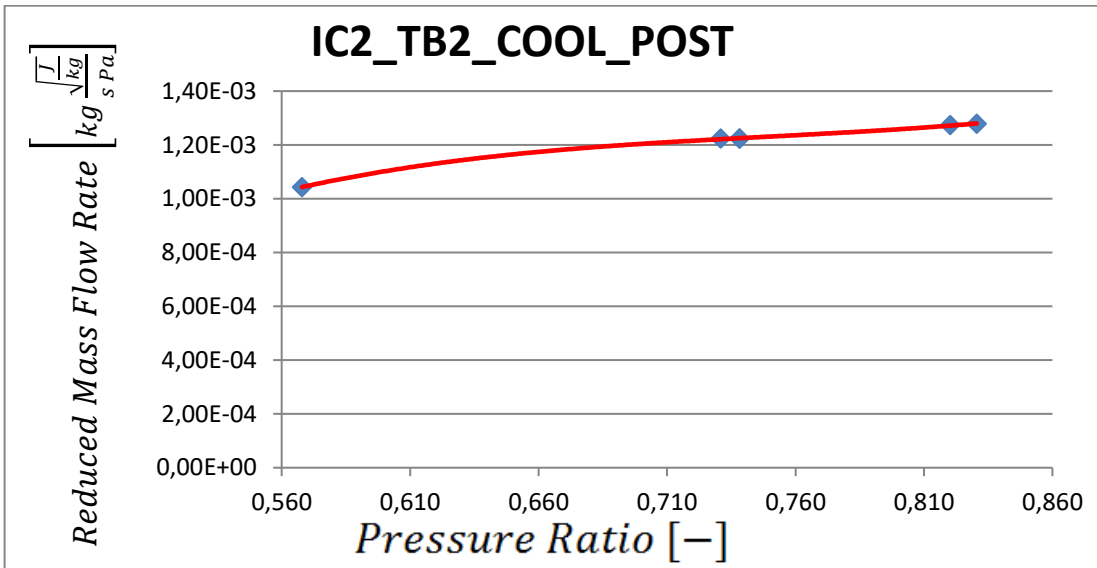
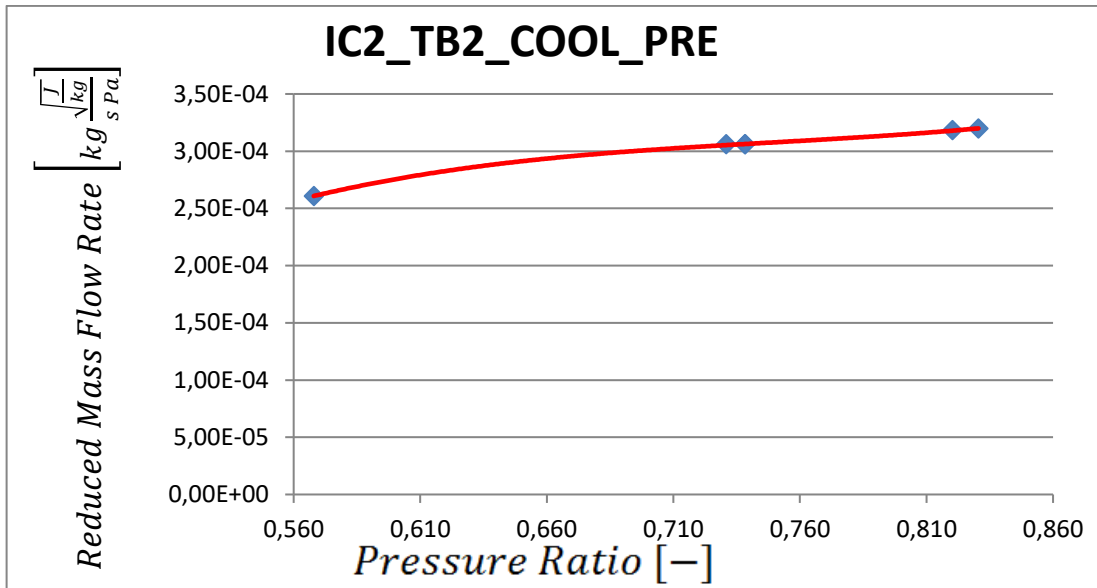


Fig. 6.7 - Cooling characteristic curves for 2<sup>nd</sup> turbine blade row

All the blade cooling working points lie on the “plateau” region of the characteristic curve: with the same boundary conditions ( $p_{turb\ inlet}^0$  and  $p_{comp\ outlet}^0$ ) according to the test matrix (Tab. 6.1), the blade working points are in a more stable and safer region than the vane ones.

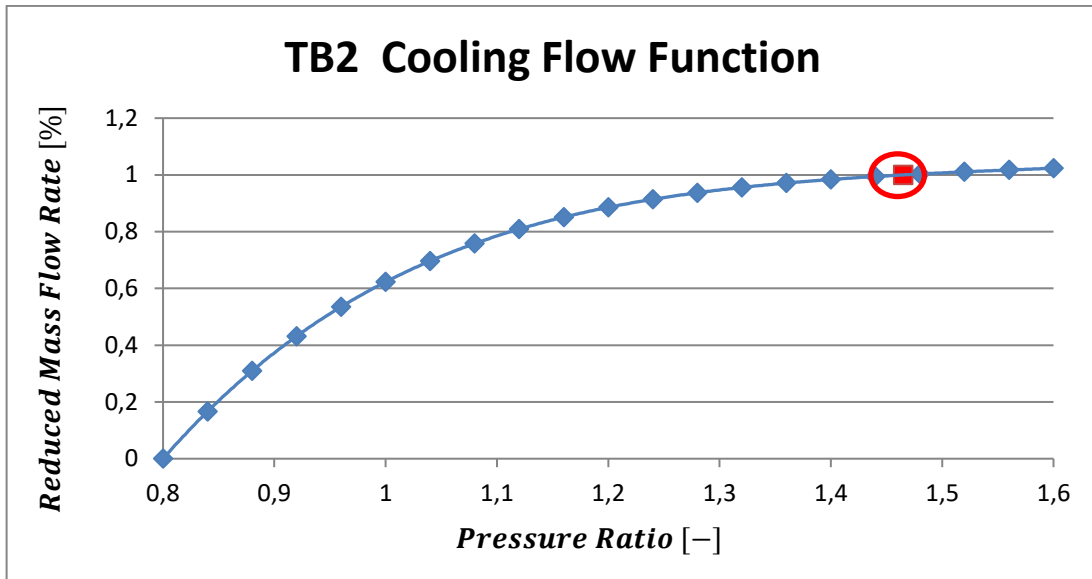
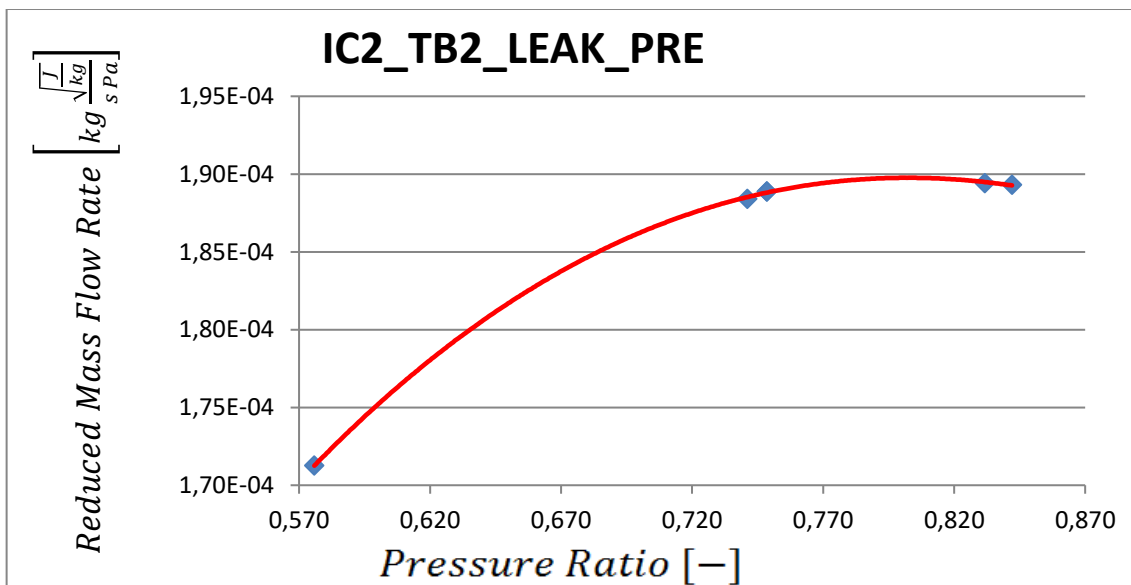


Fig. 6.8 - 2<sup>nd</sup> turbine blade row cooling flow characteristic curve (blue) and base working point (red)

From this curve a critical review of the engine design may be carried on: assuming the same risk margins for internal and external lines, for this specific imaginary turbine engine, the internal line flow rate may be reduced without any problem for the blade life and with an increase of the global produced power.



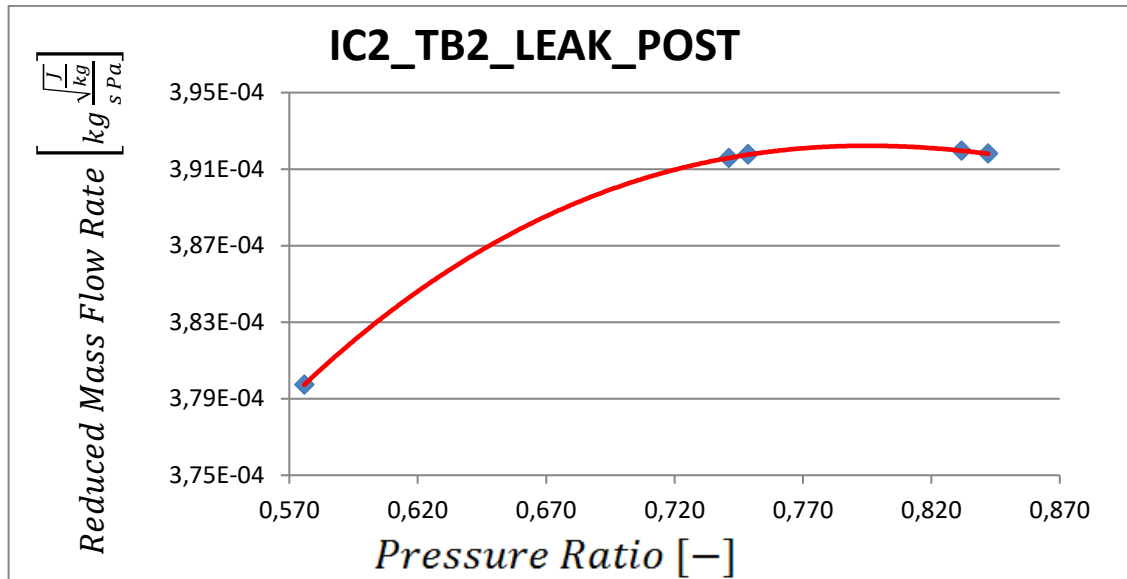


Fig. 6.9 - Leakage characteristic curves for 2<sup>nd</sup> turbine blade row

The leakage flows show a different behaviour from the vane ones: the trend has a peak trend. The stationary point, in this case the maximum, is present only in the reduced mass flow rate trend: it's necessary to recall that the dimensional quantities, such as the mass flow rate, are functions both of the pressure ratios and of the supply pressures.

According to the procedure discussed in paragraph 4.7 the above graphs show the characteristic curves based on a polynomial fitting obtained from 6 test results also if only 5 points appear: this is due to a perfect overlap of 2 different test points. This overlap, in terms of DoE, is something undesirable because the exploration of the design space, for a fixed number of test points, would be lower but, for an educational application like this thesis, is a confirm of the validity of the  $\Pi$  theorem and of the routine implemented: for a fixed pressure ratio only one value of the reduced mass flow rate exists.

Tab. 6.3 - Cooling flow data for the overlapped points

	$p_{turb\ inlet}^0$ [Bar]	$p_{relid\ end\ line}^0$ [Bar]	$\beta_{int}$ [-]	$\dot{m}$ [kg/s]	$\dot{m}_{red}$ [-]
Test point 1	20.3	14.987	0.738	1.0443	$3.059205 \cdot 10^{-4}$
Test point 2	21.315	15.736	0.738	1.0965	$3.059205 \cdot 10^{-4}$

Tab. 6.4 - Leakage flow data for the overlapped points

	$p_{turb\ inlet}^0$ [Bar]	$p_{relid\ end\ line}^0$ [Bar]	$\beta_{int}$ [-]	$\dot{m}$ [kg/s]	$\dot{m}_{red}$ [-]
Test point 1	20.3	15.195	0.748	0.6525	$1.888781 \cdot 10^{-4}$
Test point 2	21.315	15.955	0.748	0.6851	$1.888775 \cdot 10^{-4}$

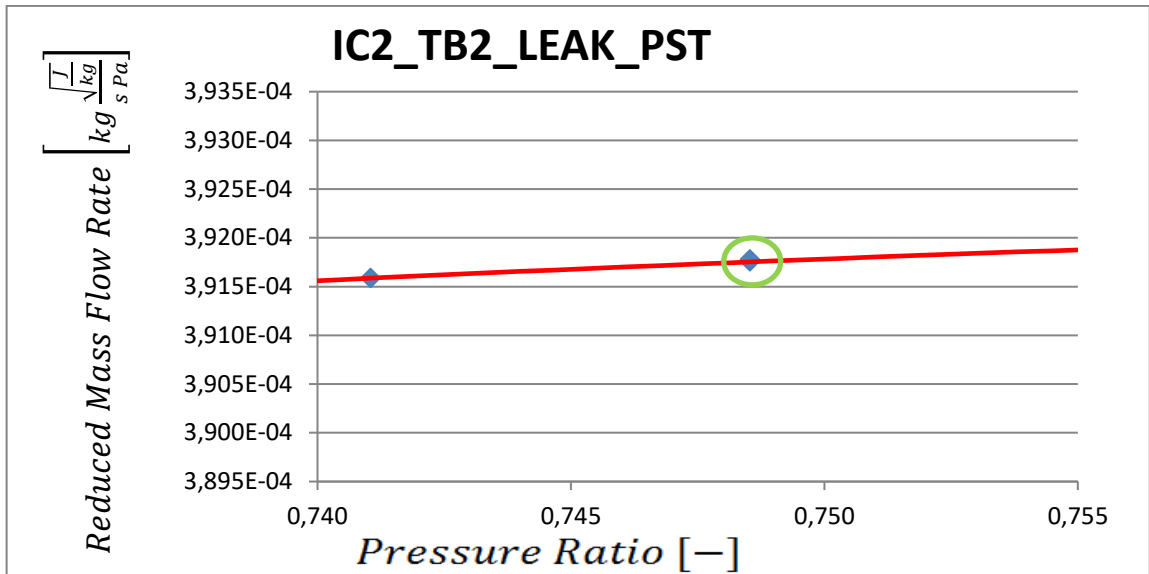


Fig. 6.10 - Detail of the overlapped points in the turbine leakage characteristic curve

## 7. Conclusions

In a fast changing and competitive market like the today energy market, the necessity of an integrated and fast simulation method of the Gas Turbine engine performances is everyday more important. To reach an adequate solution in a strict time scheduling and with a low resources demand a simplified 0D fluid network of the SAS network has been implemented in a wider routine for performance prediction: the routine has been based on the Riabouchinsky - Buckingham's  $\Pi$  theorem and on the components' characteristic curve generation. With many simplifying assumptions the SAS circuits have been successfully integrated with the other main components of the GT engine such as the compressor and the turbine. To obtain a realistic solution, alongside the SAS line, the fluid network simulates the behaviour of the blade and vane cooling, by the adoption of specifically designed flow functions. Many correlations, both incompressible and compressible, based on literature and experimental data have been implemented in the fluid network to model the SAS lines. The fluid network and the correlations implemented inside itself, as they have been designed, are open to be tuned with data from experimental campaigns or more complex 3D CFD analyses with possible improvements in the results' fidelity. After the assembly of the entire SAS circuit inside the 0D fluid network the conditions of pressure at the boundaries have been modified, according to a user-defined Design of Experiments, in order to simulate the wide off-design range of the gas turbine engine working points. The validity of the characteristics' method chosen has been validated and the interpolation error, due to the necessary fitting of the results, has been quantified: the errors have been proved to be overcome by the time and resources savings. The application of the method described in this thesis can also be extended from the off-design simulation to the critical review of a chosen design.

## References

- [1] Ansaldo Energia, brochure
- [2] Lozza G., 2016, Turbine a Gas e Cicli Combinati, Esculapio edizioni, Italia
- [3] Sorce A., Lecture notes of ‘Solutions for combined cycle flexibility’ seminar
- [4] Tanda G. Lecture notes of course ‘Heat Transfer’
- [5] Massardo A. F., Lecture notes of course ‘Energy Plants’
- [6] Galliani A., 2017, Lecture notes from ‘Evoluzione del mix produttivo di energia elettrica e suoi effetti sul sistema’ seminar
- [7] ARERA Autorità di Regolazione per l’energia reti ed ambiente, website
- [8] TERNA – Rete Elettrica Nazionale, website
- [9] Innocenti L., Lecture notes of ‘Introduzione ai Sistemi Aria Secondaria di turbine a gas’
- [10] Ludwig L. P., Johnson R. L., 1974, Sealing technology for aircraft gas turbine engines, American Institute of Aeronautics and Astronautics and Society of Automotive Engineers, California, 21-24
- [11] Becker B., 2002, Robust gas turbine design, proceedings of ASME TURBO EXPO, Netherlands
- [12] Atkins N. R., Knjirakkad V., 2014, Flow in a rotating cavity with axial throughflow at engine representative conditions, ASME Turbo Expo 2014 Turbine Technical Conference and Exposition, Germany, 1-14
- [13] Reichert A.W., Janssen M., 1996, Cooling and sealing air system in industrial gas turbine engines, ASME International Gas Turbine and Aeroengine Congress and Exhibition, England
- [14] Dhondt G., CalculiX CrunchiX user’s manual
- [15] Chapra S., Canale R. P., 2018, Numerical Methods for engineers, McGraw-Hill Education, USA
- [16] Bottaro A., Lecture notes of course ‘Fluid Mechanics’
- [17] Kudela H., Dimensional analysis, Lectures of course ‘Fundamentals of Fluid Mechanics’
- [18] Cohen H., Saravanamuttoo H.I.H., Rogers G.F.C., Straznicky P., Nix A.C., 2017, Gas Turbine Theory, Pearson, USA
- [19] Dixon S. L., 2017, Fluid mechanics and Thermodynamics of turbomachinery, Butterworth-Heinemann, USA.
- [20] McGreehan W.F., Schotsch M.J., 1988, Flow Characteristics of Long Orifices With Rotation and Corner Radiusing, Journal of Turbomachinery, vol.110, 213-218.
- [21] Reichert A.W., Brillert D., Simon H., 1997, Loss Prediction for Rotating Passages in Secondary Air Systems, ASME International Gas Turbine and Aeroengine Congress and Exhibition, Florida, 1-8.

- [22] Idel’Cik I. E., 1999 , Memento des pertes de charge, Eyrolles, France
- [23] Moody, L. F., 1944, Friction factors for pipe flow, Transactions of the ASME, Vol. 66, 671–684
- [24] Haaland S.E., 1983 Simple and Explicit Formulas for the Friction Factor in Turbulent Flow, Journal of Fluids Engineering Vol.105, 89–90.
- [25] Swamee, P.K., Jain, A.K., 1976, Explicit equations for pipe-flow problems, Journal of the Hydraulics Division, Vol. 102, 657–664
- [26] Anderson J. D., 2003, Modern Compressible flow, McGraw-Hill Education, USA

## Nomenclature

### Notations

$k$	specific heat ratio
$c_p$	constant pressure specific heat capacity
$p$	pressure
$\eta$	efficiency
$\beta$	compression ratio
$L_n$	useful/net work
$\dot{m}_{red}$	reduced mass flow rate
$sw$	swirl coefficient
$u$	blade speed
$c$	absolute flow velocity

### Subscripts

red	reduced
blade root	blade root cavity
end line	end of the SAS circuit
c	compressor
t	turbine
e	expander
is	isentropic
rel	relative
abs	absolute
id	ideal
supply	supply cavity
int	internal line
ext	external line
$\theta$	tangential
0	stagnation quantity

### Definitions and acronyms

SAS	Secondary Air System
GT	Gas Turbine
IC	Internal Circuit
EC	External Circuit
BL	Base Load
ML	Minimum Load
MEL	Minimum Environmental Load
IGV	Inlet Guide Vane
TP	Test Point